UNIVERSITY OF SOUTHERN QUEENSLAND

USING TOPOLOGY OPTIMISATION IN TUNNEL REINFORCEMENT DESIGN

A dissertation submitted by

TIN NGUYEN

B.Eng., Danang University of Technology, Vietnam, 2005

M.Eng, Asian Institute of Technology, Thailand, 2009

For the award of the degree of

Doctor of Philosophy

2015

Dedication

To my family

Abstract

In tunnel reinforcement design, having a suitable tool which is able to capture complex ground material and various tunnelling conditions is definitely significant. Since early stages of tunnelling engineering, empirical approaches using rock mass classification and accumulated experiences have been commonly used. Nevertheless, as developed from long-term accumulated knowledge in older projects, it is not always applicable to new ground conditions and also hardly guarantees a best design to be obtained. Analytical method is another tool to provide explicit calculations, however, its applications are limited to only some simple scenarios such as circular tunnel. It is also noted that these two approaches are only applicable to free-field conditions. Owing to the ability in modelling complex ground conditions with consideration of discontinuities or adjacent structures, numerical simulations has been constantly developing and applying in tunnel excavation design in the last decades. An appropriate incorporation of numerical analysis and optimisation techniques, if applicable, would provide a powerful tool for obtaining an optimal tunnel design.

In spite of effectiveness of topology optimisation theory, which is proved to work effectively in a broad range of engineering disciplines, its applications in geotechnical engineering and specifically in tunnelling design is fairly humble. Some research works have already attempted to incorporate topology optimisaton techniques in tunnel reinforcement design and proposed some initial achievements in the area. However, simple assumptions on the material models and modelling techniques of geomaterials and reinforcement materials have essentially limited its applications and practicality in a complicated structure like underground excavations.

This thesis explores the incorporation of topology optimisation methods in tunnel reinforcement design. The main focus of the study is to improve some critical shortcomings of the previous works on reinforcement optimisation and propose new optimisation algorithms in searching for the best distribution of reinforcement material.

As the first step in this study, material nonlinearities are accounted for in optimisation techniques to improve the linear elastic material model assumption of previous studies. Practical behaviours of material, hence, can be captured. The Bidirectional Evolutionary Structural Optimisation (BESO) method is extended to consider nonlinear material behaviour. An elastic perfectly-plastic Mohr-Coulomb model is utilised for both host ground and reinforced material. External work along the tunnel wall is considered as the objective function. Various *in situ* stress conditions with different horizontal stress ratios and different geostatic stress magnitudes are investigated through several examples. The outcomes show that the proposed approach is capable of improving tunnel reinforcement design. Also, significant difference in optimal reinforcement distribution for the cases of linear and nonlinear analysis results proves the importance of the influence of realistic nonlinear material properties on the final outcome.

Another serious shortcoming of the previous studies is that reinforced areas were modelled as homogenised isotropic elements. Optimisation results, therefore, do not clearly show reinforcement distributions, leading to difficulties in explaining the final outcomes. In order to overcome this deficiency, a more advanced modelling technique in which reinforcements are explicitly modelled as truss elements embedded in rock mass media is employed. Corresponding optimisation algorithm are proposed to seek for an optimised bolt layout. Also, a topology optimisation technique is employed to simultaneously optimise all bolt parameters including pattern for bolts, spacing between the bolts and size of the bolts. The external work along the opening is selected as the objective function with a constraint on volume of bolt. To demonstrate the capabilities of the methods, numerical examples of nonlinear material models are presented. Various tunnelling characters and geological conditions with presence of discontinuities in the host rock have been successfully investigated in numerous examples, showing

the broad applicability and usefulness of the proposed approaches.

In reality, minimisation of certain displacements such as heave issues or ground displacements in shallow tunnel is sometimes of concern. Extending optimisation methods to capture these objective functions is crucial. A general displacement-based objective function is introduced with a constraint on a bolt volume. Sensitivity analysis is conducted and details on identification of necessary parameters are provided. Using the presented optimisation algorithm, an example on optimising bolt layout to minimise a heave function is performed. It is shown that the displacement-based objective function can be effectively captured by the proposed optimisation technique.

This study focuses on applying topology optimisation in tunnel reinforcement design to take advantage of both numerical analysis and optimisation methods. The presented techniques are applicable to any material models of host ground and reinforcements and provides clear and practical final outcomes. Using the proposed methods, all significant factors including geological conditions, construction sequences and tunnel characters can be taken into account to obtain an optimised reinforcement distribution. It is also demonstrated that various objective functions can be employed and usefully optimised by the methods. The obtained results proves that the optimisation techniques presented in this thesis are promising tools to reinforcement design of underground excavations.

Certification of Dissertation

I certify that the idea, experimental work, results and analyses, software and conclusions reported in this dissertation are entirely my own effort, except where otherwise acknowledged. I also certify that the work is original and has not been previously submitted for any other award.

Tin NGUYEN ENDORSEMENT	Date
Dr. Kazem GHABRAIE, Principal supervisor	Date
Prof. Thanh TRAN–CONG, Co-supervisor	Date

Acknowledgements

Firstly, my sincere thanks are extended to Prof. Thanh Tran-Cong for giving me an opportunity to pursue my PhD at the University of Southern Queensland (USQ), opening up a new and bright chapter of my academic career. His financial and academic support are also appreciated. I would like to express my profound gratitude to my principle supervisor, Dr. Kazem Ghabraie, for his invaluable supervision, fruitful discussions, useful writing corrections and inspirations during the period of my PhD research.

I owe this work to my dear parents. Their endless love, unconditional lifetime sacrifices and continued encouragements are invaluable sources that constantly keeps me move forward.

My sincere appreciations are due to my beloved wife for being beside me through the ups and downs, sharing many tough times in our personal life and especially giving a birth of our little daughter, Emma. Without her supportive encouragement, I have never made this to the end. Special thanks are also due to my lovely daughter for all much happiness she has brought to me during my period of intensive research.

I would like to extend my gratitude to all members of my parents-in-law's family, my brother, Thien, my sister-in-law, Nhung and my nephew, Duc Trong, for their warm love and selfless support.

The project was jointly funded by the University of Southern Queensland (USQ), Faculty of Health, Engineering and Surveying (FHES), and the Computational Engineering and Science Research Centre (CESRC). This financial support is gratefully acknowledged.

Papers resulting from the Research

Journal papers

1. **Nguyen, T.**, Ghabraie, K., and Tran-Cong, T. (2014). Applying Bi-directional Evolutionary Structural Optimisation method for tunnel reinforcement design considering nonlinear material behaviour. *Computers and Geotechnics,* 55, 57-66.

2. **Nguyen, T.**, Ghabraie, K., Tran-Cong, T., and Fatahi, B. (2015). Improving Rock Bolt Design in Tunnels Using Topology Optimisation. *International Journal of Geomechanics (accepted 9 Jan 2015).*

3. **Nguyen, T.**, Ghabraie, K., and Tran-Cong, T. (2015). Simultaneous pattern and size optimisation of rock bolts for underground excavations. *Computers and Geotechnics (accepted 10 Feb 2015).*

Conference papers

1. **Nguyen, T.**, Ghabraie, K., and Tran-Cong, T. (2012). Tunnel Reinforcement Optimization for Nonlinear Material. *The 4th International Conference on Computational Methods (ICCM2012)*, Gold Coast, Australia, November 2012.

Contents

List of Figures

List of Tables

Chapter 1

Introduction

1.1 General

Design of underground structures like shafts, caverns or tunnels in rock media faces a number of challenges owing to complex rock mass properties and ground conditions. Having a relevant tool which is able to capture a variety of rock mass conditions is definitely essential to obtain a technically safe and economically reasonable design. Various types of design tools and methods normally employed in rock engineering can be named as analytical calculations, numerical modellings, empirical systems and observational methods. Each of these methods has both advantages and disadvantages and can be applied to various phases of planning and construction period.

Development of high speed computers and improvements in optimisation algorithms have supported not only academic interests but also a large number of engineers to work on and benefit from optimisation methods. Optimisation techniques have been continuously developed in the last decades and achieved some significant practical applications in manufacturing industry (particularly in car and aerospace industries) (Rozvany, 2009). They have also been broadly expanded to a wide variety of physical problems including structure, heat transfer, fluid, electromagnetics, photonics and their combinations. In geotechnical engineering design, there is a considerable number of design problems where optimisation techniques can be applied to such as slope design with and without

reinforcement, foundation engineering, tunnel design, etc. Despite its promising potential, there are few applications employing modern optimisation techniques to obtain a more rational design in geotechnical engineering, particularly in tunnelling design.

Given available information on ground conditions and design requirements, the conventional methods combined with engineers's experiences would provide eventual outcomes of the required tunnelling features and the ground behaviour around the opening. Nevertheless, no one can guarantee that the proposed design is the most appropriate one. An incorporation of the conventional design tools with optimisation techniques would expectedly provide an advanced and useful tool in design of underground structure. Finding optimal shape of underground excavations or optimal size and patterns of reinforcement materials around the opening are some of typical achievements by such an approach.

1.2 Levels of optimisation

In structural design, optimisation can be classified into three categories, namely size optimisation, shape optimisation and topology optimisation. The earliest approach is size optimisation which finds the optimal structural dimensions with predefined shape by changing size variables. Problems such as seeking out an optimal cross section area of truss elements or an I beam have been solved by sizing optimisation in structural design. Shape optimisation is performed to modify predetermined boundaries on continuum structures to achieve the best shape. Searching for the best shape of a hole in a loaded plate is a typical example of shape optimisation. Topology optimisation in a discrete structure can be used to find the optimal spatial order and its connectivity. For continuum structures, it can be used to search for the best locations and geometries of cavities in the domain. Topology optimisation is by far the most technically challenging as well as economically rewarding among these types. Conceptual illustration of these optimisation levels is depicted in Fig. 1.1.

Benefiting from the significant improvements of numerical analysis and powerful

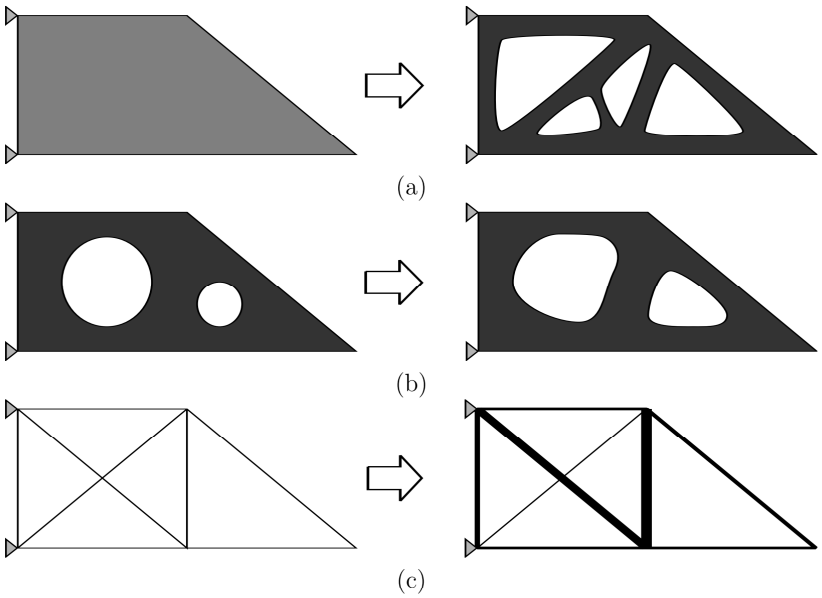

Figure 1.1: Three levels of optimisation: a)Topology optimisation; b)Shape optimisation; c)Sizing optimisation (Ghabraie, 2009)

digital computers, the optimisation techniques, especially topology optimisation techniques, have been rapidly expanded in the last two decades. Topology optimisation has not been limited to structural engineering applications, but widely applied in material design, micro- and nanotechnologies and wave propagation problems (Bendsøe and Sigmund, 2003). Achievements in both theoretical implications and important practical applications have been obtained.

1.3 Applications of Topology Optimisation in Tunnelling Design

Topology optimisation techniques are utilised in this study to search for the optimal reinforcement design for underground excavations by economically distributing reinforced material where it is mostly required. The obtained outcomes are expected to provide goetechnical engineers with an overview on tunnel reinforcement design and specific suggestions on optimal reinforcement distribution for underground excavations.

In geotechnical engineering design, there is a considerable number of design problems where topology optimisation techniques can be applied to such as tunneling

engineering, slope design with and without reinforcement, foundation engineering, etc. However, there are only few publications on employing the well-known robustness of topology optimisation in geomechanics problems due to complex behaviour of geomaterials.

Generally, natural geological materials like rock and soils are discontinuous, inhomogeneous, anisotropic and not-elastic (Harrison and Hudson, 2000). Also, the presence of fluids and discontinuities in rock mass such as bedding planes, joints, and faults makes rock a fractured porous media. Compared to manufactured materials with clearly defined physical and engineering properties, the properties of geomaterials needs to be established based on laboratory test and empirical knowledge. These special features give rise to difficulties in mathematical representation of geomaterials and subsequently in modelling.

Another dominant feature of geotechnical engineering is the effects of loading sequence on ground behaviours. Specifically in underground excavation design, a change in the opening shape during excavation process causes stress relief around the opening and alters the loading conditions. Also, tunnel advancement and reinforcement installation significantly affect the reaction of surrounding ground and their interactions with the reinforcements. This interaction is an important factor to determine the types and amounts of the reinforcements required.

Some studies have attempted to optimise shape and reinforcement distribution of underground excavation. Shape optimisation of underground opening was explored by Ren et al. (2005); Ghabraie et al. (2008); Ren et al. (2014). Also, tunnel reinforcement optimisation have been studied by several optimisation methods (Yin et al., 2000; Yin and Yang, 2000a,b; Liu et al., 2008b; Ghabraie, 2009; Ghabraie et al., 2010). A rigorous review of these works will be detailed in chapter 2.

Finding the optimal shape of underground openings is beyond the scope of this study. With regards to reinforcement optimisation, a common limitation of the above-mentioned earlier works is linear elastic analysis which is not valid for most of the cases in geomechanics and can only be considered as the initial step in analysis (Jing, 2003). Additionally, in the previous studies, homogeneous re-

inforced material models were used to model reinforcement material, which leads to difficulties in explicitly simulating anisotropy of material and interpreting the final outcomes. Common reinforcement types like rock bolts or nails are steel bars being fixed at their ends and pretensioned or connected to the surrounding rock over their entire length by grouting. Obviously, using these reinforcement types, the reinforced area will have different mechanical properties in different directions. Considering this effect explicitly in tunnel reinforcement optimisation can capture the behaviour of reinforced rock mass more accurately and be seen as an essential improvement to the existing studies. Furthermore, existence of discontinuities in rock mass such as joints, bedding planes etc. can heavily influence the rock mass behaviour. A thorough consideration of discontinuities is therefore crucial in securing more reliable and practical design.

1.4 Objectives and Scope of Study

In this research, the most critical shortcomings of the previous studies will be improved and further developments in applying topology optimisation techniques on tunnel reinforcement design will be conducted. Specifically, the following research objectives are to be addressed:

1. Considering elasto plastic material models and using nonlinear finite element analysis in tunnel reinforcement optimisation.

2. Considering anisotropic properties of reinforced material by explicit modelling of rock bolts.

3. Proposing an optimisation approach to optimise rock bolt size.

4. Proposing a simultaneous optimisation approach of bolt size and pattern.

5. Capturing the effects of geological conditions on optimised bolt configurations

6. Considering various objective functions in the proposed optimisation techniques.

1.5 Outline of the Thesis

An overall literature review is conducted in the next chapter. Paricularly, in the first part, an overview of geotechnical materials and tunnel reinforcement design issues is presented. A careful discussion is given to analyse difficulties and limitations of using various conventional approaches in design of underground excavation. In the second part, details of the topology optimisation techniques and their potential applications on underground excavation design are presented. Previous works on applying topology optimisation on tunnel design are summarised to show their limitations and also to propose some possible improvements and further developments in the area.

Chapter 3 removes a serious assumption in the previous reinforcement optimisation works by taking into account material nonlinearities. Examples on both elastic and elasto-plastic cases are illustrated to show that the proposed approach is applicable to any material models used. Various factors affecting optimised distribution of reinforcement material are discussed via examples.

As a further improvement, in chapters 4 and 5, an explicit modelling method is used to simulate tunnel reinforcements and corresponding optimisation approaches are proposed to seek for optimised reinforcement configurations. Chapter 4 provides an optimisation approach to search for optimised bolt sizes. An advanced optimisation approach to simultaneously optimise bolt size and pattern is proposed in chapter 5. A series of examples are presented in each chapter to demonstrate effects of various important inputs on bolt design including tunnelling features, geological conditions and construction sequences.

In chapter 6, attempts are made to extend the the proposed optimisation methods by considering a general displacement-based objective function. A typical example is shown to illustrate the usefulness of the method.

A summary of this research outcomes is presented in the conclusion chapter, chapter 7. Ideas and recommendation for future research is also listed.

Chapter 2

Literature Review

The aim of this study is to propose algorithms which are able to optimise reinforcement distribution around underground openings satisfying given objective functions and constraint conditions. This chapter is devoted to a review of published literature related to both tunnel reinforcement design issues and topology optimisation techniques.

2.1 Overview of rock mechanics

In the design of underground excavations, a comprehensive understanding of geomaterial behaviour and its interaction with external structures are important inputs for modelling and designing tunnel structures. In the following sections, details on material properties of rock mass and modelling issues are presented.

2.1.1 Special character of rock mass

Unlike other engineering properties, a special character of rock material is the existence of discontinuities which may be filled with liquid or gas or solids under complex *in situ* stress conditions. The characters of discontinuities are dominant factors, to a large extent, governing rock mass behaviour (Bieniawski, 1989). These characters can be categorised in two types, geometric and non-geometric properties. The geometric properties covers the fabric of discontinuities in the

rock mass while the non-geometric captures the infill material mechanical properties and shear strength of intact rock close to discontinuities (Hack, 1998). However, obtaining all of these features is normally impossible in reality. Instead, information obtained from borehole cores, field observations and rock mass classification system provides designers with an overall picture of discontinuties within a rock mass.

2.1.2 Strength of rock mass

Strength of a rock mass depends on the strength of intact rock and the shear strength of discontinuities. In the case of a rock mass with few discontinuities, the strength of discontinuities should be explicitly determined by a shear strength criterion while the strength of intact rock is considered by using a failure criterion for intact rock. On the other hand, in the case of heavily jointed rock, the strength of discontinuities can be implicitly combined with the strength of intact rock to utilise a failure criterion for the whole rock mass.

Mohr-Coulomb model is widely used to model both the shear strength of surfaces and jointed rock mass while Hoek-Brown is among the most renowned empirical failure criterion of jointed rock mass.

a. Mohr-Coulomb failure criterion

In the Mohr-Coulomb criterion, yielding starts when the relation between a normal stress σ_n and a shear stress τ satisfies the following condition:

$$\tau = c + \sigma_n \tan\phi, \tag{2.1}$$

where c is the cohesion and ϕ the friction angle.

The criterion can be expressed in terms of principal stresses $\sigma_1 \geq \sigma_2 \geq \sigma_3$ as follows

$$f = (\sigma_1 - \sigma_3) - (\sigma_1 + \sigma_3) \sin\phi - 2c \cos\phi = 0. \tag{2.2}$$

b. Hoek-Brown failure criterion

The empirical Hoek-Brown failure criterion was originally proposed by Hoek and

Brown (1980). Over the years, this criterion has been modified by Hoek et al. (1992, 1997); Hoek and Brown (1980); Hoek et al. (2002) to improve its practicality and usefulness. The most general form, called the generalised Hoek-Brown failure criterion (Hoek et al., 2002), is written as follows

$$\sigma_1' = \sigma_3' + \sigma_{ci}\left(m_b\frac{\sigma_3'}{\sigma_{ci}} + s\right)^a, \tag{2.3}$$

where m_b is a reduced value of the material constant m_i and expressed as

$$m_b = m_i \exp\left(\frac{GSI - 100}{28 - 14D}\right). \tag{2.4}$$

s and a are constants for a rock mass and given by

$$s = \exp\left(\frac{GSI - 100}{9 - 3D}\right), \tag{2.5}$$

$$a = \frac{1}{2} + \frac{1}{6}\left(e^{-GSI/15} - e^{-20/3}\right). \tag{2.6}$$

GSI is the Geological Strength Index, D a factor accounting for the degree of disturbance of the rock mass, σ_1' and σ_3' the major and minor effective stresses and σ_{ci} the uniaxial compressive strength of the intact rock.

As the Mohr-Coulomb is a popular model in many geotechnical software packages, it is a necessity to work out a correlation between the Hoek-Brown and the Mohr-Coulomb model parameters. Hoek et al. (2002) proposed equivalent friction angle and cohesion for each rock mass under a stress range as

$$\phi' = \sin^{-1}\left[\frac{6am_b\left(s + m_b\sigma_{3n}'\right)^{a-1}}{2(1+a)(2+a) + 6am_b\left(s + m_b\sigma_{3n}'\right)^{a-1}}\right], \tag{2.7}$$

$$c' = \frac{\sigma_{ci}\left[(1+2a)s + (1-a)m_b\sigma_{3n}'\right]\left(s + m_b\sigma_{3n}'\right)^{a-1}}{(1+a)(2+a)\sqrt{1 + (6am_b)s + m_b\sigma_{3n}')^{a-1})\,/((1+a)(2+a))}}. \tag{2.8}$$

2.1.3 Rock mass classification systems

Due to rock mass complexity, rock mass classification systems flourished as powerful tool to have an overall picture of physical and mechanical properties of rock

mass. Over the years, many rock mass classification systems have been developed for the sake of characterising rock mass and establishing empirical design tools.

Based on a certain field of application, either for rock mass characterisation or for empirical method formalisation, or for both of these, various classification systems put different weights on various engineering geological parameters (Russo et al., 1998). The most commonly used classifications systems can be named as the Rock Mass Rating (RMR) system (also called Geomechanics Classification System), the Q system and the GSI system . A summary of these systems is detailed below.

The *Q* system

Barton et al. (1974) proposed a rock classification system, Tunneling Quality Index (Q), to estimate support requirements for rock tunnels. The Q index value is a function of rock mass quality and defined as

$$Q = \left(\frac{RQD}{J_n}\right)\left(\frac{J_r}{J_a}\right)\left(\frac{J_w}{SRF}\right), \tag{2.9}$$

where RQD is the Rock Quality Designation, J_n the Joint Set Number, J_r the Joint Roughness Number, J_a the Joint Alteration Number, J_w the Joint Reduction Factor and SRF the Stress Reduction Factor.

The three quotients in Eq. (2.9) respectively represent block size, inter-block frictional shear strength and active stress of a rock mass. The value of Q ranges from 0.001 to 1000 in which a small value represents a poor rock mass and inversely, a high value determines a good one. Using this range of Q, nine classes of rock mass are defined varying from 'exceptionally poor' to 'exceptionally good'.

The Q-system is widely employed as an empirical design method for rock support. Knowing the size of the opening, the *Excavation Support Ratio (ESR)* and the Q value, the amount of rock support can be estimated. Similar to the RMR system, the Q value can also be used to approximate rock mass deformation modulus (Grimstad and Barton, 1993) and the parameters m and s in the Hoek-Brown failure criterion (Hoek, 1983; Hoek and Brown, 1988) detailed in 2.1.2.

The RMR system

The *RMR* system was firstly published by Bieniawski (1973) and significantly revised in the later years (Bieniawski, 1974, 1976, 1989). The following presents the latest version of the RMR system (Bieniawski, 1989), classifying the rock mass using six parameters

1. Uniaxial compressive strength of intact rock
2. Rock Quality Designation (RQD)
3. Spacing of discontinuities
4. Conditions of discontinuities
5. Ground water conditions
6. Orientation of discontinuities

A rating value is assigned for each parameter and the RMR value is determined by adding up these individual parameters. The value of RMR is in the range of 0 to 100 and based on this, five rock mass classes are defined from a "very good rock" to a "very poor rock".

Extending the applications of the RMR system, Bieniawski (1989) proposed guidelines for rock support applied in tunnels. Also, some empirical relations between RMR value and rock mass properties have been established, such as the relationship between RMR and rock mass deformation modulus (Serafim and Pereira, 1983; Bieniawski, 1984, 1989), and RMR and m and s parameters in the Hoek-Brown failure criterion (Hoek, 1994; Hoek and Brown, 1997).

The *GSI* system

Hoek (1994); Hoek and Brown (1997) introduced a rock mass classification scheme known as *Geological Strength Index (GSI)* based on visual exposures of a rock structure. Specifically, two features of a rock mass are accounted for, which are conditions of the discontinuity surfaces and its blockiness. It is noted that the

GSI values merely represent the visual descriptions and do not explicitly include quantitative inputs as in the case of RMR and Q systems.

2.1.4 Numerical analysis methods in rock mechanics

Due to the complicated behaviour of material such as jointed rock mass, a closed-form solution is unavailable for most of the practical cases and numerical method is an effective alternative for such problems. With the development of digital computer, numerical analysis has become an effective and powerful means for predicting rock mass behaviour (stresses and strains at specific points). Particularly, it is capable of providing us with an understanding of progressive changes in rock mass due to engineering actions (excavation/reinforcement installation).

An issue arises in jointed rock modelling as whether a rock mass should be treated as continuum or not. Depending on the size of the analysed structure, simulation of rock mass behaviour can be considered as intact rock or rock mass with few discontinuities or heavily jointed rock mass. For the intact rock and heavily jointed rock cases, the medium can be modelled as continuum or equivalent continuum while in the case of rock with few discontinuities, the continuum assumption is not valid and discontinuum models need to be used (Brady and Brown, 2006). A number of numerical methods have been developed and broadly applied for continuous and discrete systems in the design of rock engineering structures and some of the commonly used ones are listed below:

- Continuum methods
  - Finite Difference Method (FDM)
  - Finite Element Method (FEM), and
  - Boundary Element Method (BEM)
- Discontinuum methods
  - Discrete Element Method (DEM)
  - Discrete Fracture Network Method (DFN)

- Hybrid continuum/discontinuum methods
  - Hybrid FEM/BEM
  - Hybrid DEM/DEM
  - Hybrid FEM/DEM, and
  - Other hybrid models

This study aims to work on optimisation algorithms which can be extended to tunnel reinforcement design. Numerical method is simply a means of conducting numerical analysis to provide input for such optimisation engines. A detailed investigation of these numerical methods is beyond the scope of this study and therefore not presented herein. Rigorous reviews of these methods in rock modelling can be found in Jing (2003); Bobet et al. (2009). Because of its capabilities and widespread usage, FEM is used in this research.

The degree of approximation of numerical modelling depends on the quality of the geometrical characterization of discontinuity systems, understanding of physical properties of the discontinuities and their interactions. Obviously, in rock mechanics, a full validation of numerical models by experiments is impossible due to incomplete knowledge of the geometry and properties of jointed rock mass. Only a partial validation can be conducted. Furthermore, uncertainty and variability of the rock properties, loadings, initial and boundary conditions are parts of rock mechanics. As a consequence, it is a crucial requirement to have a clarification of the input information and a thorough understanding of assumptions employed.

2.2 Tunnel Support and Reinforcement

2.2.1 Terminology

In the excavation process, the surrounding rock displaces and squeezes, which results in movement of a whole or some rock blocks towards the opening. Failure may happen if displacement is larger than an admissible value. Moreover, loss of shear strength at the opening may cause failure due to disruption of *in-situ*

stresses. As a result, additional reinforcement or support during and after excavation is necessary to prevent such failures and maintain stability of an excavation.

Tunnel support can be divided into two types: reinforcement (active) and support (passive) (Windsor and Thompson, 1993). The term reinforcement refers to a means of improving rock mass properties by stimulating the ground material to sustain a portion of external loads. Some examples in this group can be listed as rock bolts, cable bolts and ground anchors. On the other hand, the term support refers to employing external structures to support the rock mass. Timber, shotcrete and steel liners can be listed in this category. To the extent of this research, only mechanical behaviour of underground excavation with reinforcement is considered. From the topology optimisation point of view, external support design is similar to structural design and is well understood.

2.2.2 Ground and support interaction

As a tunnel face advances, a considerable change of stress distributions in the surrounding rock mass is observed and needs to be captured. Also, a rational support design has to account for the interaction between reinforcement or support systems and the rock mass. A significant factor controlling a design of support and reinforcement systems is the rock displacement. Particularly, enough displacement of rock mass has to be allowed to sufficiently mobilise the required support load. However, an excessive displacement, if occurred, would result in a loosening of the rock mass and a decrease in its load-carrying capacity. The reinforcement stiffness and time of installation are the dominant factors affecting the rock mass displacements.

Fig. 2.1 shows a *ground reaction curve* which illustrates a close relation between internal pressures and inward radial displacements as excavation proceeds. It can be seen that the internal pressure p_i which is initially equal to the *in situ* stress p_0 starts decreasing as excavation proceeds. The rock mass yields as the internal pressure becomes less than a critical value, p_{cr}. When $p_i \geq p_{cr}$, elastic behaviour is observed. When $p_i < p_{cr}$, plastic displacement occurs. The function of a support system is like an extra internal pressure added to p_i. As displacement

increases, the internal pressure decreases and the support stress increases. The equilibrium is obtained once the ground response curve intersects the support reaction curve. Clearly, the installation of support system is more effective if the support system takes more stress before reaching an equilibrium. But this stress needs to be less than the yield stress of reinforcing bars.

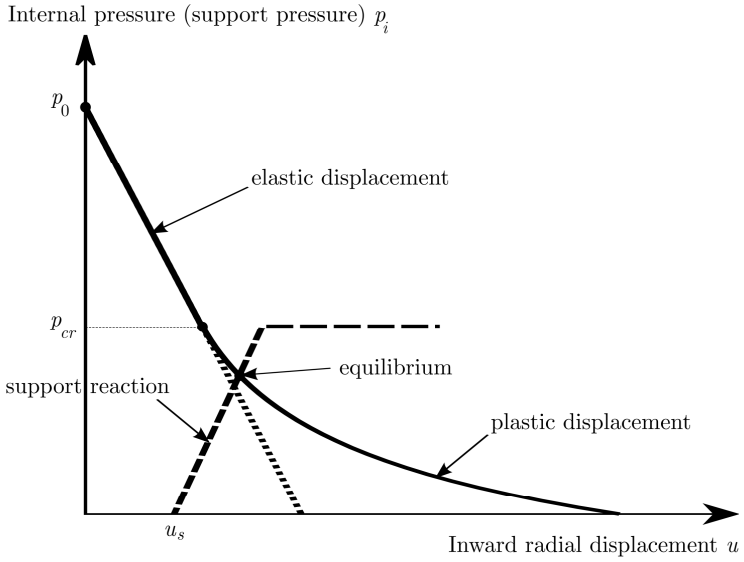

Figure 2.1: Ground reaction curve and support interaction (Ghabraie, 2009)

2.2.3 Rock bolt

Finding an optimal distribution of reinforcement around the opening is of concern in this study. Owing to the popularity and effectiveness, design of rock bolt is selected to be optimised. Rock bolt reinforcement system was developed since the 1940s and has become one of the most dominant support methods in underground structures (Kovári, 2004). It belongs to the active support category with the effective principle of employing the ground itself to stabilise the rock mass system. Also, rock bolt is believed to be more economic than other methods in terms of both material and manpower consumptions. More importantly, bolt can be used together with other various support methods like concrete lining, shotcrete and also is applicable to various geological conditions. Practical descriptions of how rock bolts work, are installed and the design-related criteria can be found in a standard book on the topics of rock engineering design or tunnelling design such

as Hoek et al. (1997) or Brady and Brown (2006).

The ultimate goal of a bolt design is achieved by proposing bolt parameters including density, orientation, length, size and pretension. However, due to the complexity and varieties of geological conditions, rock bolt pattern design has been more of an art rather than a science. In conventional design, rock bolt is assumed to be distributed evenly around the opening with a certain length and spacing depending on specific class of rock mass and structure size (Grimstad and Barton, 1993; Bieniawski, 1993). Many other crucial factors in rock engineering design such as fracture presence, *in situ* stress state or tunnel features have not been fully accounted for. Additionally, it cannot be guaranteed that the conventional design is an optimal one with respect to different objective functions. Solving the rock bolt design problem as an optimisation problem can provide us with more reasonable designs and also improve our understanding in this area.

2.2.4 Modelling of rock bolts

The effect of rock bolts can be simulated by two approaches.

One is the homogenisation approach in which the reinforcement effect is considered by using a stiffer and stronger material for the reinforced areas. The method then consists of simulating the reinforced rock mass as a homogeneous material with anisotropic strength and stiffness properties (Bernaud et al., 1995; Wong and Larue, 1998). An advantage of this technique is the reduced effort and computational time in the modelling process. However, it should be noted that the homogenisation approach assumes a perfect bonding between the surrounding rock and the bolts which might overestimate the effect of reinforcement (de Buhan et al., 2008). Also, using such modelling technique does not give us a clear bolt pattern and might require post-processing of the final results.

Another method is a direct numerical simulation which treats the bolts as individual elements embedded in the rock mass. Such approach can give us a higher level of accuracy but also requires more computation time and more powerful computational tools.

2.3 Rock engineering design tools

This section will detail the approaches used in a rock engineering design, including methods for rock bolt design. Generally, the following input needs to be provided for a rock engineering design

- Geological and geotechnical features including properties of intact rock and discontinuities
- Conditions of the in-situ and induced stresses
- Specific design requirements such as acceptable deformation, lifetime of the structure, etc.

2.3.1 Procedures of rock engineering design

From an engineering point of view, Schubert et al. (2001) summarised the general procedures of an underground excavation design from pre-construction stage to tunnel construction into three steps.

1. Step 1: Rock mass characterisation

   For characterising rock mass, rock mass type needs to be defined. Using data from lithology, field observations and laboratory tests, key parameters describing rock types are determined

2. Step 2: Determination of rock mass behaviour types.

   This step is to determine behaviour of rock mass by combining rock mass type with other system factors such as discontinuities feature, effects of ground water, shape and size of the opening. Potential failure modes such as sliding, shear failures are identified and the displacements are estimated. Analytical and numerical methods are also employed in this step to verify the predicted behaviour. From the obtained rock mass behaviour approximations, concepts of a support system is proposed to be analysed in the subsequent steps.

3. Step 3: Analysis of system behaviour

Monitoring and observation are conducted during the construction stage to capture the system behaviour. The system behaviour is analysed considering the rock mass and support interaction and the obtained system behaviour is then verified with the specific design requirements. Some examples of such requirements can be named as allowable surface settlement for shallow tunnels or the allowable load in the lining for deep tunnels.

Generally, at various construction phases, various tools are utilised. The following sections will summarise these tools and also specify benefits and drawbacks of each of them.

2.3.2 Empirical systems

As mentioned in section 2.1.3, apart from the aim of providing an experience-based tool to characterise the properties of rock mass, the rock mass classification systems have been also developed for use in reinforcement design. Some of the common empirical support design methods are tabulated in Table 2.1.

Among these, the two most commonly employed empirical systems in underground design are the RMR and the Q systems with simple and practical applications (Riedmüller and Schubert, 1999)

Table 2.1: Some empirical methods for the underground support design (revised from Palmstrom and Stille (2007))

Name	Applications	Reference
The Terzaghi rock load classification system	For steel support design in tunnels	Terzaghi (1946)
The New Austrian Tunnelling Method (NATM)	For excavation and design in incompetent ground	Rabcewicz (1964, 1965)
The Rock Structure Rating (RSR) classification	For steel support design in tunnels	Wickham et al. (1972)
The Rock Mass Rating (RMR) classification	Design of tunnel, mine and foundation	Bieniawski (1973)
The Q Classification System	For support design in underground excavations	Barton et al. (1974)
The RMi Rock Support Method	For support design in underground excavations	Palmstrom (1995, 2000)

The Q system

Inputs of the Q system include the calculated Q value from Eq. (2.9), size of an opening and an Excavation Support Ratio (ESR). The amount of rock support can be estimated using a chart proposed by Barton et al. (1974) and later revised by Grimstad and Barton (1993). Palmstrom and Broch (2006) presented some critical comments on the use and limitations of the system, and pointed out an area in the chart that the Q system works best. Also, some of the other shortcomings of the Q system were mentioned below.

- The stress reduction factor (SRF) is not clear for rock burst, squeezing rock or weakness zones.
- Characterisation of the degree of jointing by RQD reveals some limitations.
- The effects of water on rock support requirements is not clear.

The RMR system

The RMR system as presented in section 2.1.3 provides some guidelines on support design against block fall instability (Bieniawski, 1993). However, these recommendations are proposed only for a 10 m horseshoe shaped tunnel with vertical stress of under 25 MPa. This approach also shares the last two shortcomings of the Q system listed above.

Due to the complexity of rock mass conditions as well as the ease of use of the empirical systems, these approaches are widely employed in underground reinforcement design. However, these methods contains a couple of disadvantages. A common feature of empirical design systems is that they are defined using the accumulative knowledge of previous projects. A direct application of these approaches into practical designs therefore imposes some inherent shortcomings. Firstly, behaviour of an underground excavation is fundamentally unique for a particular ground condition while the empirical systems characterise or identify

rock support for a certain type of rock mass. Hence, the actual ground reactions may not be reasonably captured, leading to inappropriate predictions of the system behaviour especially for heterogeneous and poor rock mass (Riedmüller and Schubert, 1999). Another critical drawback of the empirical systems is the incapability of separate definitions of the common requirements in modern design codes like structural resistance, serviceability and durability. It is noted that the currently available empirical systems merely consider the matter of structural resistance which covers only one requirement in a typical design while other project requirements cannot be addressed. It is also obvious that the empirical systems are unable to define the degree of safety of a certain design.

2.3.3 Analytical calculations

The analytical approach is an advantageous tool to provide explicit solutions of system behaviour with particular material models of rock mass and support elements. Also, these approaches enable us to study the interaction between rock and structure or investigate structural resistance related issues such as block stability. However, given the scope of being only capable of applying in simplified cases such as a circular tunnel with isotropic stress field, the application range of this method is really limited.

2.3.4 Numerical simulations

Behaviour of rock mass and rock support can be modelled in the form of complex differential equations and the aim of any numerical modelling is to work out numerical solutions to these differential equations. Numerical methods are powerful tools to deal with a broad range of problems in rock mechanics including impacts of construction sequences, existence of nearby structures or rock-support interaction (de Farias et al., 2004). Various geological conditions and tunnel features can also be handled by suitable numerical methods. However, the most significant issue arising in numerical simulations is the reliability of the input data, especially the following information (Palmstrom and Stille, 2007).

- characters of *in situ* stress
- models of rock mass and their input parameters
- extent and location of various geological conditions

Like the empirical systems and analytical calculations, the numerical approaches are unable to account for non-calculable load cases such as frost, weathering as they have been primarily developed to capture structural resistance.

2.3.5 Observational methods

The complexity of rock mass characters and current limitations of rock engineering design present some challenges in determining the responses of ground material around the opening. As a result, accurate predictions of stress and strain are not always possible. Observation of the system behaviour during construction is required to verify the estimated analysis. However, it should be noted that using the observational approach might lead to time delays or claims for unspecified and unpredictable scenarios. A strict observation program with listed requirements needs to be prepared prior to construction stage to avoid these cases.

2.3.6 Summary

The primary priority in any rock engineering design is a thorough understanding of geological and ground conditions. An appropriate tool can then be applied to propose a design satisfying the given requirements. Among various design tools, observational approach is a mandatory supplement to others to capture any unexpected scenarios. Certainly, engineering judgement is absolutely significant to evaluate the method employed and work with unforeseeable situations in construction.

2.4 Simulation of excavation sequence and reinforcement installation

2.4.1 2D/3D modelling

Underground excavation is practically a three dimensional (3D) construction process. Along with the development of numerical techniques and powerful computers, a 3D analysis is possible (Grasselli, 2005; Liu et al., 2008a). Obviously, a 3D modelling is more appropriate to capture actual geological conditions, construction sequences or exact locations of support systems. However, it requires highly powerful computer resource and also consumes a lot of time. These barriers have therefore limited its usage. On the other hand, a two dimensional (2D) analysis with appropriate assumptions, in some cases, provides an acceptable approximation. Therefore, 2D analysis is still a convenient and common approach.

When performing an optimisation problem, in which a number of analyses are required, the excessive computational time required for a 3D analysis is a major drawback. In this study, all examples will be performed in 2D analysis using plane strain assumption. It should be noted that generally the proposed optimisation approach can be applicable to 3D analysis without any modifications. To capture 3D effects in a 2D analysis, assumption will made by prescribing rather than predicting the volume loss and appropriate modelling techniques need to be followed as will be mentioned in the next section.

2.4.2 Simulating tunnel excavation

When a two dimensional simulation is chosen, an assumption needs to be made to account for the volume loss and deformation of the excavation boundary before reinforcement activation. Several methods to consider these 3D effects can be named as the gap method (Rowe et al., 1983; Lee and Rowe, 1991), the progressive softening method (Swoboda, 1979; Swoboda et al., 1994), the volume loss control method (Potts and Zdravković, 2001) and the convergence-confinement method (Panet and Guenot, 1982). In this study, the convergence-confinement method

is employed. Using this method, a proportion of unloading is prescribed before reinforcement introduction to predict the volume loss value. By applying an internal force vector, $\beta \mathbf{n} \cdot \boldsymbol{\sigma_0}$ (where $\boldsymbol{\sigma_0}$ is the initial stress, $\mathbf{n}$ the inward unit vector normal to the opening surface) at the nodes on the opening, a definition of the relationship between internal pressure - radial displacement can be established. Initially, β is equal to 1 to represent the initial stress condition and then gradually decreased to 0 to represent the excavation process. At a prescribed value of β_t that the reinforcement is activated, the stress reduction is determined as $(1 - \beta_t)\boldsymbol{\sigma_0}$. Details of this modelling procedure are presented in §4.2.

2.5 General form of optimisation problems

A general optimisation problem consists of objective function (f) and constraints (g and h) and can be stated in the following form

$$\begin{aligned} &\min_{x_1, x_2, \ldots, x_n} f(\mathbf{x}) \\ &\text{such that } h_j(\mathbf{x}) = 0,\ j = 1, 2, \ldots, n_h; \\ &\qquad g_k(\mathbf{x}) \leq 0,\ k = 1, 2, \ldots, n_g \end{aligned} \tag{2.10}$$

where $\mathbf{x} = (x_1, x_2, \ldots, x_n)$ are the design variables, and n_h and n_g are the number of equality and inequality constraints, respectively.

Mathematical programming methods which directly optimise the objective function are commonly used to deal with general optimisation problems. However, in topology optimisation problems, this approach is usually costly and time consuming due to a huge number of design variables which are proportional to the number of elements in the design domain. Moreover, in structural optimisation problems, a huge amount of numerical calculation is needed for determination of objective functions, constraints conditions and their derivatives (Haftka and Gurdal, 1992; Kirsch, 1993). Therefore, using mathematical programming method is practically ineffective. On the other hand, if the objective function and/or constraints are not expressed as explicit functions of the design variables, classical analytical approaches are incapable of dealing with it. "Optimality criteria" approach is a

good alternative to overcome these difficulties.

The optimality criteria method usually relies on Karush-Kuhn-Tucker (KKT) optimality conditions (Karush, 1939; Kuhn and Tucker, 1951) to test whether a candidate point is a minimum or not instead of solving a set of nonlinear equations. If $\mathbf{x}$ is a local minimum for the problem Eq. (2.10), there exist constants λ_j and ν_k such that:

$$\begin{cases} \frac{\partial f}{\partial x_i} + \sum_{j=1}^{n_h} \lambda_j \frac{\partial h_j}{\partial x_i} + \sum_{k=1}^{n_g} \nu_k \frac{\partial g_k}{\partial x_i} = 0 \quad i = 1, \ldots, n, \\ h_j = 0, \quad j = 1, \ldots, n_h, \\ g_k \leq 0, \quad k = 1, \ldots, n_g, \\ g_k \nu_k = 0, \quad k = 1, \ldots, n_g, \\ \nu_k \geq 0, \quad k = 1, \ldots, n_g \end{cases} \tag{2.11}$$

where λ_j and ν_k are Lagrangian multipliers.

In order to apply the KKT conditions, sensitivity analysis of the objective function is required. In the following section, commonly used topology optimisation methods which solve optimisation problems indirectly based on the optimality criteria approach are introduced.

2.6 Methods of topology optimisation

In an underground excavation design, the optimal shape of the opening and the optimal pattern of the reinforcement material are two design objectives which can be solved (and have been solved in some previous studies) by topology optimisation. The opening shape is usually determined by functional requirements and methods of construction (Hoek and Brown, 1980), and it is beyond the scope of this work. This study only focuses on developing optimisation methods to seek out an optimal reinforcement design.

Topology optimisation includes a determination of the best locations and geometries of holes in a continuum domain or the optimal spatial order and its connectivity in a discrete structure. Using topology optimisation techniques, tunnel

reinforcement design can be transformed into a material distribution optimisation problem.

2.6.1 Overview

In a milestone paper, Bendsøe and Kikuchi (1988) introduced the first practical general-purpose structural topology optimisation method. Commonly referred to as the "homogenisation method", this method set up the basis for many further studies in the field. The main concept of this method is to simulate the design domain by complex material with periodic microstructures.

Among other notable topology optimisation methods, one can name the Solid Isotropic Material with Penalisation (SIMP) method and Bi-directional Evolutionary Structural Optimisation (BESO) method (Ghabraie, 2009). The SIMP method was introduced by Bendsøe (1989). In this method, a power-law relationship between the elasticity tensor and the density of the material is assumed and based on sensitivity analysis of a chosen objective function, material density in each element of the design domain is updated iteratively. The BESO method was initially introduced by Querin (1997), Querin et al. (1998) and Yang et al. (1999). This method approaches the optimal material distribution by iteratively removing the least efficient elements and adding more elements around the most efficient parts of the design domain.

Each of the above-mentioned topology optimisation methods has its own advantages and disadvantages. Selecting an appropriate one for a certain problem depends on a number of factors. In the light of their potential applications in an underground excavation design which composes complex geomechanics behaviour and complicated loading sequences, particular benefits and shortcomings of these methods should be well recognised.

For the homogenisation method, a huge number of design variables are required, while the final solutions are complicated and not easily implemented in construction. Another serious shortcoming is that it is hard to combine the homogenisation algorithm with commercial finite element packages using which is

a significant requirement to propose a practical tool for engineering design of underground structures.

On the other hand, the SIMP and the BESO methods have been proved to be applicable to a wide range of practical applications (Rozvany, 2009; Huang and Xie, 2010a). Being computationally efficient is an advantage of both methods. Especially, an outstanding benefit of these methods is that they are flexible and therefore it is easy to link them to an external finite element package. Although these methods are prone to some numerical instabilities as other topology optimisation methods, these issues can be usually solved by some relatively simple approaches.

Generally, working with an underground excavation design, the SIMP and the BESO methods are powerful in terms of computational linkage and convenience. In this thesis, optimisation methods based on the concepts of these two methods are going to be extended and applied to tunnel reinforcement design.

2.7 The SIMP method

2.7.1 Overview

Bendsøe (1989) introduced the SIMP method. In this method, material constitutive tensor at each element is defined as a function of material density varying from very small value (representing voids or weak elements) to 1 (representing solids or strong elements). It is noted that the optimal outcomes using this scheme consist of mostly "grey" elements, which represent intermediate density values. In order to achieve a nearly "black-white" solution, grey elements with intermediate densities need to be penalised. The simple power-law interpolation function proposed by Bendsøe (1989) is one of the most common penalisation rules which takes the form

$$E(\rho) = [\rho(x)^p]\bar{E} \tag{2.12}$$

where E is the interpolated stiffness tensor; $\bar{E}$ the elasticity constants of the base material, $\rho(x)$ the relative density function at the location represented by x and

$0 \leq \rho(x) \leq 1$, and p the penalty factor and $p \geq 1$. The penalty factor p is to penalise the intermediate density value and consequently push the elements to the two extremes of solid or void.

The interpolation scheme in Eq. (2.12) can be applied to a material-void problem in which the considered element could be either solid or void or intermediate. In a two-material problem, the considered element would be selected as either one of two given materials or intermediate, and the interpolation scheme can be stated as

$$E(x) = E^{(1)} + \rho(x)^p (E^{(2)} - E^{(1)}) \tag{2.13}$$

where $E^{(1)}$ and $E^{(2)}$ are the elasticity constants of materials (1) and (2), respectively. Other penalisation rules for suppressing the intermediate elements can also be found in Stolpe and Svanberg (2001a); Fuchs et al. (2005); Sigmund (2007); Ghabraie (2009).

Since its introduction, there have been a number of publications developing and applying the SIMP method. A detailed review of these works can be found in Rozvany (2001). Especially with the publications of an educational article on a 99-line topology optimisation code (Sigmund, 2001) (with an improved version provided by Andreassen et al. (2011)) and a web-based topology optimisation program (Tcherniak and Sigmund, 2001), the SIMP method has been broadly known in the optimisation area. Applications of the SIMP method have been extended to a wide range of problems including compliant mechanism (Sigmund, 1997), geometrically nonlinear structures (Sigmund, 1997), phonotic crystal structures (Jensen and Sigmund, 2004), reliability-based problems (Kharmanda et al., 2004), and design-dependent load (Du and Olhoff, 2004a,b).

2.7.2 Details of the method

Selecting mean compliance as the objective function, which is very common in structural optimisation, the optimisation problem using the SIMP method can

be expressed as

$$\begin{aligned} \min_{\rho_1,\rho_2,\ldots,\rho_n} \quad & W(\boldsymbol{\rho}) = \mathbf{f}\cdot\mathbf{u} \\ \text{such that} \quad & \mathbf{K}(\boldsymbol{\rho})\mathbf{u} = \mathbf{f}, \\ & 0 \le \rho_i \le 1, \qquad i = 1,\ldots,N \\ & \sum_{i=1}^{N}(\rho_i V_i) - \bar{V} \le 0 \end{aligned} \tag{2.14}$$

where $\mathbf{f}$ is the vector of nodal forces, $\mathbf{u}$ the displacement vector, $\mathbf{K}$ the global stiffness matrix of the structure, $\boldsymbol{\rho} = [\rho_1, \rho_2, \ldots, \rho_n]$ the relative density vector which is the design variable, N the number of elements, V_i the volume of the i-th element and $\bar{V}$ the maximum alowable material volume.

The Lagrangian functional for the optimisation problem takes the following form

$$\mathscr{L} = W + \sum_{i=1}^{N}\left(\overline{\lambda}_i(\rho_i - 1) - \underline{\lambda}_i\rho_i\right) + \Lambda\left(\sum_{i=1}^{N}(\rho_i V_i) - \bar{V}\right) \tag{2.15}$$

where $\overline{\lambda}_i$, $\underline{\lambda}_i$ and Λ are non-negative Lagrange multipliers. Stationariness of $\mathscr{L}$ with respect to ρ_i implies that

$$\frac{\partial W}{\partial \rho_i} + \overline{\lambda}_i - \underline{\lambda}_i + V_i\Lambda = 0, \quad i = 1,\ldots,N \tag{2.16}$$

If we define

$$B_i = \frac{-\frac{\partial W}{\partial \rho_i}}{V_i\Lambda}, \quad i = 1,\ldots,N \tag{2.17}$$

the update scheme for ρ can be expressed as follows (Bendsøe, 1995)

$$\rho_i^{[k+1]} = \begin{cases} \max\{(1-\zeta)\rho_i^{[k]}, 0\}, & \text{if } \rho_i^{[k]}(B_i^{[k]})^\eta \le \max\{(1-\zeta)\rho_i^{[k]}, 0\} \\ \min\{(1+\zeta)\rho_i^{[k]}, 1\}, & \text{if } \rho_i^{[k]}(B_i^{[k]})^\eta \ge \min\{(1+\zeta)\rho_i^{[k]}, 1\} \\ \rho_i^{[k]}(B_i^{[k]})^\eta, & \text{otherwise} \end{cases} \tag{2.18}$$

Here the superscript $[k]$ indicates that the values are from the k-th iteration. ζ is the move limit and η is a tuning parameter.

To calculate the values of B, we need to know the Lagrange multiplier for the volume constraint (Λ). The value of Λ in Eq. (2.17) is found using an inner loop

such that the volume constraint is satisfied.

A general algorithm of the SIMP method is summarised in Fig. 2.2

1. Discretise the design domain
2. Select initial values of densities
3. **repeat**
4. Perform finite element analysis
5. **repeat**
6. Update design variables (Eq. (2.18))
7. Update Lagrangian multiplier Λ
8. **until** volume constraint is satisfied
9. **until** convergence criteria are met
10. **print** results
11. **end**

Figure 2.2: An algorithm of the SIMP method

2.7.3 Numerical instabilities and solutions

Numerical instabilities are common and sometimes a serious problem in most topology optimisation methods (Sigmund and Petersson, 1998). This causes some critical obstacles in obtaining the optimal results or interpreting the final outcomes. Three numerical instabilities in topology optimisation can be mentioned as checkerboard, mesh-dependency and local minima.

Checkerboard problem corresponds to the formation of regions with alternating void and solid elements resulting in difficulties in interpreting the final optimum and also manufacturing process (Diaz and Sigmund, 1995). An example of the checkerboard problem can be observed in Fig. 2.3. It has been believed earlier that these regions represent some sort of optimal microstructures; however, by theoretical approach, Jog and Harber (1996) demonstrated the numerical causes of checkerboard formation rather than physical one.

Mesh dependency issue is due to nonexistence or nonuniqueness of final solutions under different discretisations or mesh-sizes.

Firstly proposed by Sigmund (1994), the filtering technique has been widely used to overcome both mesh dependency and checkerboard problems encountered in

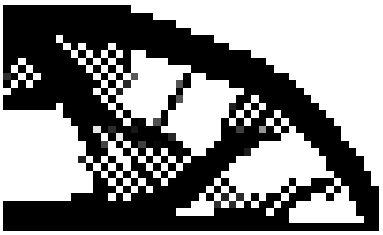

Figure 2.3: Checker board problem

the SIMP method. The filtered sensitivities are expressed as

$$\frac{\widehat{\partial W}}{\partial \rho_i} = \frac{\sum_{j=1}^{N} \rho_j \frac{\partial W}{\partial \rho_j} \omega_{ij}}{\rho_j \sum_{j=1}^{N} \omega_{ij}} \tag{2.19}$$

where ω_{ij} is the weighting factor defined as

$$\omega(r_{ij}) = \max\{r_f - r_{ij}, 0\} \tag{2.20}$$

where r_f is a predefined filtering radius, and r_{ij} the distance between the centres of elements i and j. By choosing r_f less than the size of elemens, the filtering scheme is inactive and the filtered sensitivities are the original sensitivities.

Another technique to cope with this numerical problem is setting gradient constraints (Petersson and Sigmund, 1998). Also, Matsui and Terada (2004) presented a method of continuous approximation of material distribution for topology optimisation to obtain a checkerboard-free optimum results without using any additional constraint parameters. There are also other techniques proposed in the literature to overcome these numerical instabilities but studying them is beyond the scope of this project.

Local minima relates to not obtaining the same final solution under the same discretisation with different algorithm parameters or initial guess designs. The presented SIMP method is a gradient-based approach, and therefore is not guaranteed to yield the global optimum. A popular approach which sometimes can overcome this issue is to employ a continuation technique (Sigmund and Petersson, 1998). For example, Harber et al. (1996) started the algorithm with low penalties then gradually increased them to the desired value. Also, Sigmund (1997) utilised a large value of filtering radius initially then gradually lowered

it. Although sometimes local minima can be solved with continuation technique, much more time and efforts are demanded by this technique.

2.7.4 Example

To demonstrate the application of the SIMP method, a simply supported beam sketched in Fig. 2.4 is optimised topologically. The magnitude of the load is $P = 1$. The width and the length of the beam are $l = 10$ and $w = 3$ respectively. The material has the Young modulus of $E = 1$ and Poisson's ratio of $\nu = 0.3$. The design domain is discretised into 100×30 square shaped elements. A penalty factor (p) of 3 is applied. The move limit and the tuning parameter are selected as $\zeta = 0.2$ and $\eta = 0.5$, respectively. The filtering scheme (Sigmund, 1994) with a filtering radius of 1.5 times the element size is applied to tackle checkerboard problem and mesh dependency. Using the 99 line code proposed by Sigmund (2001), the obtained evolution of topologies and objective function variations are shown in Fig. 2.5.

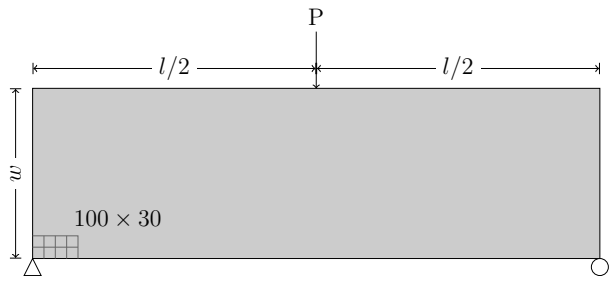

Figure 2.4: Design domain of a simply supported beam

In Fig. 2.5, the darkness in grey-scale is used to represent the densities of elements. It can be seen that although penalisation is applied, the final topology still contains some intermediate elements, resulting in a blurred image. In relation to the objective function variation, the initial mean compliance corresponding to a uniform material distribution is 245 J. An optimised value of 50.6 J is then obtained after optimisation.

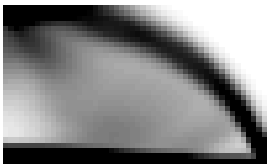

(a) $K = 5$

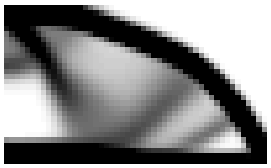

(b) $K = 10$

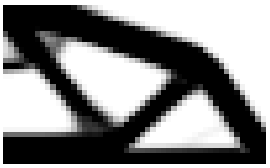

(c) $K = 20$

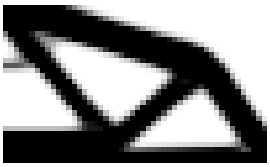

(d) $K = 30$

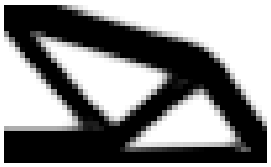

(e) $K = 50$

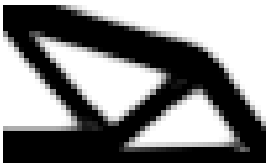

(f) $K = 64$ (final topology)

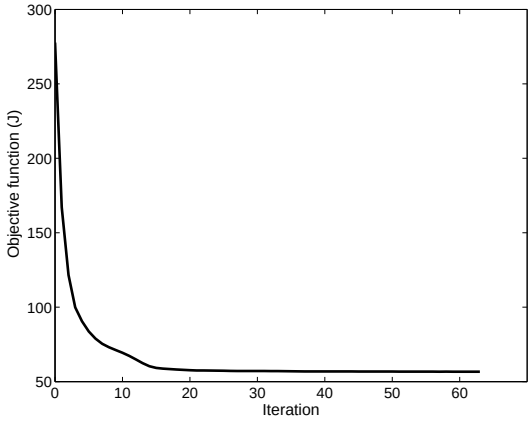

(g) Objective function evolution

Figure 2.5: Topologies obtained by the SIMP method for a simply supported beam (K is the iteration number). Owing to symmetry, only half of the beam is shown.

2.8 The BESO method

2.8.1 Overview

The BESO method was initially introduced as an extension of the Evolutionary Structural Optimisation (ESO) method. Proposed by Xie and Steven (1992), the concept of the ESO method is fairly simple: by gradually removing inefficient elements from the structure, it can move towards its optimal shape and topology. A rejection criterion is set to manage the removal process with an introduction of a threshold value. Mechanical responses of elements are represented by a scalar function, and the elements with values smaller than the threshold value will be removed.

From engineering point of view, the ESO method seems to be an attractive approach because it is simple and can be easily implemented with the aid of a FEA package with a small amount of time. However, a removed element cannot be reintroduced, which can cause non-optimal solution. Also, if a large value of element removal ratio or inappropriate constraint is utilised, a much worse solution than the optimal would probably be obtained. Recent detailed discussion on the ESO method and its shortcomings can be found in a paper by Ghabraie (2015a).

To remedy the deficiencies of the ESO method, beside removal of inefficient elements, addition of efficient elements are considered in the BESO method (Querin, 1997; Querin et al., 1998; Yang et al., 1999; Rispler et al., 2000). In the BESO method, a ground structure covering the whole design domain including both solid elements and void elements is considered. Different from the SIMP method, the BESO method uses binary design variables by assigning the value of either 1 or 0 to a solid or void element respectively. For example, the compliance minimisation

problem using the BESO method can be expressed as

$$\begin{aligned} \min_{x_1,x_2,\ldots,x_N} \quad & W(\mathbf{x}) = \mathbf{f} \cdot \mathbf{u} \\ \text{such that} \quad & \mathbf{K}(\mathbf{x})\mathbf{u} = \mathbf{f}, \\ & x_i \in \{0,1\}, \qquad i = 1,\ldots,N \\ & \sum_{i=1}^{N} x_i V_i \leq \bar{V} \end{aligned} \tag{2.21}$$

As the void elements are not present in the mechanical analysis, their sensitivity numbers cannot be directly calculated. Instead, information from the neighbouring elements can be used to estimate their sensitivity numbers. For instance, Querin (1997) assumed that void elements having a common node with the most efficient elements take those elements' sensitivity numbers and are to be added. In another work, Li et al. (1999) and Yang et al. (1999) presented an approximation technique to extrapolate the nodal displacements of the surrounding solid elements to the nodal displacements of the void elements. Then the sensitivity numbers of the voids can be calculated. In a newer version of the BESO method, Huang and Xie (2007) applied a linear filtering technique to approximate the sensitivity numbers of the voids as

$$\hat{\alpha}_i = \frac{\sum_{j=1}^{N} w_{ij}\bar{\alpha}_j}{\sum_{j=1}^{N} w_{ij}} \tag{2.22}$$

where N is the total number of nodes in the sub-domain Ω_i of the i-th element. The sub-domain Ω_i for element i is defined by drawing a circle centred at its centroid with a radius of length scale r_{min}. $w(r_{ij})$ is the weight factor determined by

$$w(r_{ij}) = \max\{0, r_{min} - r_{ij}\} \tag{2.23}$$

where r_{ij} is the distance between centroids of element i and element j. It was suggested that r_{min} should be larger than half of the element size and a value of 1-3 times the element size was recommended.

Since its introduction, the BESO method has attracted a large number of publications in both theoretical and practical aspects. History of the method devel-

opment, improvement and its applications are consolidated in a book by Huang and Xie (2010a) and review papers by Rozvany (2009); Huang and Xie (2010b).

2.8.2 Details of the method

In the original version of the BESO method, the stress-based objective function was developed with a Von Mises-based stress criterion by Querin (1997); Querin et al. (1998, 2000). The algorithm selected under-stressed elements to be removed and void elements near the over-stressed elements to be changed to solid elements. Numbers of elements in removal and addition process for each iteration were controlled by two separate parameters: rejection ratio (RR) and inclusion ratio (IR), respectively. Due to the irrelevance of RR and IR, their values need to be carefully chosen to achieve corresponding optimal design. It can be seen that separation of removing and adding process based on ranked elements is somewhat illogical and cumbersome. Some other issues also exist in initial versions of the BESO method such as mesh-dependency, checkerboard pattern, and convergence problem.

In newer versions, Huang et al. (2006); Huang and Xie (2007) improve these shortcomings by proposing a single parameter called as *Evolutionary Volume Ratio (EVR)* to control the process of adding and removing elements. This parameter controls the volume of the structure in each iteration using the following relation

$$V^{k+1} = V^k(1 \pm EVR) \tag{2.24}$$

where V^k is the volume at the iteration k. Once the objective volume ($\bar{V}$) is reached, the volume will remain constant ($V^{k+1} = \bar{V}$).

The switching process is controlled based on the rank of the sensitivity numbers. Solid elements with lower values are to be removed and void elements with higher values are to be added. The void elements' sensitivity numbers are determined using the filtering scheme in Eq. (2.22). It is noted that this filtering scheme is also effective to cope with numerical instabilities as discussed in the next section.

The addition and removal of elements are controlled by the following steps

1. Sort sensitivity numbers in an ascending order
2. Assign the sensitivity number α_{th} corresponding to the target volume V^{k+1}
3. Calculate Admission Ratio $AR = \frac{V^{add}}{V}$, where V^{add} is the volume of void elements whose sensitivity numbers are greater than α_{th} and V the volume of solid and void elements.
4. Compare AR and AR_{max} in which AR_{max} is a prescribed maximum admission ratio. If $AR \leq AR_{max}$, skip to step 7. Otherwise, continue to step 5.
5. Sort the sensitivity numbers of void elements in descending order. Assign α_{th}^{add} equal to the sensitivity number of the void element corresponding to the new volume of adding elements V^{add} which is calculated as $V^{add} = AR_{max} \times V$.
6. Assign α_{th}^{del} equal to the sensitivity number of the solid element corresponding to the volume of removing elements V^{del} with $V^{del} = V^{add} + V^{k+1} - V^{k}$.
7. Void elements will be added (switched to 1) if $\alpha_i \geq \alpha_{th}^{add}$ and solid elements will be removed (switched to 0) if $\alpha_i \leq \alpha_{th}^{del}$.

A general algorithm of the BESO method is summarised in Fig. 2.6

1. Discretise the design domain
2. Select initial values of EVR and AR_{max}, set value of $\bar{V}$
3. **repeat**
4. Conduct finite element analysis and calculate sensitivity numbers
5. Filter sensitivity numbers (Eq. (2.22))
6. Add and remove elements
7. **until** Convergence criteria
8. **print** results
9. **end**

Figure 2.6: An algorithm for the BESO method

The BESO methods can be divided into two categories: hard-kill and soft-kill techniques. In the hard-kill BESO approach, inefficient elements are completely removed from the design domain. Permanently removing an element may cause nonoptimal final solution as there could be possibly considerable change in stress

patterns between various stages of iteration. The soft-kill alternative was introduced to overcome the issue by replacing the removed elements by soft elements with significantly small elastic modulus. Hinton and Sienz (1995) replaced the removed elements by elements with the elastic modulus scaled to a factor of 10^{-6}. Rozvany and Querin (2002) considered the void elements as soft elements with significantly small density in their proposed Sequential Element Rejection and Addmission (SERA). Zhu et al. (2007) introduced a similar method to BESO in which an orthotropic cellular microstructure (OCM) element is utilised to replace the deleted element. Huang and Xie (2009) further improved the BESO method by using material interpolation scheme with penalisation used in the SIMP method. It is noted that the hard-kill BESO method can be seen as a special case of the soft-kill when stiffness of the soft material approaches zero.

The hard-kill approach is naturally suitable for single material problems. On the other hand, applications of the soft-kill approach is more broader and can be extended to multi-material problems. The optimisation problem of finding an optimised reinforcement distribution can be seen as a problem of searching for an optimised distribution of multi-materials, i.e. host ground and reinforcement materials. In this research, the soft-kill BESO method is therefore employed.

2.8.3 Numerical instabilities and solutions

Similar to the SIMP method, the BESO method also encounters numerical instabilities including checkerboard problems, mesh dependency and local minima. The following presents solutions applied to these problems for the BESO method.

Checkerboard problem:
Li et al. (2001) applied a filtering technique for the ESO method by simply averaging the sensitivity numbers of surrounding elements to suppress the formation of checkerboard patterns. However, this smoothing scheme does not overcome the mesh-dependency issue. In the improved BESO version proposed by Huang and Xie (2007), the proposed filtering technique is capable of effectively dealing with both mesh dependency and checkerboard issues. The sensitivity number of void elements which are initially assumed to be zero are modified by the fil-

tering scheme. Elemental sensitivity numbers are converted to nodal sensitivity numbers by averaging elemental sensitivity numbers connected to each node as

$$\bar{\alpha}_j^n = \frac{\sum_{i=1}^{M} V_i \alpha_i^e}{\sum_{i=1}^{M} V_i} \tag{2.25}$$

where $\bar{\alpha}_j^n$ is nodal sensitivity number of node j, M the total number of elements, V_i the volume of the element i with elemental sensitivity number α_i^e. The nodal sensitivity numbers are then converted to elemental sensitivity numbers and only nodes inside a defined sub-domain are considered in the calculated elemental sensitivity numbers as defined in Eq. (2.22). Also, historical information of the elemental sensitivity number is taken into account to stabilize the optimisation process. To do so the sensitivity numbers of the current iteration are assigned as follows

$$\hat{\alpha}_i = \frac{\hat{\alpha}_i^k + \hat{\alpha}_i^{k-1}}{2} \tag{2.26}$$

where k is the current iteration number.

The above filtering scheme is effective with single material distribution but ineffective with multi-material problems (soft-kill BESO) (Ghabraie, 2015b). To tackle this deficiency, Huang and Xie (2009) applied a material interpolation scheme with penalisation employed in the SIMP method in BESO. Alternatively, Ghabraie (2015b) proposed another filtering scheme by replacing Eq. (2.25) by the following equation

$$\tilde{\alpha}_j^n = \frac{\sum_{i=1}^{M} V_i E_i \alpha_i^e}{\sum_{i=1}^{M} V_i E_i} \tag{2.27}$$

It is noted that although no theoretical justification has been offered, the filtering technique is simple to implement without introducing any extra constraints and produces acceptable results.

Mesh dependency:

The perimeter control method (Harber et al., 1996; Jog, 2002) is a solution to tackle mesh dependency problem. It is known that among two topologies, one with fewer holes also contains a smaller perimeter. By introducing a constraint on the perimeter, the method would be able to control the obtained topologies and the mesh dependency issue can be prevented (Yang et al., 2003). However,

physical significance of perimeter control is somewhat meaningless, and selecting an appropriate value for a topology optimisation design is a difficult task.

Apart from the perimeter constraint approaches, the aforementioned filtering technique is also effective to overcome mesh dependency problem.

Local minima:
Applying the concept of the continuation approach utilised in the SIMP method, Ghabraie (2015b) proposed a *gradual BESO* (*g*BESO) method to tackle the local minima problem in the soft-kill BESO method. In the first step, elastic moduli of all materials are selected very close to the softest material. These values of stiffer materials are then gradually increased in next steps as optimisation algorithm proceeds till the elastic moduli reach their prescribed values.

2.8.4 Examples

An example of finding an optimal topology of a cantilever beam is performed to illustrate the application of the BESO method. The design domain and boundary condition of the problem is shown in Fig. 2.7. A load of $P = 1$ is applied. The beam has a length of $l = 5$ and a width of $w = 3$. The material properties are Young modulus of $E = 1$ and Poisson ratio of $\nu = 0.3$. A discretisation of 50×30 square elements is applied to the design domain. A full design is used as an initial design. The maximum allowable volume of material is assigned as 50% of the design domain volume. The evolutionary volume ratio is set as $EVR = 0.01$. The filtering radius (Eq. (2.22)) is set as three times as the element size. Fig. 2.8 shows the obtained topologies and the evolutionary of the objective function and volume fraction.

2.9 Applying topology optimisation in underground excavation design

The complicated nature of rock mass behaviour introduces a number of challenges in the rock engineering design as mentioned in previous sections. Another special

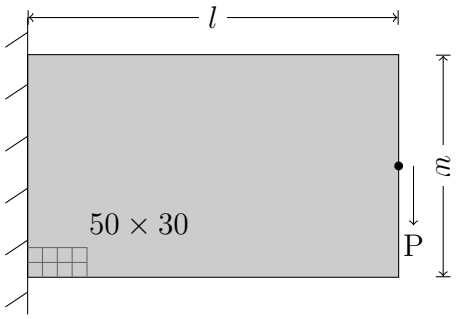

Figure 2.7: Design domain of a cantilever beam

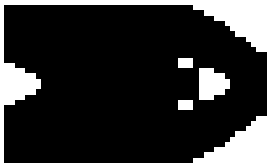

(a) $K = 15, VF = 86.0\%$

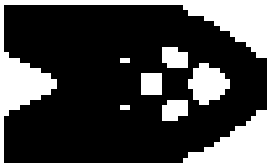

(b) $K = 25, VF = 77.8\%$

(c) $K = 35, VF = 70.3\%$

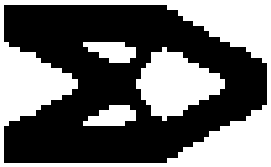

(d) $K = 45, VF = 63.5\%$

(e) $K = 55, VF = 57.6\%$

(f) $K = 79, VF = 50.0\%$ (final topology)

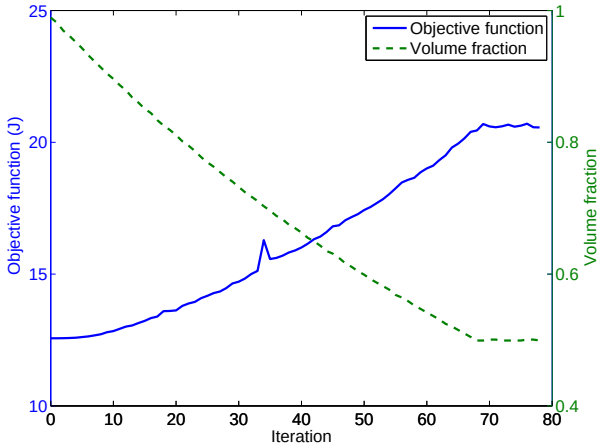

(g) Evolutionary histories of the objective function and the volume fraction

Figure 2.8: Topologies obtained by the BESO method for the cantilever beam problem (K is the iteration number and VF is the volume fraction)

feature of underground excavations is the changes of stress-strain patterns due to excavation and installation of support/reinforcement. These obstacles results in several limitations and difficulties in using topology optimisation in tunnelling engineering. This section is devoted to review published works on applying topology optimisation in underground excavation design and their corresponding limitations.

2.9.1 Shape optimisation of underground excavations

Numerical shape optimisation of underground openings was firstly investigated by Ren et al. (2005). They used an intuitive stress-based criterion using the mean principal compressive stress expressed as

$$\bar{\sigma} = \frac{\sigma_1 + \sigma_2 + \sigma_3}{3} \tag{2.28}$$

where $\bar{\sigma}$ is the mean stress, σ_1, σ_2 and σ_3 the principal stresses. The ESO method is used to gradually eliminate elements with lower $\bar{\sigma}$ in the finite element mesh until a control condition is satisfied. Some examples in both two and three dimensions were demonstrated and verified with analytical solutions. The ground material was assumed to follow linear elastic regime.

Applying the ESO concept, an attempt was made by Ghabraie et al. (2008) to optimise the opening shape considering nonlinear material properties. An elastic-perfectly plastic Mohr-Coulomb model was used to simulate ground material. A rejection criterion based on Mohr-Coulomb yield function was proposed to control the elimination process.

Replacing the intuitive stress-based optimisation, Ren et al. (2014) studied the shape optimisation based on a stiffness rejection criterion. The BESO method was employed and nonlinear behaviour of material was incorporated in the sensitivity analysis. The proposed approach was demonstrated by presenting a shape optimisation of an underground excavation under biaxial stress. Also, three dimension example optimising a shape of a mine pillar was shown to demonstrate to the applicability of the approach.

2.9.2 Reinforcement optimisation of underground excavations

In civil and mining engineering, underground reinforcement have been routinely designed using empirical methods. This tool is credited for its usefulness and convenience, however, it imposes some limitations in practicality as discussed in §2.3.2. To improve the conventional design method, some attempts have been made recently to apply topology optimisation in tunnel reinforcement design.

The application of topology optimisation in tunnel reinforcement design was initially studied by Yin et al. (2000). In this work, the homogenisation method is used to minimise the external work along the opening defined as

$$W = \int_{\Gamma} \mathbf{f} \cdot \mathbf{u} d\Gamma \tag{2.29}$$

where $\mathbf{u}$ is the displacement vector, Γ the tunnel's boundary, and $\mathbf{f}$ the surface traction on the opening before excavation. Elements in the design domain were modelled by a square cell made of original rock at the centre surrounded by reinforced rock.

Yin and Yang (2000a) conducted further research on tunnel reinforcement distribution in various layered geological conditions. Four cases of rock structures were investigated including isotropic soft, hard/soft, soft/hard, and hard/soft/hard rock layers. A displacement-based objective function which is the sum of relative displacements around the tunnel boundary is considered in the optimisation problem. The SIMP method is employed to determine the optimum distribution of reinforcement density in the design domain. The power-law interpolation similar to Eq. (2.13) is employed.

Using the same approach, another important issue in tunnel reinforcement design, namely tunnel and sidewall heave caused by squeezing rock, was also addressed by Yin and Yang (2000b).

Liu et al. (2008b) studied the displacement-based objective function to optimise reinforcement distribution around the opening by a Fixed-Grid Bidirectional Evolutionary Structural Optimisation (FG BESO) method. This approach was used

to overcome mesh-dependency and zigzag boundary problem in intermediate and final results. A linear interpolation scheme is used to represent the material properties of elements in the design domain in the form

$$E(x_e) = x_e E^{(r)} + (1 - x_e)E^{(o)} \tag{2.30}$$

where x_e is the design variable of the e-th element, taking the value of 0 if the element e is not reinforced or 1 if the element e is reinforced. We have $E(x_e) = E^{(o)}$ for $x_e = 0$ and $E(x_e) = E^{(r)}$ for $x_e = 1$.

A simultaneous optimisation of shape and reinforcement distribution of an underground excavation was explored by Ghabraie et al. (2010) using the BESO method. Some numerical examples on single and twin tunnels considering the *in situ* stress and traffic loadings were demonstrated.

It is noted that a linear elastic material behaviour was assumed to model both the original rock and reinforced in all the above-mentioned works. Also, all these works used isotropic homogenised material properties to model reinforced areas.

2.9.3 Limitations of the previous works and potential improvement

The two main limitations of the previous works on reinforcement optimisation include the linear elastic assumption for material behaviour and the modelling techniques of reinforcement material.

The elastic material model as assumed in the existing reinforcement optimisation works is a serious shortcoming as it is incapable of illustrating practical behaviour of geomaterials. Applications of these methods in tunnelling engineering is, hence, limited. This assumption will be removed in chapter 3 by considering nonlinear elastic-perfectly plastic material models.

Also, modelling reinforcement materials as homogenised isotropic elements causes inevitable inaccuracies in considering specific properties of reinforcement and also in explaining and processing the final outcomes. An advanced explicit modelling technique and relevant optimisation algorithm will be introduced in chapter 4 to

optimise bolt sizes in a given pattern around a tunnel. Further development of the reinforcement optimisation will be presented in chapter 5 in which the bolt pattern is also optimised.

The objective function of the external work around an opening has been widely used in the literature and also in the first chapters of this thesis. To consider other practical problems such as minimisation of heave or ground displacements due to tunnel excavation, a general formulation for displacement-based objective functions is introduced in chapter 6. The proposed optimisation techniques are then extended to that objective function.

Chapter 3

Nonlinear behaviour of geomaterial in optimisation

It is noted in §2.9.2 that the previous works on optimising tunnel reinforcement assumed linear elastic model for both host ground and reinforced material. As mentioned earlier this assumption is not always valid especially for geomechanics materials and should only be considered as the initial step to model geotechnical problems (Jing, 2003). Therefore, considering nonlinear material behaviour in topology optimisation is a reasonable extension of the previous studies towards obtaining proper and more reliable designs. In this chapter, the BESO method is improved and extended to search for an optimal reinforcement distribution in an underground excavation design modelled with nonlinear material model.

The work in this chapter has been published in a journal paper by Nguyen et al. (2014).

3.1 Motivations

Nonlinearity is a natural character of geomaterials (Jing, 2003). The behaviour of geomaterials is generally stress dependent. Particularly in tunnelling engineering, the stress-strain behaviour of ground material is continuously altered under repeated acts of tunnel advancement and support installation. It is therefore significant to capture practical material behaviour under various phases of

construction to gain an overall understanding of the system behaviour.

However, using such nonlinear material models in topology optimisation is somewhat challenging. The first and the most notable difficulty is the sensitivity analysis if the material nonlinearity or the construction sequence is to be concerned. Additionally, a typical optimisation algorithm normally requires a considerable number of finite element analyses. Solving such problems demand a huge computational effort and time, and is another barrier. Despite this, however, incorporation of material nonlinearities would provide us with more practical results and therefore be a crucial contribution to the area.

Historically, the topology optimisation methods mentioned in §2.6 are all initially applied for optimisation problems with linear material behaviour. Effects of nonlinear material behaviour on topology optimisation design have been studied later in some works by Maute et al. (1998); Bruns and Tortorelli (2001); Jung and Gea (2004) and Huang and Xie (2008). However, consideration of topology optimisation for multiple nonlinear materials working together has not been fully studied.

The previous works on tunnel reinforcement optimisation merely considered homogeneous, linear elastic material behaviour. This work is going to improve and extend the BESO to multimaterial problems with nonlinear materials and apply it into tunnel reinforcement design. It will be shown that the derived sensitivities could be used with any material model employed.

3.2 Tunnel modelling

The typical tunnel used in illustrative examples in this chapter is assumed to be long and straight enough to satisfy plane strain assumption. The geometry of the tunnel is a rectangle of size $w \times h = 10\text{m} \times 5\text{m}$ augmented at the top with a semicircle of radius 5m. After some numerical testings, the design domain geometry is selected as a square of side length $8h$. This is to ensure that the design domain size does not have a noticeable effect on topology optimisation results.

Fig. 3.1 shows the initial guess reinforcement design which represents a uniform

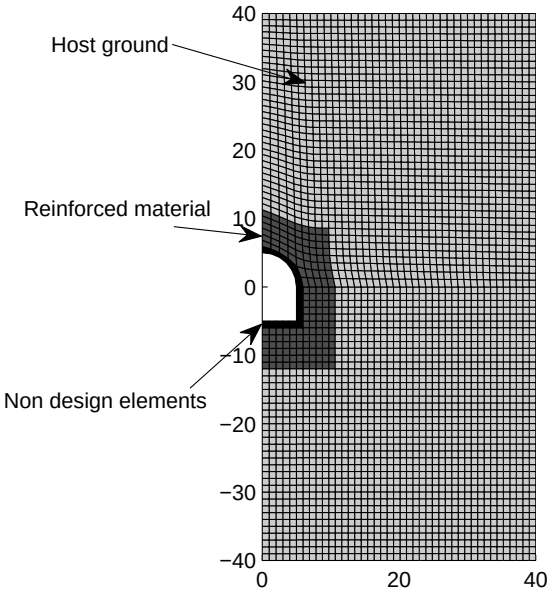

Figure 3.1: Initial guess design

distribution of reinforcements based on current empirical recommendations. In this figure, the reinforced zone is illustrated by dark grey elements. Elements around the tunnel opening are assigned as non-designable elements, printed black and assumed to have the same properties as the reinforced material. Using symmetry, only half of the design domain is modelled in the finite element analysis with proper symmetric conditions. Excavation process is analysed by finite element method using ABAQUS (version 6.11). Since the case of deep tunnel is investigated, the effect of difference in gravity force is ignored here. Also, the materials are assumed to be weightless.

Unlike linear material models, loading history affects the response of nonlinear materials. Thus, the tunnel excavation is modelled in two separate steps. Firstly, pre-excavation conditions are obtained by restraining the nodal displacements of elements at the tunnel surface and at the boundary regions between the reinforced rock and the original rock. In the subsequent step, the displacement restraints along the boundary of the opening are removed.

It is clear from the tunnel model that two types of materials, i.e. host ground and reinforced material, are of concern. Mohr-Coulomb constitutive model which has been broadly used in geotechnical engineering applications is employed to

model host ground and reinforced material owing to its simplicity and acceptable accuracy. Yield function and flow potential of the elasto plastic Mohr-Coulomb model with a non-associated flow rule are expressed as (Menétrey and Willam, 1995)

$$F = R_{mc}q - p\tan\phi - c = 0 \tag{3.1}$$

$$G = \sqrt{(\epsilon C|_0 \tan\psi)^2 + (R_{m\omega}q)^2} - p\tan\psi \tag{3.2}$$

where

$$R_{mc}(\Theta,\phi) = \frac{1}{\sqrt{3}\cos\phi}\sin\left(\Theta+\frac{\pi}{3}\right) + \frac{1}{3}\cos\left(\Theta+\frac{\pi}{3}\right)\tan\phi, \tag{3.3}$$

$$R_{mw}(\Theta,e) = \frac{4(1-e^2)\cos^2\Theta + (2e-1)^2}{2(1-e^2)\cos\Theta + (2e-1)\sqrt{4(1-e^2)\cos^2\Theta + 5e^2 - 4e}} R_{mc}(\frac{\pi}{3},\phi), \tag{3.4}$$

$$R_{mc}(\frac{\pi}{3},\phi) = \frac{3-\sin\phi}{6\cos\phi}, \tag{3.5}$$

$$p = -\frac{1}{3}\text{trace}(\boldsymbol{\sigma}) \tag{3.6}$$

$$q = \sqrt{\frac{3}{2}\mathbf{S}:\mathbf{S}} \tag{3.7}$$

ϕ, c and ψ are the friction angle, cohesion and dilation angle of the rock, respectively. Θ is the deviatoric polar angle, ϵ the meridional eccentricity, e the deviatoric eccentricity, and C_0 the initial cohesion yield stress. p is the mean stress, q the Mises stress, and $\mathbf{S}$ the deviatoric stress. The values adopted for the material parameters are shown in Table 3.1.

Table 3.1: Engineering properties of host ground and reinforced material

Material properties	Host ground	Reinforced material
Young modulus (GPa)	0.1	0.5
Poisson's ratio	0.3	0.3
Friction angle (°)	27	32
Cohesion (MPa)	0.1	0.3

It should be emphasised, however, that as will be clear later, the approach proposed here is not dependent on the material model used.

3.3 Statement of objective function

The aim of the tunnel reinforcement design is to employ a minimum amount of reinforcements while tunnel deformation after activating the reinforcements needs to be limited. This objective can be reformulated as minimising tunnel deformation after reinforcement installation under a prescribed reinforcement volume. In the proposed method below, the optimisation process minimises the external work along the tunnel wall which is a functional of the tunnel deformation under a constrained reinforcement volume. The outcomes provide an optimal distribution for a certain amount of reinforcement volume in order to obtain a minimum external work. It can be shown that any solution to this problem is also a solution to finding a minimum reinforcement volume subject to a constrained external work. The optimisation problem can be stated as

$$\begin{aligned} \min\ W &= \int \mathbf{f} \cdot d\mathbf{u} = \lim_{n\to\infty} \left[\frac{1}{2} \sum_{i=1}^{n} (\mathbf{u}_i - \mathbf{u}_{i-1}) \cdot (\mathbf{f}_i + \mathbf{f}_{i-1}) \right] \\ \text{subject to:}\quad V_R &= \sum_{e=1}^{M} V_e x_e \\ x_e &\in \{0, 1\} \end{aligned} \tag{3.8}$$

where W is the total external work, $\mathbf{u}$ the displacement vector, $\mathbf{f}$ the external force vector, n the number of iterations in solving the non-linear equilibrium equations, V_e the volume of element e, V_R the prescribed reinforced volume, and M the total number of elements in the design domain. x_e is the design variable of element e. $x_e = 1$ means that element e is reinforced and $x_e = 0$ means element e is not reinforced.

3.4 Nonlinear sensitivity analysis

To search for an optimal reinforcement distribution, the core task of the BESO method is to switch elements' material between two material types, host ground and reinforced material, based on the rank of their sensitivity numbers. The sensitivity analysis for the above-mentioned objective function with a consideration

of material nonlinearities is presented herein.

Equilibrium requires the residual force vector to be eliminated, i.e.,

$$\mathbf{R} = \mathbf{f} - \mathbf{p} = 0 \tag{3.9}$$

where $\mathbf{p}$ is the internal force vector. The internal force vector can be expressed as

$$\mathbf{p} = \sum_{e=1}^{M} \int_e \mathbf{C}_e \mathbf{B} \boldsymbol{\sigma} d\nu = \sum_{e=1}^{M} \int_e \mathbf{C}_e \mathbf{B} \mathbf{D}_e \boldsymbol{\varepsilon} d\nu \tag{3.10}$$

where $\mathbf{C_e}$ is the matrix which transforms local force vector of element e to global force vector, $\mathbf{B}$ the strain-displacement matrix, and $\mathbf{D_e}$ the matrix defining the stress-strain relationship. The sensitivity of the objective function to a change in variable x is

$$\frac{\partial W}{\partial x} = \lim_{n\to\infty} \left[\frac{1}{2} \sum_{i=1}^{n} (\mathbf{u}_i - \mathbf{u}_{i-1}) \cdot \left(\frac{\partial \mathbf{f}_i}{\partial x} + \frac{\partial \mathbf{f}_{i-1}}{\partial x} \right) + \frac{1}{2} \sum_{i=1}^{n} \left(\frac{\partial \mathbf{u}_i}{dx} - \frac{\partial \mathbf{u}_{i-1}}{dx} \right) \cdot (\mathbf{f}_i + \mathbf{f}_{i-1}) \right] \tag{3.11}$$

Note that the second sum vanishes because at any point either the external force is zero or the displacement is fixed.

The adjoint method is applied by adding an adjoint term to the objective function (3.8).

$$W = \lim_{n\to\infty} \left[\frac{1}{2} \sum_{i=1}^{n} (\mathbf{u}_i - \mathbf{u}_{i-1}) \cdot (\mathbf{f}_i + \mathbf{f}_{i-1}) - \lambda_i \cdot (\mathbf{R}_i + \mathbf{R}_{i-1}) \right] \tag{3.12}$$

Differentiating Eq. (3.12) and using Eq. (3.9), we obtain

$$\frac{\partial W}{\partial x} = \lim_{n\to\infty} \frac{1}{2} \sum_{i=1}^{n} \left[(\mathbf{u}_i - \mathbf{u}_{i-1}) \cdot \left(\frac{\partial \mathbf{f}_i}{\partial x} + \frac{\partial \mathbf{f}_{i-1}}{\partial x} \right) - \lambda_i \cdot \left(\frac{\partial \mathbf{f}_i}{\partial x} - \frac{\partial \mathbf{p_i}}{\partial x} + \frac{\partial \mathbf{f}_{i-1}}{\partial x} - \frac{\partial \mathbf{p_{i-1}}}{\partial x} \right) \right] \tag{3.13}$$

In order to eliminate the unknown part $\frac{\partial \mathbf{f}_i}{\partial x} + \frac{\partial \mathbf{f}_{i-1}}{\partial x}$, λ_i is selected as

$$\lambda_i = \mathbf{u}_i - \mathbf{u}_{i-1} \tag{3.14}$$

Substituting Eq. (3.14) into Eq. (3.13), the sensitivity of the objective function

is

$$\frac{\partial W}{\partial x} = \lim_{n\to\infty} \frac{1}{2} \sum_{i=1}^{n} (\mathbf{u}_i - \mathbf{u}_{i-1}) \cdot \left(\frac{\partial \mathbf{p_i}}{\partial x} + \frac{\partial \mathbf{p_{i-1}}}{\partial x} \right) \tag{3.15}$$

In order to calculate the sensitivity of the internal force vectors, we use the material interpolation scheme suggested by Stolpe and Svanberg (2001a). Using this interpolation scheme, the matrix $\mathbf{D}_e$ in terms of design variables is expressed as

$$\mathbf{D}_e(x_e) = \mathbf{D}_e^{(2)} + \frac{x_e}{1 + q(1 - x_e)} \left(\mathbf{D}_e^{(1)} - \mathbf{D}_e^{(2)} \right) \tag{3.16}$$

where $\mathbf{D}_e$ is the stress-strain matrix of the e-th element and $\mathbf{D}_e^{(1)}$ and $\mathbf{D}_e^{(2)}$ the stress-strain matrices of the same element if it was made of the reinforced material (material 1) and unreinforced material (material 2) respectively. x_e is the design variable of the e-th element and we have $\mathbf{D}_e = \mathbf{D}_e^{(2)}$ for $x_e = 0$ and $\mathbf{D}_e = \mathbf{D}_e^{(1)}$ for $x_e = 1$. A value of $q = 0$ results in a linear interpolation. Ghabraie (2015b) showed that using linear interpolation in the BESO can result in unrecognisable topologies when filtering techniques are adopted to overcome numerical instabilities. In this work, a value of $q > 0$ is used to prevent such situations.

Differentiating Eq. (4.2), yields

$$\frac{\partial \mathbf{D}_e}{\partial x_e} = \frac{\left(\mathbf{D}_e^{(1)} - \mathbf{D}_e^{(2)} \right) (1 + q)}{\left[1 + q(1 - x_e) \right]^2} \tag{3.17}$$

From Eq. (4.3) and Eq. (3.17), we have

$$\begin{aligned} \frac{\partial \mathbf{p}}{\partial x_e} &= \frac{1 + q}{\left[1 + q(1 - x_e) \right]^2} \sum_{e=1}^{M} \int_e \mathbf{C}_e \mathbf{B} (\mathbf{D}_e^{(1)} - \mathbf{D}_e^{(2)}) \varepsilon d\nu \\ &= \frac{1 + q}{\left[1 + q(1 - x_e) \right]^2} \left(\mathbf{p_e^{(1)}} - \mathbf{p_e^{(2)}} \right) \end{aligned} \tag{3.18}$$

Substitute Eq. (4.5) into Eq. (3.15), we have

$$\begin{aligned}\alpha = \frac{\partial W}{\partial x_e} &= \frac{1+q}{\left[1+q\left(1-x_e\right)\right]^2} \lim_{n\to\infty} \frac{1}{2} \sum_{i=1}^{n} \left(\mathbf{u}_i - \mathbf{u}_{i-1}\right) \cdot \left(\mathbf{p_i^{(1)}} - \mathbf{p_i^{(2)}} + \mathbf{p_{i-1}^{(1)}} - \mathbf{p_{i-1}^{(2)}}\right) \\ &= \frac{1+q}{\left[1+q\left(1-x_e\right)\right]^2} \left[\lim_{n\to\infty} \frac{1}{2} \sum_{i=1}^{n} \left(\mathbf{u}_i - \mathbf{u}_{i-1}\right) \cdot \left(\mathbf{p_i^{(1)}} + \mathbf{p_{i-1}^{(1)}}\right) \right. \\ &\qquad \left. - \lim_{n\to\infty} \frac{1}{2} \sum_{i=1}^{n} \left(\mathbf{u}_i - \mathbf{u}_{i-1}\right) \cdot \left(\mathbf{p_i^{(2)}} + \mathbf{p_{i-1}^{(2)}}\right)\right] \\ &= \frac{(1+q)}{\left[1+q\left(1-x_e\right)\right]^2} \left(\Pi_e^{(1)} - \Pi_e^{(2)}\right)\end{aligned} \tag{3.19}$$

where $\Pi_e^{(1)}$ and $\Pi_e^{(2)}$ are the total strain energies of element e if it was made of material 1 and 2 respectively.

The sensitivity number α is a direct measure of variation of the objective function due to switching the two materials. It is interesting to note that the sensitivities are local, i.e., they only depend on the local responses of the considered element. It can also be seen that the sensitivities are independent of size of displacement increments. It is worth noting that in this sensitivity analysis, no assumption has been made on the behaviour of the material or the failure model. Thus, this result is valid for all types of material models.

The utilised optimisation method requires a switching procedure of material between the original rock and the reinforced rock. The elements themselves can be considered as the design variable during the optimisation process.

3.4.1 Numerical calculation of sensitivity numbers

The elastic perfectly plastic Mohr-Coulomb model is employed for both the original (material 2) and the reinforced materials (material 1). Two cases need to be considered as follows.

Case 1: the element is made of material 1 ($x_e = 1$). In this case, $\Pi_e^{(2)}$ in Eq. (4.9) takes the form

$$\Pi_e^{(2)} = \lim_{n\to\infty} \frac{1}{2} \sum_{i=1}^{n} \left(\boldsymbol{\varepsilon}_i - \boldsymbol{\varepsilon}_{i-1}\right) \cdot \left(\boldsymbol{\sigma}_i^{(2)} + \boldsymbol{\sigma}_{i-1}^{(2)}\right) V_e \tag{3.20}$$

where V_e is the volume of the element e.

If the element is in its elastic region under the final strain $\boldsymbol{\varepsilon}$, we have

$$\Pi_e^{(2)} = \frac{1}{2} V_e \boldsymbol{\varepsilon} \cdot \boldsymbol{\sigma}^{(2)} \tag{3.21}$$

and Eq. (4.9) takes the form

$$\alpha = (1+q)\left(\Pi_e^{(1)} - \frac{1}{2} V_e \boldsymbol{\varepsilon} \cdot \boldsymbol{\sigma}^{(2)}\right) \tag{3.22}$$

Otherwise, the strain energy of the element is made of elastic and plastic components and we have

$$\Pi_e^{(2)} = \frac{1}{2} V_e \left[\boldsymbol{\varepsilon}_y^{(2)} \cdot \boldsymbol{\sigma}_y^{(2)} + \left(\boldsymbol{\varepsilon} - \boldsymbol{\varepsilon}_y^{(2)}\right) \cdot \left(\boldsymbol{\sigma}^{(2)} + \boldsymbol{\sigma}_y^{(2)}\right)\right] \tag{3.23}$$

and Eq. (4.9) takes the form

$$\alpha = (1+q)\left\{\Pi_e^{(1)} - \frac{1}{2} V_e \left[\boldsymbol{\varepsilon}_y^{(2)} \cdot \boldsymbol{\sigma}_y^{(2)} + \left(\boldsymbol{\varepsilon} - \boldsymbol{\varepsilon}_y^{(2)}\right) \cdot \left(\boldsymbol{\sigma}^{(2)} + \boldsymbol{\sigma}_y^{(2)}\right)\right]\right\} \tag{3.24}$$

or

$$\alpha = (1+q)\left\{\Pi_e^{(1)} - \frac{1}{2} V_e \left[\boldsymbol{\varepsilon} \cdot \left(\boldsymbol{\sigma}^{(2)} + \boldsymbol{\sigma}_y^{(2)}\right) - \boldsymbol{\varepsilon}_y^{(2)} \cdot \boldsymbol{\sigma}^{(2)}\right]\right\} \tag{3.25}$$

Case 2: the element is made of material 2 ($x_e = 0$). In this case, $\Pi_e^{(1)}$ in Eq. (4.9) takes the form

$$\Pi_e^{(1)} = \lim_{n\to\infty} \frac{1}{2} \sum_{i=1}^{n} \left(\boldsymbol{\varepsilon}_i - \boldsymbol{\varepsilon}_{i-1}\right) \cdot \left(\boldsymbol{\sigma}_i^{(1)} + \boldsymbol{\sigma}_{i-1}^{(1)}\right) V_e \tag{3.26}$$

If the element is in its elastic region under the final strain ε, we have

$$\Pi_e^{(1)} = \frac{1}{2} V_e \boldsymbol{\varepsilon} \cdot \boldsymbol{\sigma}^{(1)} \tag{3.27}$$

and Eq. (4.9) takes the form

$$\alpha = \frac{1}{1+q}\left(\frac{1}{2} V_e \boldsymbol{\varepsilon} \cdot \boldsymbol{\sigma}^{(1)} - \Pi_e^{(2)}\right) \tag{3.28}$$

Otherwise, the strain energy of the element is made of elastic and plastic components and we have

$$\Pi_e^{(1)} = \frac{1}{2} V_e \left[\boldsymbol{\varepsilon}_y^{(1)} \cdot \boldsymbol{\sigma}_y^{(1)} + \left(\boldsymbol{\varepsilon} - \boldsymbol{\varepsilon}_y^{(1)} \right) \cdot \left(\boldsymbol{\sigma}^{(1)} + \boldsymbol{\sigma}_y^{(1)} \right) \right] \tag{3.29}$$

and Eq. (4.9) takes the form

$$\alpha = \frac{1}{1+q} \left\{ \frac{1}{2} V_e \left[\boldsymbol{\varepsilon}_y^{(1)} \cdot \boldsymbol{\sigma}_y^{(1)} + \left(\boldsymbol{\varepsilon} - \boldsymbol{\varepsilon}_y^{(1)} \right) \cdot \left(\boldsymbol{\sigma}^{(1)} + \boldsymbol{\sigma}_y^{(1)} \right) \right] - \Pi_e^{(2)} \right\} \tag{3.30}$$

or

$$\alpha = \frac{1}{1+q} \left\{ \frac{1}{2} V_e \left[\boldsymbol{\varepsilon} \cdot \left(\boldsymbol{\sigma}^{(1)} + \boldsymbol{\sigma}_y^{(1)} \right) - \boldsymbol{\varepsilon}_y^{(1)} \cdot \boldsymbol{\sigma}^{(1)} \right] - \Pi_e^{(2)} \right\} \tag{3.31}$$

where ε is the final strain, σ the final stress caused by ε, and $\sigma_y^{(1)}$, $\varepsilon_y^{(1)}$, $\sigma_y^{(2)}$, $\varepsilon_y^{(2)}$ the yield stresses and yield strains of material 1 and material 2, respectively.

3.5 BESO procedures

The BESO procedure repeatedly switches elements between the two phases of material based on the obtained sensitivity numbers. In the initial design, the reinforcement volume is chosen to satisfy the volume constraint given in Eq. (3.8) and is maintained during the optimisation process. The volume of elements to be reinforced is thus equal to the volume of elements to be unreinforced in each iteration. This is beneficial for observing the objective function variations clearly in each iteration and also in the final optimal result. Additionally, a limit is imposed on the maximum volume of changing elements to ensure that there is no sudden change in the design. This limit is referred to as evolutionary volume ratio (EVR).

The volume of switched elements in each iteration is calculated from

$$\min \{EVR, VR, VO\} \tag{3.32}$$

where VR is the total volume of all reinforced elements with sensitivity numbers smaller than the maximum sensitivity number of the original elements, and VO

the total volume of all original elements with sensitivity numbers larger than the minimum sensitivity number of the reinforced elements.

Additionally, to overcome mesh dependency and eliminate checkerboard patterns, the linear filtering technique (Huang and Xie, 2007) presented in §2.8.3 is also employed.

The process of finite element analysis and material switching continues until the following convergence criterion is met (Huang and Xie, 2010a)

$$\text{error} = \frac{\sum_{k=1}^{n} \left(W_{i-k+1} - W_{i-n-k+1}\right)}{\sum_{k=1}^{n} W_{i-k+1}} \leq \tau \tag{3.33}$$

where W_i is the value of objective function in the i-th iteration, n is chosen as 5, and τ is the convergence tolerance selected as 10^{-4}. The flow chart for the whole program is depicted in Fig. 3.2.

3.6 Examples and discussion

In order to verify and demonstrate the applicability and robustness of the presented approach, some problems with both linear and nonlinear material models are solved here. The tunnel reinforcement design presented in Fig. 3.1 is optimised in all these examples.

For verification, tunnel reinforcement design is firstly carried out assuming linear elastic material analysis. Both host ground and reinforced material are assumed to work in elastic regime with Young modulus (E) and Poisson's ratio (ν) shown in Table 3.1. Volume of reinforcing material is predefined as 5 percent of that of the whole design domain. The filtering radius is chosen as 2.5 m. Hoek and Brown (1980) reported that the ratio between horizontal and vertical stress, k, may be in the range of 0.4 to 5. In this example, two cases of k are investigated and the obtained outcomes are depicted in Fig. 3.3. As expected, tunnel reinforcement is distributed evenly around the tunnel wall in hydrostatic stress condition ($k = 1$) (Fig. 3.3a). For $k = 0.7$, reinforcement areas are more skewed in vertical direction which agrees well with the results of Yin et al. (2000) (Fig. 3.3b). The objective

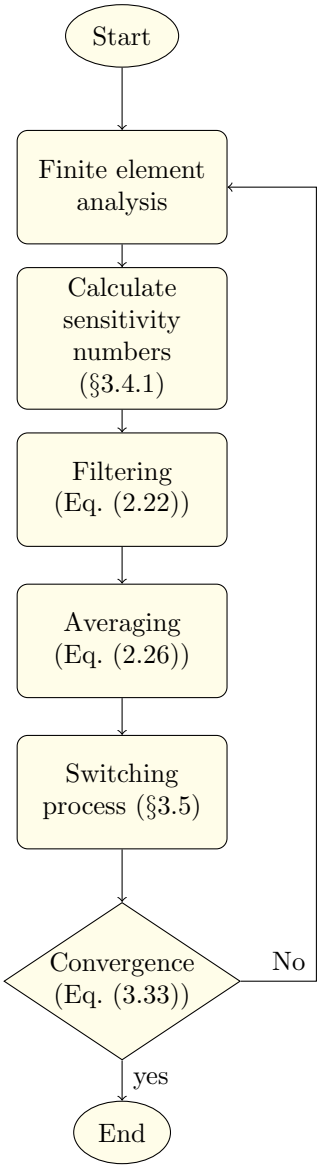

Figure 3.2: Flowchart of tunnel reinforcement optimisation using the BESO method

function variations for these two cases are shown in Fig. 3.3c. It can be seen that the objective function reduces gradually with smooth changes and converges after a few iterations.

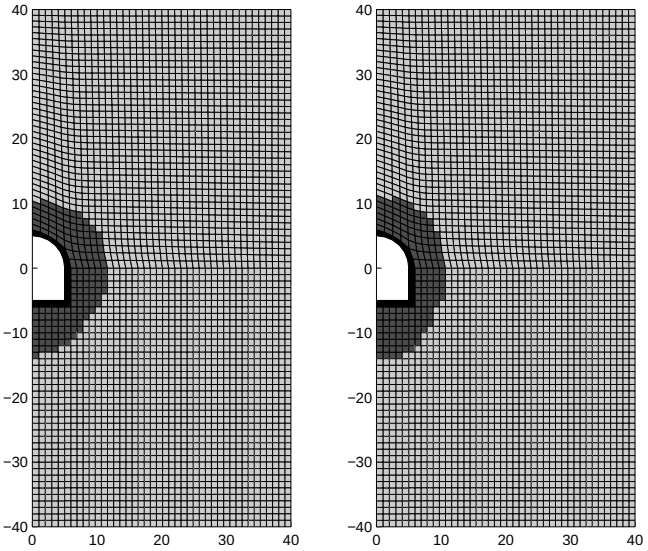

(a) $k = 1$ (b) $k = 0.7$

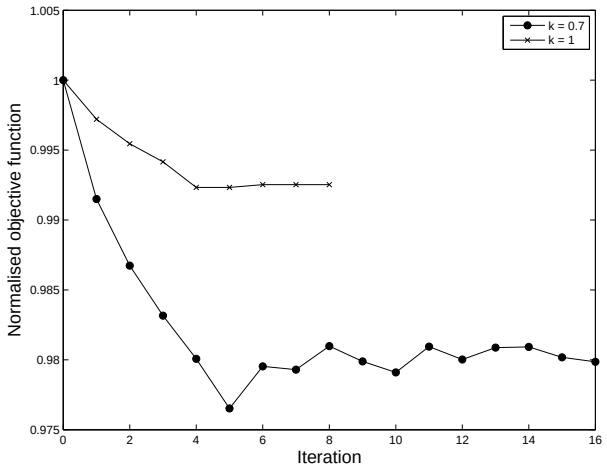

(c) Objective function variations

Figure 3.3: Optimal tunnel reinforcement with an elastic material model

It has been proved that reinforcement design for underground excavation is highly affected by horizontal stress ratio (Ghabraie, 2009). In the following examples, various *in situ* stress conditions including horizontal stress ratios and stress magnitudes are investigated.

3.6.1 Examples of various horizontal stress ratios in plastic cases

The tunnel described in section 3.2 is analysed with the elastic perfectly plastic Mohr-Coulomb material model. Since the tunnel is assumed to be deep enough, vertical stress in the vicinity of the opening can be assumed to be independent of depth. Various horizontal stress ratios, $k = 0.4,\ 0.7,\ 1,\ 1.4$ and 2 are investigated in these examples under the same vertical stress of 0.8 MPa. Filtering radius is selected as 1 m. Fig. 3.4 shows the obtained reinforcement distributions and objective function variations for these cases.

It can be observed from the results that the optimal tunnel reinforcement is significantly dependent on the horizontal stress ratio. Reinforcement distribution is even for the case of hydrostatic condition ($k = 1$) (Fig. 3.4c), while for unequal horizontal and vertical stresses, it can be easily seen that the reinforcement is aligned towards the direction of the maximum principal stress (Fig. 3.4a, 3.4b, 3.4d, 3.4e). Objective function gradually decreases and converges to the optimum in all of these examples (Fig. 3.4f).

3.6.2 Examples of stress dependency in plastic cases

The previous examples illustrated the effect of horizontal stress ratio on tunnel reinforcement design. Investigation of the effects of stress magnitude is conducted in this section. It is obvious that the effect of stress magnitude on the optimal reinforcement design only can be captured provided that material nonlinearity is taken into account.

In these examples, vertical stress (σ_1) is varied while horizontal stress ratio remains constant ($k = 0.4$). In order to obtain a clearer stress effects, a small filter radius of 1 m is used. Fig. 3.5 depicts tunnel reinforcement for linear materials and nonlinear materials with various vertical stress magnitudes.

For small vertical stresses, as expected, the optimal reinforcement design of nonlinear materials (Fig. 3.5b) is almost similar to that of linear ones (Fig. 3.5a). This is easily understandable since a large portion of elements are working in elastic

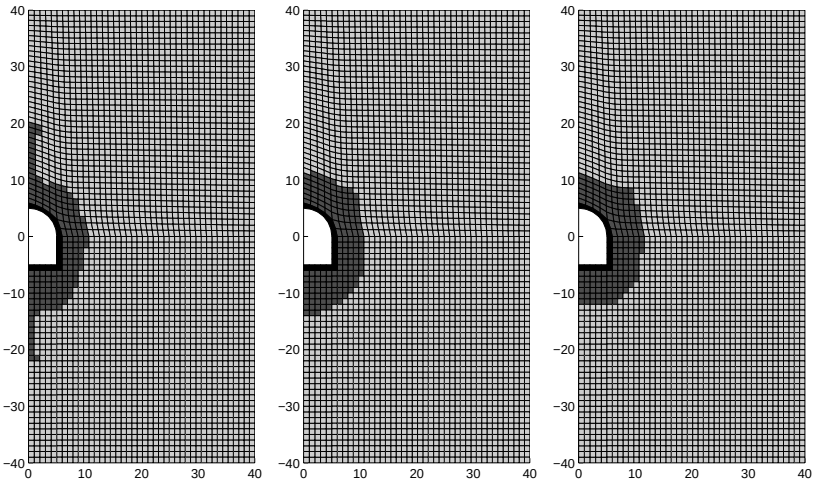

(a) $k = 0.4$ (b) $k = 0.7$ (c) $k = 1$

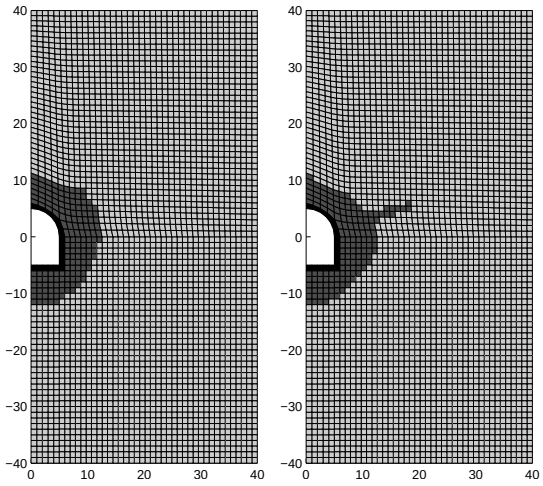

(d) $k = 1.4$ (e) $k = 2$

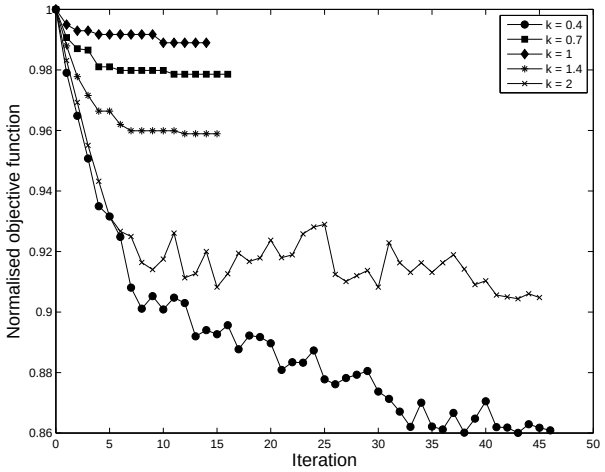

(f) Objective function variations

Figure 3.4: Nonlinear reinforcement optimisation under various horizontal stress ratios

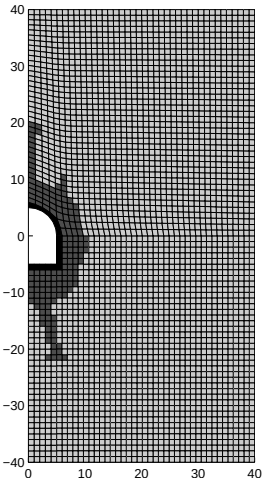

(a) Elastic case

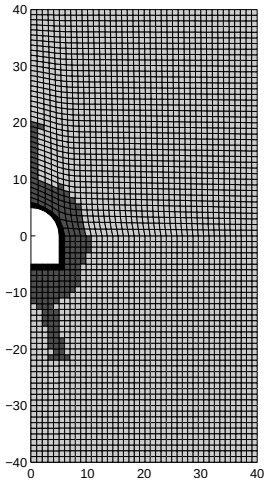

(b) Plastic case, $\sigma_1 = 0.5$ MPa

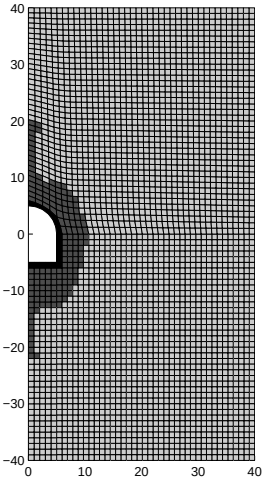

(c) Plastic case, $\sigma_1 = 0.8$ MPa

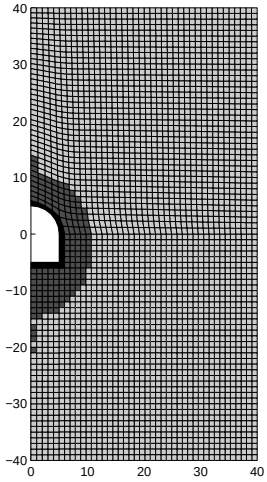

(d) Plastic case, $\sigma_1 = 1.1$ MPa

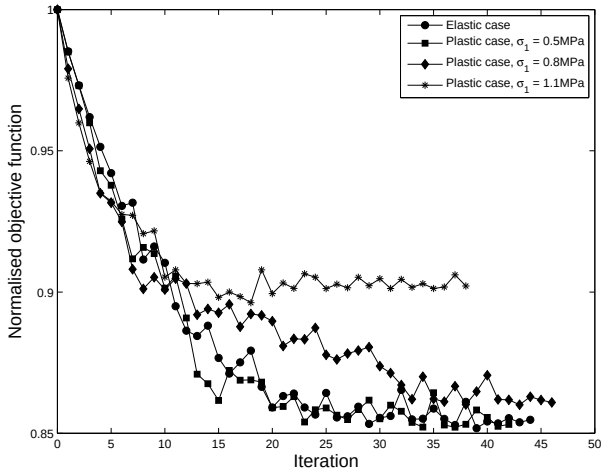

(e) Objective function variations

Figure 3.5: Stress dependency of nonlinear optimal tunnel reinforcement

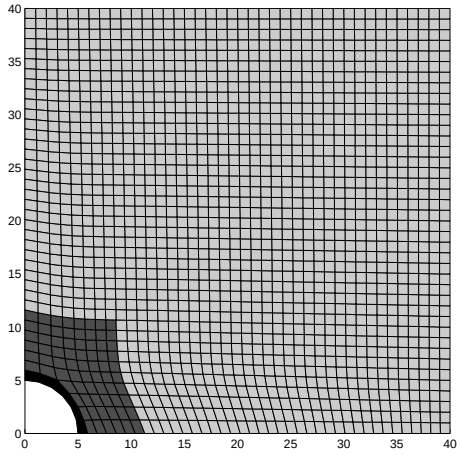

Figure 3.6: Initial guess design

regime in this condition. Under various stress values, it can be generally observed that the reinforcement distribution patterns are almost similar and oriented with the direction of the maximum principal stress (Fig. 3.5b, Fig. 3.5c and Fig. 3.5d). However, as the stress magnitudes increase, the reinforced elements tend to cover the areas closer to the openings whereas longer bolts seem to be preferable in particular directions under higher stress magnitudes. Relatively smooth changes in the objective function of various cases are also observed in these analyses as shown in Fig. 3.5e.

3.6.3 Effects of tunnel shape on the reinforcement distributions

In order to investigate the effects of tunnel shape on the optimal reinforcement distributions, a circular tunnel of the radius 5m is considered with the initial guess reinforcement design denoted by the dark grey areas as shown in Fig. 3.6. *In situ* stress conditions of vertical stress of 0.8 MPa and various horizontal stress ratios of $k = 0.4,\ 1$ and 2 are investigated. Owing to symmetry, only a quarter of the tunnel is modelled. Results on the optimal reinforcement distributions and the objective function variations are displayed in Fig. 3.7.

For the case of hydrostatic stress condition, it can be seen that the initial uniform guess design is also the optimal reinforcement distribution (Fig. 3.7b) and certainly, no further objective function improvement is observed (Fig. 3.7d). On the other hand, the optimal reinforcement distribution in the case of $k = 0.4$

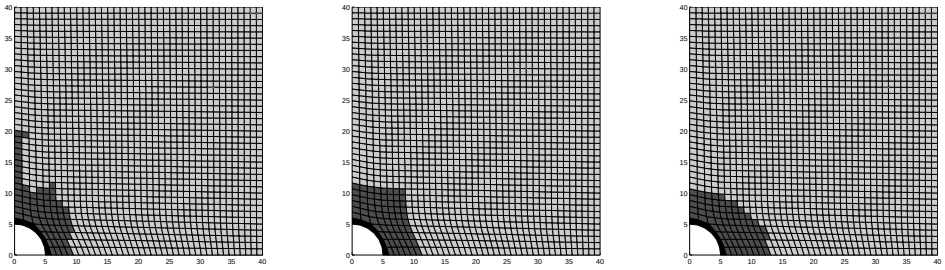

(a) $k = 0.4$ (b) $k = 1$ (c) $k = 2$

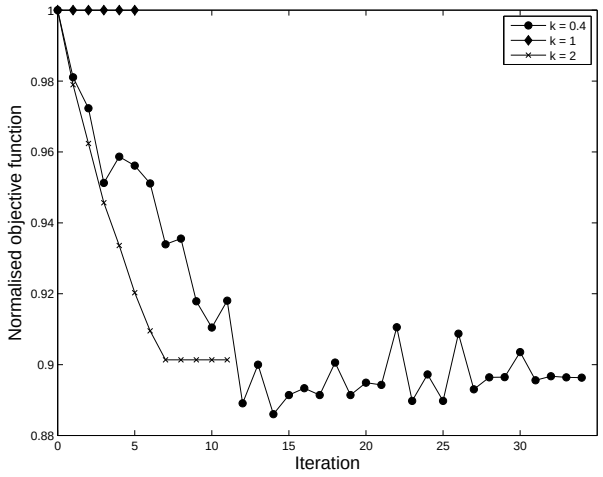

(d) Objective function variations

Figure 3.7: Reinforcement distribution for circular tunnel with $\sigma_1 = 0.8$ MPa. An even distribution of reinforcement, which is similar to the proposed initial design, is expected for the condition of the hydrostatic stress state (k=1) and the circular deep tunnel, where material weight is not considered.

for the circular tunnel (Fig. 3.7a) is almost similar to that for the tunnel shape presented in Fig. 3.4a. This is expected as the augmented parts of both tunnels are semi-circular. However, for the case of $k = 2$, the optimal reinforcement distribution for the circular tunnel is aligned with the horizontal direction and slightly different from that in Fig. 3.4e. The shape factor for the circular tunnel has redistributed the stress around the opening while the rectangle part of the tunnel in Fig. 3.4e has resulted in stress concentration at the corner, leading to a difference in the reinforcement distribution. It can be concluded that other than the *in situ* stress conditions, tunnel shape also affects the reinforcement design.

3.6.4 Demonstrations of effectiveness of the proposed approach

Based on rock engineering classification systems, empirical methods suggest certain tunnel reinforcement designs for corresponding ground conditions in which even reinforcement distribution is commonly observed. On the other hand, obtained results in previous sections show that optimal reinforcement distribution in the design domain changes with stress conditions and tunnel shape. This section is to demonstrate how the proposed approach could be used to improve the conventional reinforcement design.

Following the example presented in section 3.6.1 for the case of horizontal stress with $k = 2$, two openings reinforced by shotcrete lining and differently distributed rock bolt are presented. One is to illustrate the conventionally even distribution (Fig. 3.1) as displayed in Fig. 3.8a and another is to illustrate the distribution optimised by the present method (Fig. 3.4e) as displayed in Fig. 3.8b. Shotcrete lining and rock bolts are assumed to be elastic perfectly-plastic and their specific physical and mechanical properties are listed in Table 3.2. Total length of rock bolts for two designs are 43.54 m and 43.67 m, respectively. This negligible difference is due to mesh discretisations and has no considerable effects on optimality conditions pointed out in Eq. (3.8).

With the initial design based on an empirical recommendation (Fig. 3.8a), a finite element analysis using ABAQUS yields a value of 8.12×10^5 J for the objective function. On the other hand, starting with the above initial design, the present

Table 3.2: Physical and mechanical properties of shotcrete lining and rock bolts

Material	Shotcrete lining	Rock bolts
Young Modulus (GPa)	20	200
Poisson's ratio	0.2	0.3
Yield stress (MPa)	20	200
Thickness (mm)	100	-
Cross section area (mm^2)	-	$\pi(15)^2$

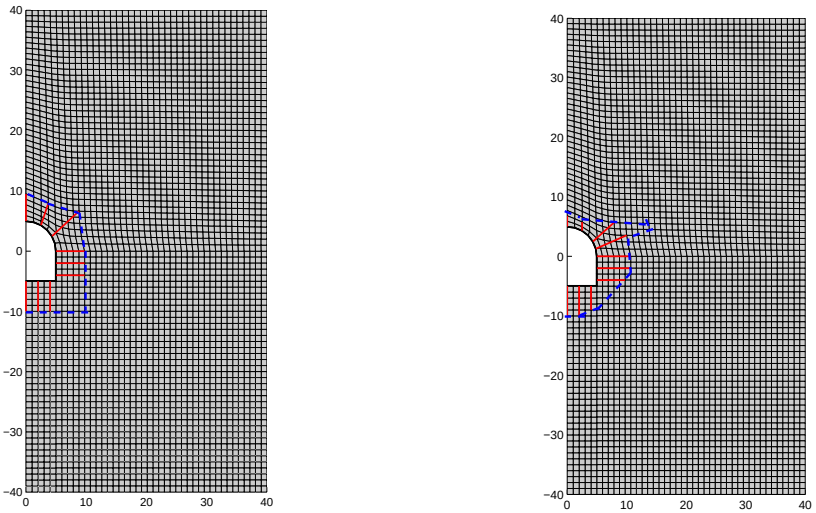

(a) Conventional design (b) Optimal design

Figure 3.8: Conventional and optimal rock bolt distribution

optimisation approach yields a final configuration as shown in Fig. 3.8b with a value of 7.5×10^5 J for the objective function. Thus, nearly 10% improvement is observable which is completely consistent with the results achieved in section 3.6.1.

3.7 Summary

Nonlinear material behaviour, a prominent and realistic character of geomechanical materials, has been captured in topology optimisation. Sensitivity analysis, one of the most significant part of topology optimisation methods, has been conducted for two nonlinear materials. To the extent of this study, the obtained results then can be utilised to search for an optimised tunnel reinforcement distribution. However, the approach can also be applicable to other topology optimisation problems considering material nonlineartities. Additionally, the method can be easily extended to a multi-material optimisation problem.

The BESO method has been extended to optimise tunnel reinforcement design in presence of nonlinear material behaviours of the host ground and the reinforced material. The proposed method is tested with both linear and nonlinear materials and the effectiveness of the method has been confirmed.

Some examples on investigating the effects of *in situ* stress conditions and tunnel shapes have been performed. Interestingly, various reinforcement designs are recommended for corresponding stress conditions and shapes of the openings. Also, to display the post-processing of the final outcomes, a simple example using the obtained final outcome and an assumed practical reinforcement design has been demonstrated. Based on the obtained results, it can be concluded that more advanced and rational designs can be achieved using the proposed optimisation technique compared to the commonly-employed method.

The presented method can be applied to a computer-aided tunnel support design, taking into account nonlinear material behaviours, ground conditions and tunnel shapes. Although only biaxial stress conditions are examined in the presented numerical demonstrations, this approach can be easily applied to other loadings

and geometrical conditions such as transport loading condition, twin tunnels, etc.

Apparently, modelling reinforcement material as homogenised elements causes some inconveniences in interpreting the final outcomes, leading to inflexibility of the proposed method. In the next chapter, a more advanced modelling approach along with a relevant optimisation technique will be presented to overcome this limitation.

Chapter 4

Optimisation of Rock Bolt Size

The work in this chapter has been accepted for publication as a journal paper by Nguyen et al. (2015b)

4.1 Modelling issues of reinforcement material

In the previous works, to model the areas of the rock mass reinforced by rock bolts, a homoginised isotropic material which is stronger and stiffer than the unreinforced rock mass material is used (Yin et al., 2000; Yin and Yang, 2000a,b; Liu et al., 2008b; Ghabraie et al., 2010; Nguyen et al., 2014). Some limitations and assumptions are linked to this modelling simplification. Firstly, a perfect bonding between the reinforced material and the surrounding rock needs to be assumed (Bernaud et al., 2009). More importantly, such a model cannot consider the anisotropic nature of the reinforced rock which is significantly stronger in the bolt direction and weaker in the normal directions. Also, results obtained by such an approach need to be further processed to yield a clear bolt distribution design as seen in §3.6.4.

To handle these shortcomings, one should model the reinforcements explicitly using linear inclusions embedded in the rock mass. This approach may take more efforts especially in topology optimisation, but a higher level of accuracy could be achieved.

This chapter is devoted to seek for an optimal rock bolt configuration by combining an extended optimisation technique and numerical analysis. Rock bolts will be explicitly modelled and nonlinear behaviour of both rock and bolts will be taken into account in order to achieve a more practical and effective bolt design.

4.2 Modelling of reinforcement system and excavation sequence

For simplicity, the considered tunnel is assumed to be long and straight enough to satisfy plane strain assumption. The support system employed to reinforce the tunnel excavation is a combination of a 100 mm-thick shotcrete lining and rock bolts. The shotcrete elements are attached to deform together with the rock elements around the excavation boundary. Rock bolts can be generally classified into two categories, namely anchored bolts and fully grouted bolts. This study focuses on anchored bolts. Due to their small cross-section area, the bending stiffness of rock bolts can be neglected and hence truss elements are used here to model pre-tensioned bolts Coda (2001); Leite et al. (2003). Rock bolts are embedded in the rock mass by connecting two ends of the bolts to nodes of the rock elements.

The whole excavation and reinforcement installation process is modelled using three separate steps as depicted in Fig. 4.1. The first step simulates pre-excavation situation. In this step, the *in situ* stress ($\boldsymbol{\sigma}_0$) is applied while the nodes on the opening surface are restrained and the reaction forces $\mathbf{t} = \mathbf{n} \cdot \boldsymbol{\sigma}_0$ are calculated (Fig. 4.1a). Here $\mathbf{n}$ denotes the inward unit vector normal to the opening surface.

The second step simulates the convergence of the opening before installing the reinforcement system. In this step the restraints of the opening surface nodes are removed while a surface traction equal to a certain ratio of their reaction at the previous step ($\mathbf{f} = \beta\mathbf{t}$) is applied at them (Fig. 4.1b). The value of β can be assumed based on longitudinal displacement profiles. For the examples we solved in this chapter, based on the improved longitudinal displacement profiles provided by Vlachopoulos and Diederichs (2009), it is concluded that a maximum

of 30% of radial displacement will occur before bolt installation based on which, the value of $\beta = 0.7$ is adopted.

In the third and last step, the shotcrete lining and rock bolts are added to the model and the surface traction is removed (Fig. 4.1c). Here we assumed that the bolts will experience the whole excavation load of the tunnel and considered them as a permanent support system. This can be easily changed if the bolts are only used to withstand a share of excavation load before installation of the main support system. In such a case, the traction force $\beta\mathbf{t}$ in step 2 should not be removed in step 3 but only reduced to $\beta'\mathbf{t}$ where $\beta' < \beta$ and β' should be found based on the distance from the face at which the permanent support system is planned to be installed.

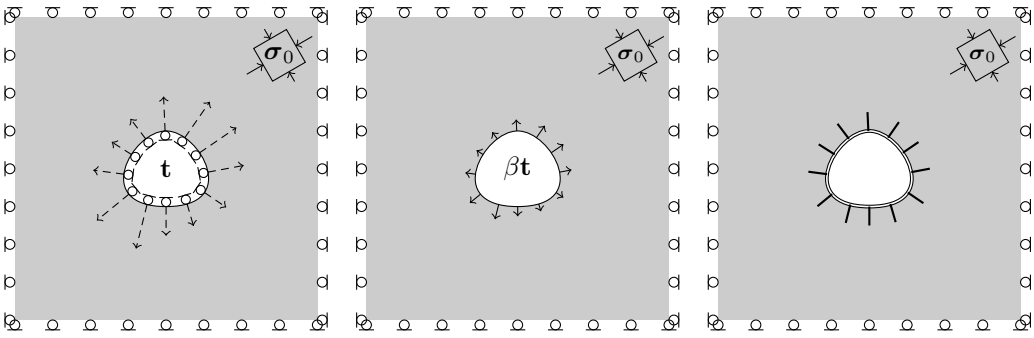

a. Step 1 b. Step 2 c. Step 3

Figure 4.1: The three steps in modelling the excavation process.

4.3 Problem statement and optimisation method

The proposed optimisation method minimises the external work along the tunnel wall introduced in §3.3 under a constrained bolt volume. The final solution is thus an optimised rock bolt distribution for a certain amount of bolt volume resulting in a minimum external work. The optimisation problem can be stated as

$$\begin{aligned} \min\ W &= \int \mathbf{f} \cdot d\mathbf{u} \\ \text{subject to:}\quad V_R &= \sum_{b=1}^{m} a_b l_b = \bar{V}_R \end{aligned} \tag{4.1}$$

where a_b is the cross section of the rock bolt b, l_b the length of the rock bolt b, m the number of rock bolts, and $\bar{V}_R$ the prescribed bolt volume.

The *ground structure* concept (Bendsøe and Sigmund, 2003) is used here. A ground structure is generated with all possibilities of rock bolts one wishes to consider in the assigned design domain. Within a given ground structure, the proposed approach seeks for an optimal layout of rock bolts. In tunnel reinforcement design, these rock bolts have one of their ends on the tunnel opening and another in the rock mass. Using the ground structure, length of each rock bolt is fixed while its cross section area is selected as a function of a design variable. A power-law interpolation scheme, which is commonly used to define intermediate material properties in the SIMP method (Bendsøe, 1989) is expressed below and employed to define the cross section area of each rock bolt.

$$a_b = \underline{a} + \alpha_b^p(\overline{a} - \underline{a}) \tag{4.2}$$

Here $\underline{a}$ and $\overline{a}$ are the lower and upper bound values of cross section area, respectively. p is the penalty factor, and $0 \leq \alpha_b \leq 1$ the design variable of rock bolt b. Selection of $\underline{a}$ and $\overline{a}$ restricts the desired range of cross section areas in the optimisation outcomes. Choosing $\underline{a} = 0$, one enables the optimisation engine to completely eliminate unnecessary bolts if required.

The penalty factor is used to penalise the intermediate values and consequently push the cross section areas of bolts to the two extremes of $\underline{a}$ and $\overline{a}$. Without penalisation ($p = 1$), the cross section area varies continuously from the lower to the upper bound values. On the other hand, a penalty factor $p > 1$ tries to push the intermediate values to the lower and upper bounds. The effect of penalisation then reduces to limiting the variety of bolt areas per unit length, ultimately leading to a reduction in the number of bolt types and/or in the number of drillings. It should be noted that using a very large value of the penalty factor results in local minima or convergence problem (Stolpe and Svanberg, 2001b). Selection of the penalty factor can have a considerable effect on optimisation results. Therefore, it needs to be carefully considered to meet technical aspects as well as economical terms. Effects of penalty factor are studied in §4.7 via a

simple example.

It should be noted that as a two dimensional model is considered here, the obtained optimisation outcomes are bolt cross section areas per unit length of the tunnel. When translating the designs back to three dimensions, based on available bolt diameters and the limitations of the drilling machine, one can work out the spacing between bolts in the third dimension to satisfy the required area per unit length.

The sensitivity analysis presented in the next section is employed to update the cross section area of each bolt in each iteration. The updating scheme employed in the SIMP method (Eq. (2.18)) is used to update these design variables. The process of finite element analysis and updating design variable continues until no design variable experiences a change of more than 10^{-4} in two consecutive iterations. The flowchart of the proposed approach is depicted in Fig. 4.2.

4.4 Sensitivity analysis

To derive the sensitivity of the objective function due to an infinitesimal change in variable α, the adjoint method utilised in chapter 3 is employed here again. Eq. (3.15) can also be obtained herein which the internal force vector ($\mathbf{p}$) is carried by both the rock material and the bolts and can be expressed as

$$\mathbf{p} = \mathbf{p}_b^S + \mathbf{p}^R \tag{4.3}$$

where $\mathbf{p}_b^S$ and $\mathbf{p}^R$ are the internal force vectors of the rock bolt b and the rock, respectively. The internal force vector carried by the rock is expressed as

$$\mathbf{p}^R = \sum_{e=1}^{M} \int_e \mathbf{C}_e \mathbf{B} \boldsymbol{\sigma} d\nu = \sum_{e=1}^{M} \int_e \mathbf{C}_e \mathbf{B} \mathbf{D}_e^R \boldsymbol{\varepsilon} d\nu \tag{4.4}$$

where M is the total number of rock elements, $\mathbf{C_e}$ the matrix which transforms the local force vector of element e to the global force vector, $\mathbf{B}$ the strain-displacement matrix and $\mathbf{D}_e^R$ the matrix defining the stress-strain relationship of the rock. As $\mathbf{C}_e$, $\mathbf{B}$ and $\mathbf{D}_e^R$ are independent of the design variable α, differentiating Eq. (4.3)

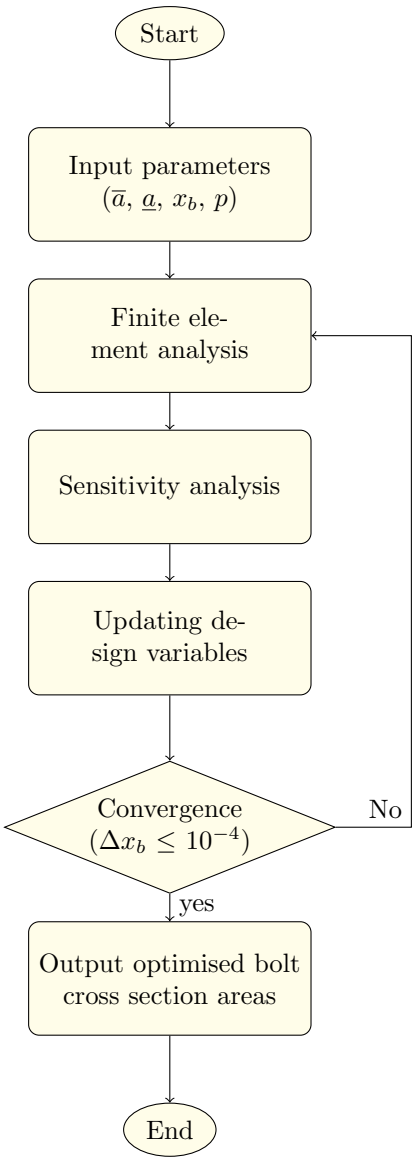

Figure 4.2: Flowchart of the bolt size optimisation approach

leads to

$$\frac{\partial \mathbf{p}}{\partial \alpha_b} = \frac{\partial \mathbf{p}_b^S}{\partial \alpha_b} \tag{4.5}$$

Substituting Eq. (4.5) into Eq. (3.15) results in

$$\frac{\partial W}{\partial \alpha_b} = \lim_{n\to\infty} \frac{1}{2} \sum_{i=1}^{n} (\mathbf{u}_i - \mathbf{u}_{i-1}) \cdot \left(\frac{\partial \mathbf{p}_{b_i}^S}{\partial \alpha_b} + \frac{\partial \mathbf{p}_{b_{i-1}}^S}{\partial \alpha_b} \right) \tag{4.6}$$

The internal force vector in a rock bolt can generally be calculated from

$$\mathbf{p}_b^S(\alpha_b, \delta_b) = a_b(\alpha_b)\boldsymbol{\sigma}(\delta_b) = a_b(\alpha_b)\mathbf{D}_b\boldsymbol{\varepsilon}_b \tag{4.7}$$

where δ_b is the elongation of the rock bolt b and $\boldsymbol{\sigma}(\delta_b)$ the stress in the rock bolt which is a function of this elongation only. $\mathbf{D}_b$ is the matrix defining the stress-strain relationship of the bolt and $\boldsymbol{\varepsilon}_b$ denotes the stress and strain vector of the bolt b. From Eq. (4.7) and Eq. (4.2), differentiation of internal force vector yields

$$\begin{aligned} \frac{\partial \mathbf{p}_b^S}{\partial \alpha_b} &= p\alpha_b^{p-1}(\overline{a} - \underline{a})g(\delta_b) \\ &= p\alpha_b^{p-1}(\mathbf{p}_b^{S_{max}} - \mathbf{p}_b^{S_{min}}) \end{aligned} \tag{4.8}$$

Substituting Eq. (4.8) and Eq. (4.5) into Eq. (3.15) results in the following

$$\begin{aligned} \frac{\partial W}{\partial \alpha_b} &= p\alpha_b^{p-1} \lim_{n\to\infty} \frac{1}{2} \sum_{i=1}^{n} (\mathbf{u}_i - \mathbf{u}_{i-1}) \cdot \left(\mathbf{p}_{b_i}^{S_{max}} - \mathbf{p}_{b_i}^{S_{min}} + \mathbf{p}_{b_{i-1}}^{S_{max}} - \mathbf{p}_{b_{i-1}}^{S_{min}} \right) \\ &= p\alpha_b^{p-1}(\Pi_b^{S_{max}} - \Pi_b^{S_{min}}) \end{aligned} \tag{4.9}$$

where $\Pi_b^{S_{max}}$ and $\Pi_b^{S_{min}}$ are the total strain energies of the bolt b when its cross section areas are $\overline{a}$ and $\underline{a}$, respectively. Setting $\underline{a} = 0$ the above equation simplifies further to

$$\frac{\partial W}{\partial \alpha_b} = p\alpha_b^{p-1}\Pi_b^{S_{max}} \tag{4.10}$$

From Eq. (4.8), it can be seen that the sensitivity of a truss element is a direct measure of its total strain energy and only depends on the considered element.

It is important to note that the sensitivity analysis outcomes can be applied to

any material models of the rock mass and bolts as no assumptions on material behaviour have been made in the above derivation.

4.5 Improving the uniform rock bolt distribution

A simple rock bolt design example is considered to illustrate the applicability and effectiveness of the proposed approach. The geometry of the tunnel is a rectangle of size $w \times h = 10\,\mathrm{m} \times 5\,\mathrm{m}$ augmented at the top with a semi-circle of radius 5 m. In order to ensure that the boundary effect is negligible, the modelled domain is chosen as a square of side length $20w$ (i.e. 200 m). Using symmetry, only half of this domain is modelled in the finite element analysis as displayed in Fig. 4.3. For a better view of the reinforcement layout, only an area around the opening with the size of $15\,\mathrm{m} \times 30\,\mathrm{m}$ will be illustrated in other figures.

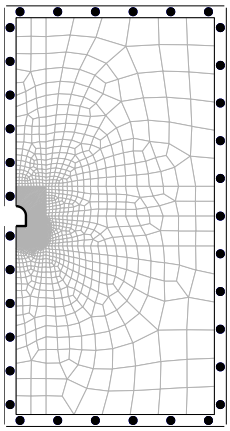

Figure 4.3: Full model of the tunnel

A typical rock bolt design practice commonly involves determining three parameters, namely, length, spacing and cross section area of bolts. The bolts are empirically distributed uniformly around the areas of the opening which need to be reinforced and normal to the opening. Generally, the selection of bolt length is based on the thickness of unstable strata to ensure that the bolts are long enough to be firmly anchored in a competent rock mass. In homogeneous rock media, however, bolt length is selected to generate a radial compression to the rock arch increasing load carrying capacity of the rock arch. For the investigation of bolts in a weak homogeneous rock, following the suggestion of Dejean and Raffoux

(1976), length of rock bolts should be in the range of $\frac{w}{3}$ to $\frac{w}{2}$, where w is the width of the opening. A fixed length of approximately 5 m is chosen here.

Fixing the rock bolt length and its orientation, a ground structure can be generated by assuming a value for rock bolt spacing. In this example, a ground structure is created with a bolt spacing of 1 m and is codenamed GS10 as displayed in Fig. 4.4. It is worth noting that the considered ground structure reflects the empirical suggestions with even distribution of bolts (Bieniawski, 1979; Grimstad and Barton, 1993). Effects of ground structure densities on optimisation outcomes will be discussed in §4.8.

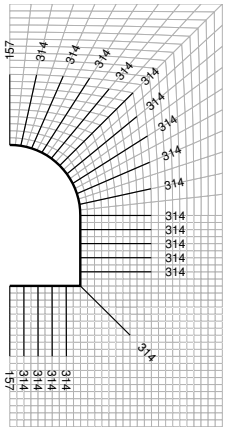

Figure 4.4: Initial bolt ditribution and the ground structure with bolt spacing of 1 m (GS10). As a symmetric model is shown in this figure, the half bolt areas of "157" are used for the bolts on the symmetry line.

Nonlinear material models are used to predict responses of the rock mass, shotcrete and rock bolts. The rock mass is modelled by the elasto plastic Mohr-Coulomb model described in §3.2. The shotcrete and rock bolts are assumed to be elastic perfectly-plastic. A non-associated flow rule Drucker-Prager model is used to govern the shotcrete behaviour with the yield function and the flow potential being defined as

$$F = t - p\tan\beta - d = 0 \tag{4.11}$$

$$G = t - p\tan\psi \tag{4.12}$$

where

$$t = \frac{1}{2}q\left[1 + \frac{1}{K} - \left(1 - \frac{1}{K}\right)\left(\frac{r}{q}\right)^3\right], \tag{4.13}$$

p is the mean stress, q the Mises stress, and K the ratio of yield stress in triaxial tension to yield stress in triaxial compression. β, ψ and d are the friction angle, dilation angle and cohesion of rock material, respectively (ABAQUS, 2013). The material properties of the rock mass, shotcrete lining and the rock bolts are summarised in Table 4.1.

The lower bound value of cross section areas ($\underline{a}$) is assigned to be zeros to allow complete elimination of unnecessary bolts and the upper bound value ($\overline{a}$) is $649 \times 10^{-6}\,\mathrm{m}^2$ (corresponding to the bolt diameter of 29 mm). No penalisation ($p = 1$) is applied in this example. The bolt volume constraint is selected as $34381\,\mathrm{mm}^2/\mathrm{m}$ (see Fig. 4.4). In this example, an *in situ* stress condition with vertical component of $\sigma_1 = 5\,\mathrm{MPa}$ and horizontal to vertical stress ratio of $k = 0.4$ is considered. The optimised results are depicted in Fig. 4.5.

Table 4.1: Properties of homogeneous rock and reinforcement materials

Material properties	Rock	Rockbolt	Shotcrete
Young modulus (GPa)	1.4	200	25
Poisson's ratio	0.3	0.3	0.2
Friction angle (°)	24	-	30
Dilation angle (°)	0	-	12
Cohesion (MPa)	0.3	-	3
Yield stress (MPa)	-	400	20

Fig. 4.5 displays the evolution of the bolt layouts with numbers at the end of bolts representing their cross section areas per unit length of the tunnel (mm^2/m) and the variation of the objective function. Since the tunnel is considered in plane strain condition, the obtained cross section areas per unit length can be converted to practical and appropriate spacings and sizes of bolts in three dimensions as noted before. It is noted that the plotted line width for each bolt is proportional to its cross section area. In order to demonstrate the plastic behaviour around the opening, plastic strain magnitudes defined as $\sqrt{\frac{2}{3}\varepsilon^{pl} : \varepsilon^{pl}}$ (where ε^{pl} is the plastic strain tensor) are shown by colour-filled contour lines with a colour-bar

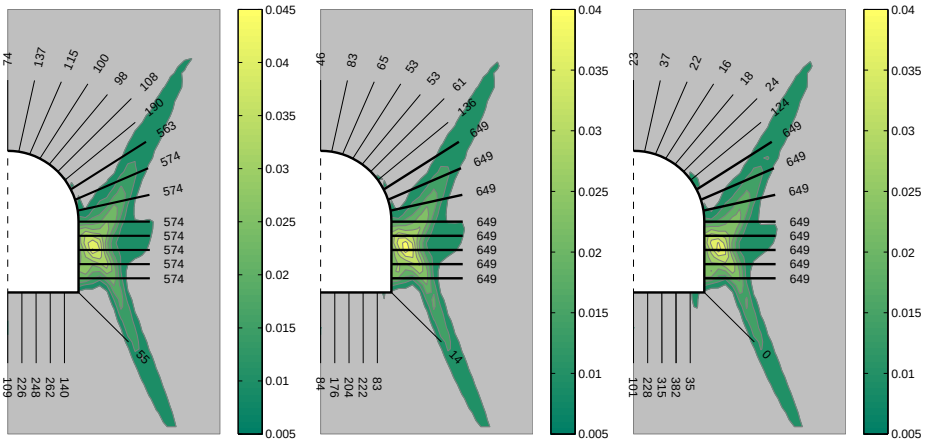

(a) Iteration 2 (b) Iteration 3 (c) Iteration 7

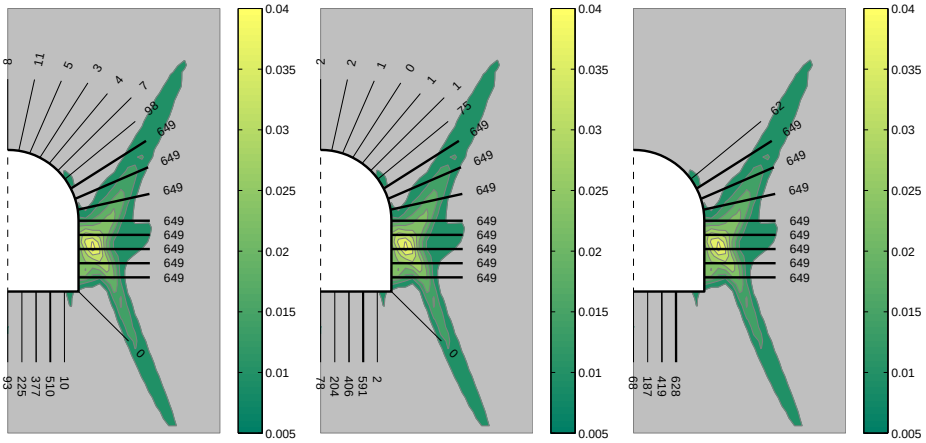

(d) Iteration 12 (e) Iteration 18 (f) Iteration 22 (final bolt layout)

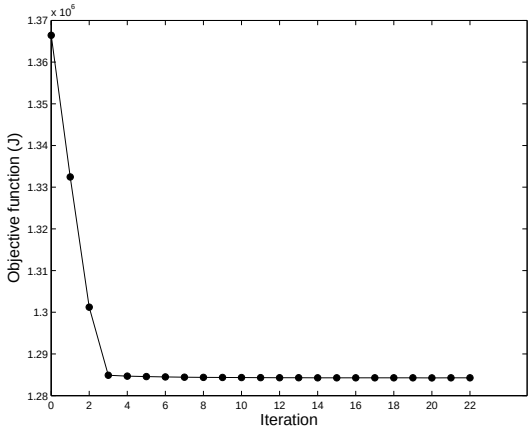

(g) Objective function variations

Figure 4.5: Bolt layouts and objective function variation for the case of $\sigma_1 = 5\,\text{MPa}$ and $k = 0.4$. Numbers at the end of bolts represent their cross section area per unit length of the tunnel in mm^2/m.

on its right to define the magnitudes. The elastic areas are coloured grey. It can be seen in the optimised bolt layout (Fig. 4.5f) that more bolts are placed at the tunnel ribs where the largest plastic strains are observed.

The initial external work of the model is 1.37 MJ. A decrease in the objective function is obtained before reaching the convergence at the external work of 1.28 MJ (Fig. 4.5g). Hence, 6% improvement of the objective function is achieved which demonstrates the advantage of the obtained result compared with the empirical design.

To illustrate and compare tunnel convergence under the initial uniform and the optimised bolt layouts, displacements around the opening are displayed in Fig. 4.6. It can be seen that the proposed bolt layout provides smaller displacements nearly everywhere around the cavity, particularly at the tunnel ribs where a considerable displacement reduction is obtained. In other words, the presented algorithm has redistributed the initially uniform bolt layout to a more effective one.

Further advantages of this approach will be pointed out via further examples by examining various *in situ* stresses and ground conditions. These examples will also demonstrate how this approach can be used to provide us with a better understanding of the effects of different factors on rock bolt design.

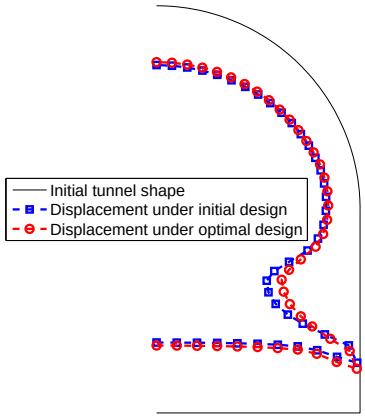

Figure 4.6: Tunnel displacements under uniform and optimised bolt layouts (tunnel deformation is multiplied by a factor of 25)

4.6 Effects of *in situ* stress conditions on rock bolt design

An investigation on effects of various *in situ* stress conditions on optimisation outcomes is conducted by varying magnitudes of vertical stress ($\sigma_1 = 3,\ 4,\ 5\,\text{MPa}$) and horizontal stress ratio ($k = 0.4,\ 1,\ 2$). A circular tunnel with a radius of 5 m is considered. The initial guess design is shown in Fig. 4.7. Other modelling and optimisation parameters are similar to the example described in §4.5. Fig. 4.8 displays all the obtained bolt layouts and the corresponding objective function variations.

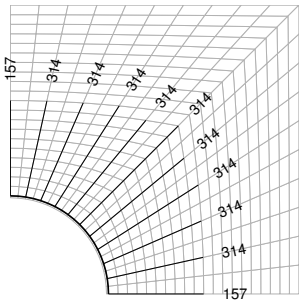

Figure 4.7: Initial design for circular tunnel

For the case of hydrostatic stress state ($k = 1$), as expected, bolts are mostly distributed evenly around the opening (Figs. 4.8b, 4.8e and 4.8h). For the case of $k = 0.4$, more bolts are observed in the horizontal direction (Figs. 4.8a, 4.8d and 4.8g). Finally, for the case of $k = 2$, bolts are distributed mostly in vertical direction (Figs. 4.8c, 4.8f and 4.8i). It can be clearly seen that bolts tend to be distributed more densely at regions with larger plastic strains.

With regards to the objective function variations, a stable convergence is observed in all cases (Fig. 4.8j). As expected, for the hydrostatic stress conditions, the optimised layouts are just slightly different from the initial design and small improvements of approximately 0.3% are obtained for the objective function. For the other stress states, higher improvements are achieved with the largest value of 4.8% observable for $\sigma_1 = 4\,\text{MPa}$ and $k = 0.4$. The magnitudes of initial and optimised objective functions and their relevant improvements are tabulated in Table 4.2 for all cases of stress states depicted in Fig. 4.8

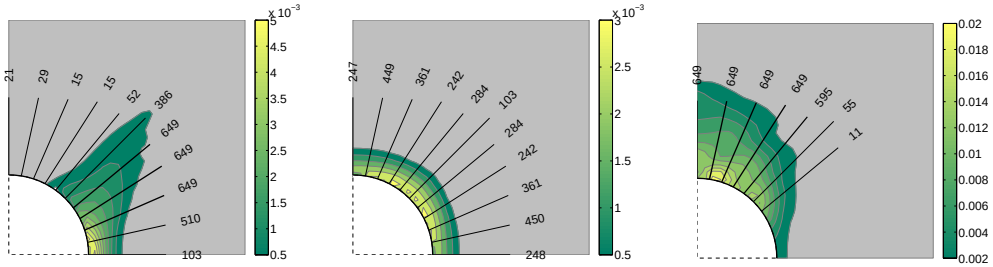

(a) $\sigma_1 = 3\,\text{MPa}$, $k = 0.4$ (b) $\sigma_1 = 3\,\text{MPa}$, $k = 1$ (c) $\sigma_1 = 3\,\text{MPa}$, $k = 2$

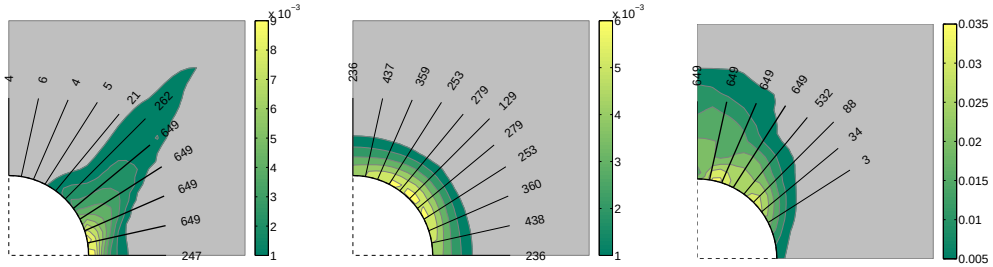

(d) $\sigma_1 = 4\,\text{MPa}$, $k = 0.4$ (e) $\sigma_1 = 4\,\text{MPa}$, $k = 1$ (f) $\sigma_1 = 4\,\text{MPa}$, $k = 2$

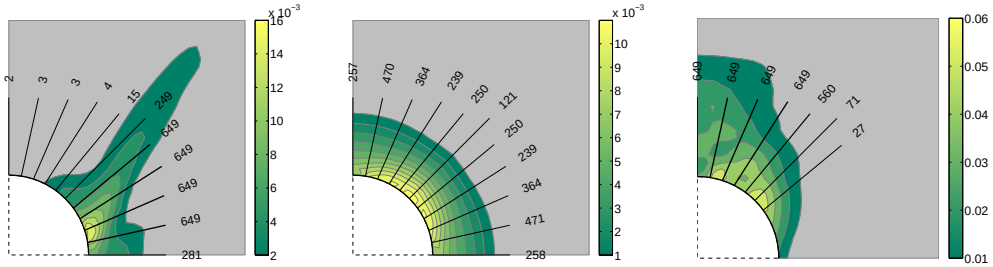

(g) $\sigma_1 = 5\,\text{MPa}$, $k = 0.4$ (h) $\sigma_1 = 5\,\text{MPa}$, $k = 1$ (i) $\sigma_1 = 5\,\text{MPa}$, $k = 2$

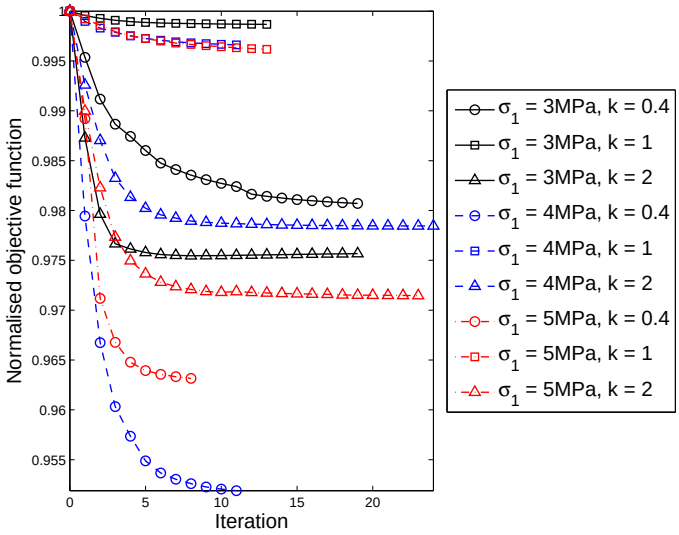

(j) Objective function variations

Figure 4.8: Effects of *in-situ* stress conditions on optimised reinforcement layouts

Table 4.2: Summary of the optimisation outcomes under various *in situ* stress conditions

In situ stress	Objective function		Improvement (%)
	Initial (J)	Optimised (J)	
$\sigma_1 = 3\,\text{MPa},\ k = 0.4$	135171	132563	1.9
$\sigma_1 = 3\,\text{MPa},\ k = 1$	191557	191302	0.1
$\sigma_1 = 3\,\text{MPa},\ k = 2$	907087	885019	2.4
$\sigma_1 = 4\,\text{MPa},\ k = 0.4$	297788	283463	4.8
$\sigma_1 = 4\,\text{MPa},\ k = 1$	422782	421350	0.3
$\sigma_1 = 4\,\text{MPa},\ k = 2$	2149557	2102266	2.2
$\sigma_1 = 5\,\text{MPa},\ k = 0.4$	467175	449962	3.6
$\sigma_1 = 5\,\text{MPa},\ k = 1$	830538	827360	0.4
$\sigma_1 = 5\,\text{MPa},\ k = 2$	4210250	4088152	2.9

4.7 Effects of penalisation on optimisation outcomes

In order to clearly show the role of the penalty factor (p) on optimisation outcomes, the example presented in Section 4.6 with the stress condition of $\sigma_1 = 4\,\text{MPa}$ and $k = 0.4$ is reconsidered with different values of penalty factor. The obtained optimised bolt layouts and variations of objective function are presented in Fig. 4.9.

By increasing the value of p from 1 to 3, the ineffective bolts are gradually eliminated, leading to a decline in the number of bolts (number of drillings) (Figs. 4.9a and 4.9b). For values of p between 3 and 7, the bolt layouts remain unchanged (Figs. 4.9b, 4.9c and 4.9d). Using these p values, the objective function converges at almost the same value (converged values are shown below each figure in Fig. 4.9). Once p reaches 8, a convergence problem occurs with fluctuation of objective function about the optimised value obtained with smaller penalty factors (Fig. 4.9f). As expected, this example shows that using penalisation might result in a reduction of bolt numbers. However, it is observed that convergence problems might occur with large values of p. Looking at the behaviour of different cases in Fig. 4.9f, the value of $p = 3$ seems to yield the best result in this example.

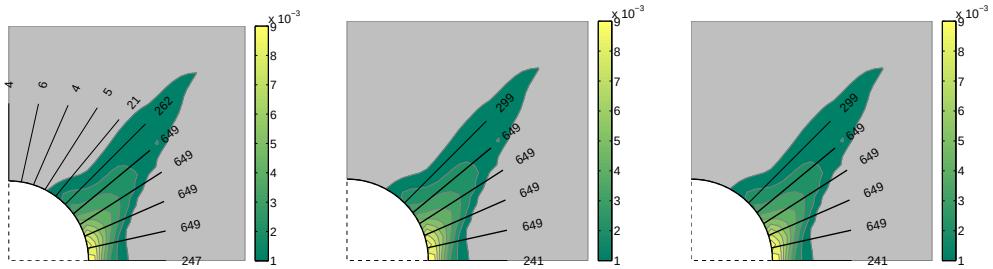

(a) $p = 1$
(converged at $283,463\,\mathrm{J}$)

(b) $p = 3$
(converged at $283,419\,\mathrm{J}$)

(c) $p = 5$
(converged at $283,419\,\mathrm{J}$)

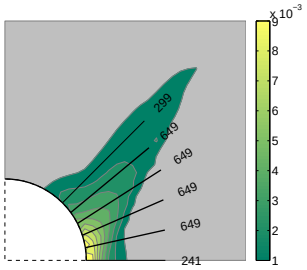

(d) $p = 7$
(converged at $283,420\,\mathrm{J}$)

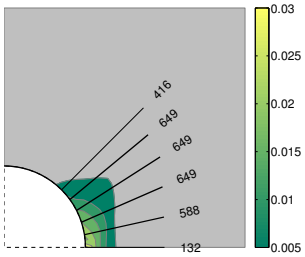

(e) $p = 8$ (not converged)

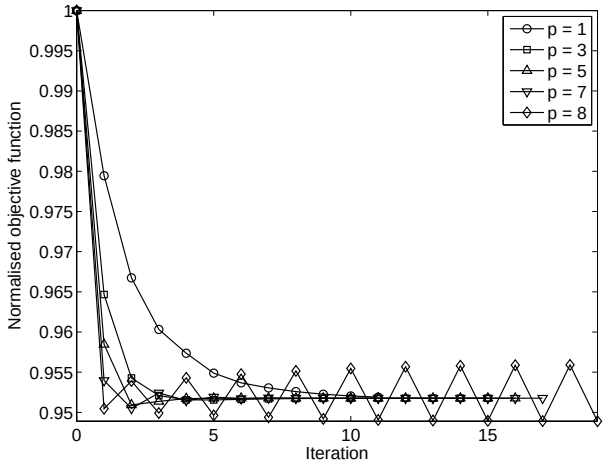

(f) Objective function variation

Figure 4.9: Effects of penalisation on optimised reinforcement outcomes ($\sigma_1 = 4\,\mathrm{MPa}$, $k = 0.4$)

4.8 Effects of ground structure density on optimisation outcomes

Along with the ground structure GS10 introduced in §4.5, two other ground structures with different densities are generated to investigate their effects on the optimisation outcomes. One is with the bolt spacing of 0.5 m (codenamed GS05) as shown in Fig. 4.10a and the other one with the spacing of 1.5 m (codenamed GS15) as shown in Fig. 4.10b.

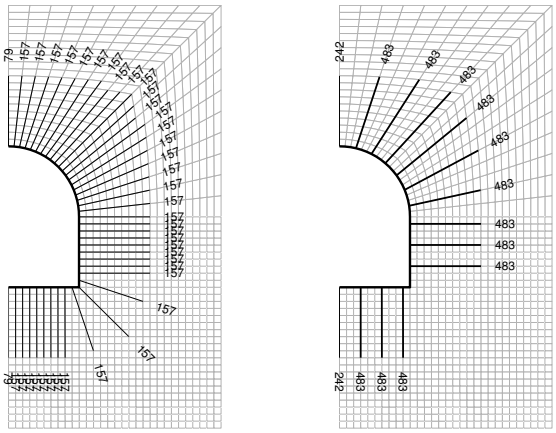

(a) GS05 (b) GS15

Figure 4.10: Ground structures with bolt spacings of 0.5 m (GS05) and 1.5 m (GS15)

The *in situ* stress condition of $\sigma_1 = 3\,\text{MPa}$ and $k = 0.4$ is investigated and the obtained outcomes are detailed in Fig. 4.11 and Table 4.3.

Table 4.3: Summary of the optimisation outcomes for different ground structure densities ($\sigma_1 = 3\,\text{MPa}$, $k = 0.4$)

Ground structure	Objective function		Improvement (%)
	Initial (J)	Optimised (J)	
GS05	344021	314947	8.4
GS10	344098	327392	4.8
GS15	343410	336584	2

It can be seen that qualitatively the optimised bolt layouts are almost similar for different ground structure densities (Fig.4.11a, 4.11b and 4.11c) with more bolts observed at the tunnel floor and tunnel ribs. However, various bolt densities result in various levels of improvements in the objective function. As tabulated

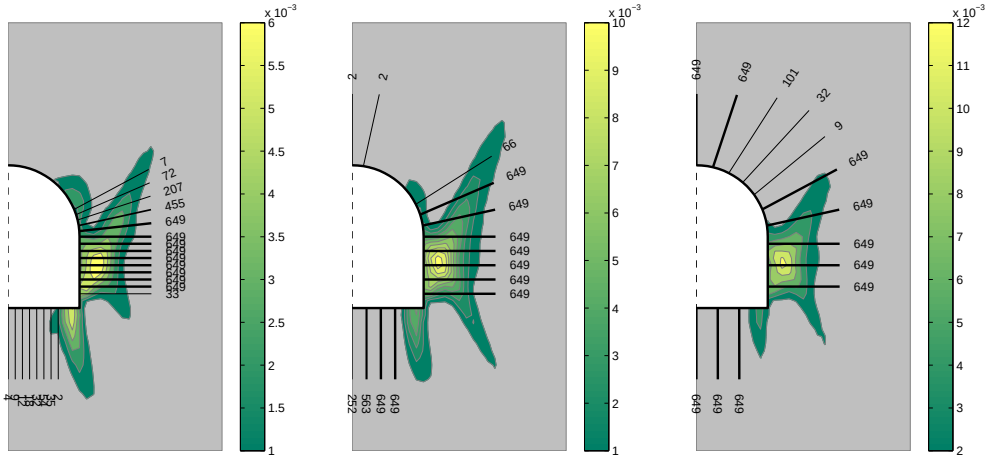

(a) GS05 (b) GS10 (c) GS15

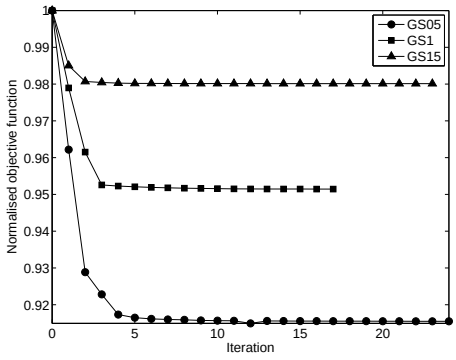

(d) Objective function variation

Figure 4.11: Effects of ground structure density on optimised reinforcement outcomes ($\sigma_1 = 3\,\text{MPa}$, $k = 0.4$)

in Table 4.3, there is not much difference in the initial values of external work for the three ground structures. Nevertheless, the objective function improvements are considerably different. While 8.4% and 4.8% improvements in the objective function are achieved for the ground structures GS05 and GS10, respectively, only 2% improvement is obtained for GS15. This is expected as denser ground structures provide more freedom and more choices to the optimisation algorithm to chose from. Therefore, to obtain higher improvements, it is beneficial to use a denser ground structure. However, in practice choosing a very small bolt spacing might result in damage around bearing plates due to stress concentration and also introduce more drilling work.

4.9 Effects of rock material on optimised bolt layout design

Rock mass is naturally discontinuous with fractures, cracks, bedding planes, etc. A thorough consideration of fractures is necessary to obtain a more accurate model and hence a more reliable tunnel reinforcement design. To demonstrate the efficacy of the proposed approach for different material models, here a heavily jointed rock mass with highly densed parallel joint surfaces in different orientations is considered. A jointed material model supported in Abaqus 6.11 library is employed to describe the jointed rock mass behaviour. The jointed material model involves two governing behaviours for the bulk material and the joint systems (ABAQUS, 2013). Bulk material is governed by the Drucker-Prager model. Additionally, the jointed material model includes a failure surface due to sliding in joint system a, which is expressed as

$$f_a = \tau_a - p_a \tan \beta_a - d_a = 0 \tag{4.14}$$

where τ_a is the shear stress magnitude resolved on the joint surface. p_a is normal pressure stress acting on the joint. β_a and d_a are the friction angle and cohesion for system a, respectively.

Replacing the homogeneous model by the above jointed material model, the tunnel geometry investigated in Section 4.5 is reconsidered here. Two models, one

with a horizontal set of joints and one with a vertical set of joints, are explored. Properties of the bulk material and the joint systems are identified in Table 4.4.

Table 4.4: Properties of jointed rock

Material properties	Bulk material	Joint surface
Young modulus (GPa)	5	-
Poisson's ratio	0.3	-
Friction angle (°)	35	26
Dilation angle (°)	5	12
Cohesion (kPa)	6×10^3	70

Fig. 4.12 displays the optimised bolt layouts for the cases of horizontal joints and vertical joints. It can be seen that the introduction of joint systems has altered the plastic strain and optimised bolt distributions around the opening. For the horizontal joints (Fig. 4.12a), the bolts are only present at the tunnel crown and tunnel floor. On the other hand, for the case of vertical joints (Fig. 4.12b), the bolts are concentrated at the corner of the tunnel crown and the tunnel ribs, and at the tunnel floor. Objective function values and obtained improvements are demonstrated in Fig. 4.12c and Table 4.5.

Table 4.5: Summary of the optimisation outcomes for different rock joint sets ($\sigma_1 = 5\,\text{MPa}$, $k = 0.4$)

Ground condition	Objective function		Improvement (%)
	Initial (J)	Optimised (J)	
Rock mass with horizontal joints	218925	216038	1.3
Rock mass with vertical joints	258340	255437	1.1

4.10 Effects of bedding plane on optimised bolt layout

This section aims to explore the effects of a bedding plane presence on optimised bolt layouts. The tunnel investigated in Section 4.5 is considered with the existence of a bedding plane at 1.5 m above the tunnel crown. A surface-based contact supported by Abaqus 6.11 is employed to model the interactions of surfaces. The mechanical behaviour of the surface interaction is governed by the Coulomb friction model in which the coefficient of friction (μ) is defined as the ratio between a shear stress and a contact pressure. A hydrostatic stress condition with a vertical

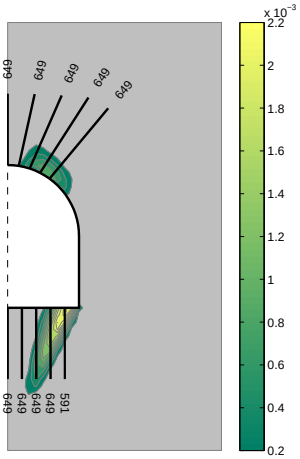

(a) Horizontal joints

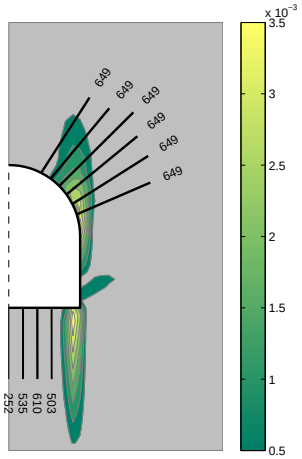

(b) Vertical joints

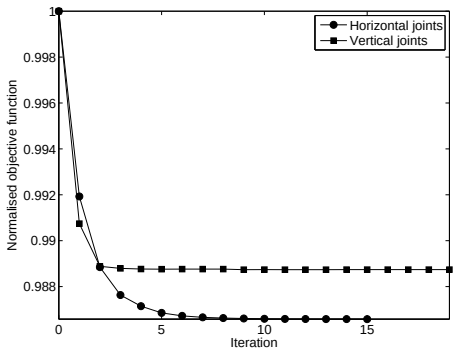

(c) Objective function variation

Figure 4.12: Effects of rock material on optimised reinforcement outcomes ($\sigma_1 = 5\,\text{MPa}$, $k = 0.4$)

stress of 5 MPa and two friction angles (ϕ) of the bedding plane, 5° and 15°, are investigated. Fig. 4.13 displays the achieved optimised bolt layouts and Table 4.6 tabulates the initial and final values of the objective function.

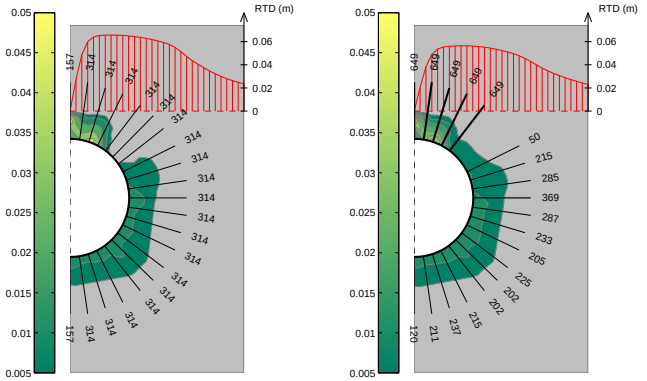

(a) Initial Design, $\phi = 5°$

(b) Optimised bolt layout, $\phi = 5°$

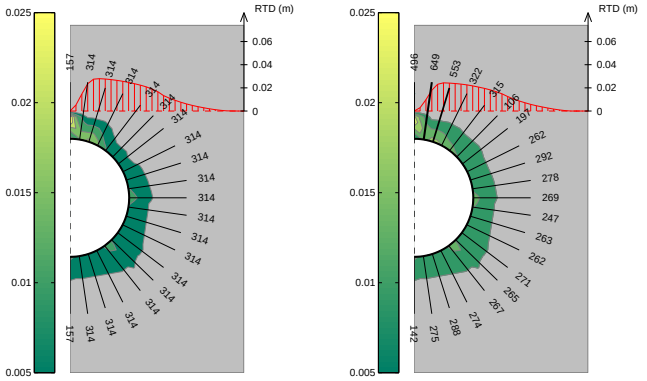

(c) Initial Design, $\phi = 15°$

(d) Optimised bolt layout, $\phi = 15°$

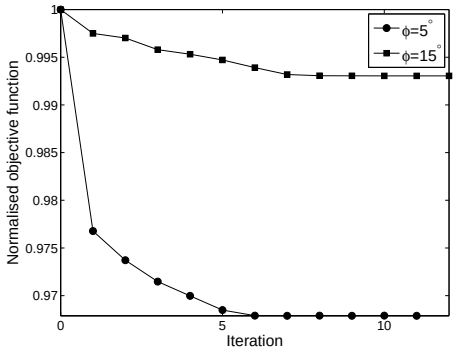

(e) Objective function variation

Figure 4.13: Effects of bedding planes on optimised reinforcement outcomes ($\sigma_1 = 5$ MPa, $k = 1$)

It can be generally seen that with both values of friction angle, more bolts are distributed at the top of the tunnel where the bedding planes are located than

Table 4.6: Summary of the optimisation outcomes considering bedding planes ($\sigma_1 = 5\,\text{MPa}$, $k = 1$)

Friction angle	Objective function		Improvement (%)
	Initial (J)	Optimised (J)	
$\phi = 5°$	1400179	1355220	3.2
$\phi = 15°$	1176049	1167870	0.6

the other positions around the opening (Figs. 4.13b and 4.13d). Also, the bolt volume at the tunnel crown of the case of friction angle of $\phi = 5°$ is more than that of the friction angle of $\phi = 15°$. In order to display slippage along the bedding planes, relative tangential displacement (RTD) is illustrated for the initial and the optimised bolt layouts. Clearly, the concentration of more bolts at the tunnel top areas has reduced slippage along the bedding planes; especially for the case of friction angle of $\phi = 5°$. Additionally, further improvements of the objective functions are obtained as displayed in Fig. 4.13e and summarised in Table 4.6. Consequently, it can be concluded that the effects of the bedding planes can be effectively captured by the proposed method.

4.11 Summary

By explicitly modelling the rock bolts, the proposed approach is capable of providing clearer, more accurate, more effective and more practical reinforcement layouts compared to the earlier works in this area. An incorporation of an optimisation technique and numerical analysis has made the presented method a significant improvement and a potential tool in tunnel reinforcement design.

The proposed optimisation algorithm is independent of material models and thus the complexity of the models adopted in this approach is only limited to the capabilities of the method used for analysis. Furthermore, as the sensitivities are directly calculable from displacements, any analysis method which can provide the values of displacements under different loadings can be easily adopted in this approach. Nonlinear behaviour of both reinforcement material and rock in homogeneous media and fractured rock mass have been considered in the presented examples and finite element method is used as the method of analysis.

It has been shown that this approach can be effectively used to study and improve our understanding of effects of different parameters on optimised bolt layouts. The examples demonstrated that the commonly-employed empirical method where a uniform distribution of bolts is used is not necessarily optimal and can be further improved by the proposed approach. In the considered examples, reductions of up to 8% have been reported in the value of external work which was selected as the objective function.

In this chapter, the effects of ground structure and penalisation factor are demonstrated through some examples. In addition, the impacts of *in situ* stresses, rock material properties and geological features such as bedding planes on optimised solutions are studied via several examples.

The proposed optimisation algorithm determines various bolt sizes around the opening to satisfy the given objective function while the bolt pattern has not been taken into account. In order to obtain an even more effective bolt design, all bolt parameters including size and pattern should be accounted for in an optimisation algorithm. The next chapter will focus on studying a simultaneous optimisation of bolt size and pattern to propose a more powerful bolt design approach.

Chapter 5

Simultaneous Optimisation of Rock Bolt Size and Pattern

The work in this chapter has been accepted for publication as a journal paper by Nguyen et al. (2015a)

5.1 Overview

The optimisation approach proposed in the chapter 4 provides an optimised distribution of the bolt sizes around the opening. It has been shown that the effects of ground conditions (see §4.10) can also be taken into account by distributing more bolt volume at more critical conditions. Nevertheless, in a more advanced scenario with presence of more complex discontinuities in rock, bolt pattern, i.e. length and orientation of the bolts, needs to be optimised to capture the ground condition effects and obtain a more reasonable and practical design.

In this chapter, an optimisation method is proposed to simultaneously optimise bolt size and pattern. In addition to the benefits discussed in chapter 4, this advanced optimisation approach would provide further objective function improvement and especially capture various complex ground conditions in a bolt design.

5.2 Design variables

Using a reinforcement system with rock bolts and shotcrete, the modelling approach described in §4.2 is employed in this chapter. Here, a conservative value of $\beta = 0.3$ is selected in the second step to simulate the convergence of the opening before introducing reinforcement materials.

The location of the end point of the bolts as well as their cross section areas are considered as design variables. We denote the location of the end point of bolt b by the coordinates (x_b, y_b) and its cross section area by a_b. The number of bolts is denoted by m. It should be noted that by allowing a_b to take the value of zero, it is possible to remove the bolt b from the design and hence change the spacing between its adjacent bolts. It is also noted that by controlling (x_b, y_b) both length and orientation of the bolt b are controlled. Hence using these three variables per each bolt we can completely define the rock bolt design around the opening.

Altogether we have $3m$ design variables. We define the design variable vectors as

$$\begin{aligned} \mathbf{x} &= [x_1, x_2, \ldots, x_m]^T \\ \mathbf{y} &= [y_1, y_2, \ldots, y_m]^T \\ \mathbf{a} &= [a_1, a_2, \ldots, a_m]^T \end{aligned} \tag{5.1}$$

and also introduce the length vector $\mathbf{l} = [l_1, l_2, \ldots, l_m]^T$ in which l_b is a function of x_b and y_b. The total volume of bolts can now be expressed as

$$V_R = \mathbf{l} \cdot \mathbf{a} \tag{5.2}$$

To simplify the modelling process in the finite element method, it is preferable to limit the possible locations of the end points (x_b, y_b) to a suitable subset of the available nodes of the finite element mesh. Such a suitable set of allowable end points for each bolt can be defined based on its allowable range of angles and lengths (Fig. 5.1).

In topology optimisation, the collection of all allowable sets for all elements in

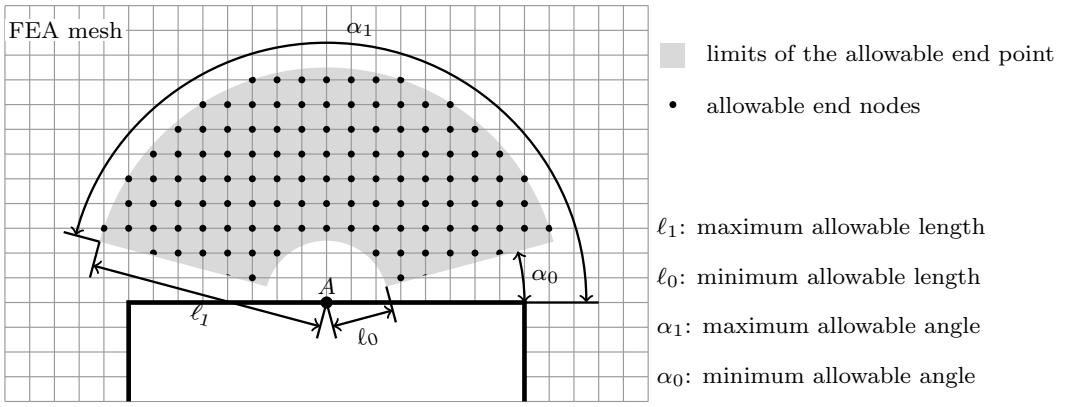

Figure 5.1: An example of finding a suitable set of allowable end points for a bolt emerging from point A.

a problem is usually referred to as the *ground structure* (Bendsøe and Sigmund, 2003). The allowable set of end nodes helps us develop a ground structure for the problem. A number of nodes along the boundary of the opening are considered as first nodes of bolts. For each of these potential nodes a sub-ground structure is determined as a group of bolt elements emerging from this node and ending at one of the corresponding allowable end nodes in the design domain. Merging all the sub ground structures, one obtains the ground structure for the problem. The ground structure shows the range of all possible solutions in the optimisation problem. Fig. 5.2 shows an example of a ground structure and one of its sub-ground structures for a tunnel rock bolt design problem.

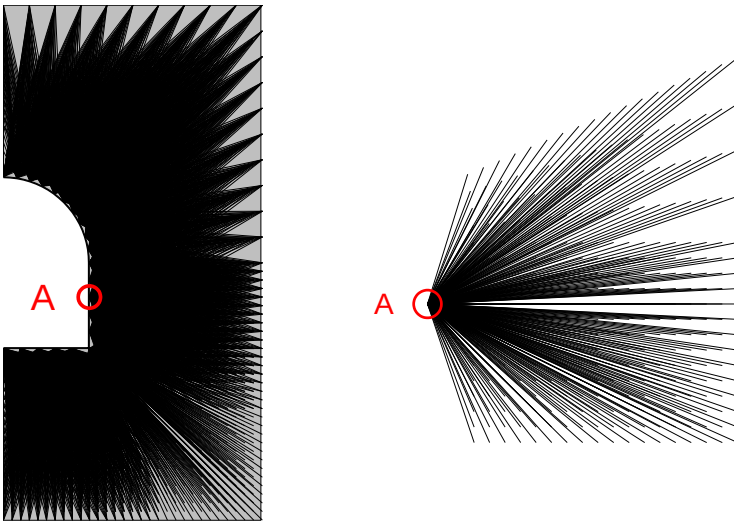

(a) Ground structure (b) Sub ground structure

Figure 5.2: Ground structure and sub-ground structure for the bolt having the first node at A.

Minimum bolt length is selected as 1.5 m in this study. The maximum length of bolts are selected such that all the bolts fall within a 30 m × 30 m square which is considered as the *design domain* of the optimisation problem. Half of the design domain is depicted in Fig. 5.2a as a shaded rectangle.

5.3 Objective function and problem statement

As a continuation of the work presented in the chapter 4, the same optimisation problem (see §4.3) is solved herein. In addition to working on bolt size optimisation, the proposed optimisation method in this chapter would provide a general optimisation of both size and pattern of the bolts. The optimisation algorithm solves the problem iteratively. Each iteration involves analysing the model using Finite Element Method, calculating the sensitivities (detailed in section 5.4), updating the design variables (detailed in section 5.5) and subsequently creating a new model for the next iteration. This process continues until a predefined convergence criterion is met. In this work, convergence is assumed when either relative changes in the design variables in two consecutive iterations is less than 1×10^{-4} or the improvement in the objective function is negligible (Eq. (3.33)).

5.4 Sensitivity analysis

From Eq. (4.6) in which the variable α_b is replaced by a general variable ξ and Eq. (4.7), it can be seen that the sensitivity numbers depend on the internal force vector in rock bolt which in turn depends on a and $\mathbf{D}$. By solving the problem with respect to a, obviously cross section areas of the bolts can be optimised. On the other hand, noting that $\mathbf{D}_b$ depends on the location of the end points of bolt b, dealing with $\mathbf{D}$ one can optimise lengths and orientations of the bolts. Sensitivity analyses with respect to cross section areas of the bolts has been presented in §4.4. Sensitivity analysis with respect to lengths and orientations of the bolts is detailed below.

5.4.1 Sensitivity analysis for lengths and orientations of the bolts

As noted previously, a ground structure is used to capture all possible lengths and orientations of different bolts. Based on the discrete nature of this part of the problem, a switching procedure is followed to update length and orientation of bolts.

For simplicity we assume a continuous linear interpolation scheme based on a normalised variable $0 \leq t_b \leq 1$ as follows

$$\mathbf{D}_b(t_b) = t_b \mathbf{D}_b^e, \quad b = 1, \ldots, m' \tag{5.3}$$

where $m' \gg m$ is the number of all potential bolt elements in the ground structure. $\mathbf{D}_b^e$ is the stress-strain matrix of bolt b if it is present in the model. We have $\mathbf{D}_b = \mathbf{0}$ for $t_b = 0$ which represents the non-existing potential bolts in the ground structure and $\mathbf{D}_b = \mathbf{D}_b^e$ for $t_b = 1$ which represents the existing bolts.

From Eq. (4.7) and Eq. (5.3), we have

$$\frac{\partial \mathbf{p}^S}{\partial t_b} = a_b \mathbf{D}_b^e \boldsymbol{\varepsilon}_b = \mathbf{p}_b^{eS}, \quad b = 1, \ldots, m' \tag{5.4}$$

Here $\mathbf{p}_b^{eS}$ is the internal force vector of bolt b if it is in the model. We clearly have $\mathbf{p}_b^{eS} = \mathbf{p}_b^S$ if b is an existing bolt (see Eq. (4.7)).

Substituting Eq. (5.4) and Eq. (4.5) into Eq. (3.15) and setting $x = t_b$, one obtains

$$\frac{\partial W}{\partial t_b} = \lim_{n \to \infty} \frac{1}{2} \sum_{i=1}^{n} (\mathbf{u}_i - \mathbf{u}_{i-1}) \cdot \left(\mathbf{p}_{b_i}^{eS} + \mathbf{p}_{b_{i-1}}^{eS} \right) = \Pi_b^e, \quad b = 1, \ldots, m' \tag{5.5}$$

where Π_b^e is the total strain energy of bolt b if it was present in the model. If b is an existing bolt, we have $\Pi_b^e = \Pi_b$.

It is important to note that in deriving these sensitivity numbers (Eq. (4.9) and Eq. (5.5)) we did not apply any assumption on the material model used. Hence, these results are applicable for all material models. It is also interesting to note that the sensitivities in both cases only depend on the strain energy results of the considered element which makes them very cheap to calculate.

5.5 Variable updating schemes

As noted earlier, the design variables are updated in two separate steps. In the first step of optimisation, the stress-strain matrix $\mathbf{D}$ is fixed while the cross section areas (a) are optimised. The updating scheme of the bolt size is already explained in §2.7.2 (Eq. (2.18)). In the second step, the values of matrices $\mathbf{D}$ are updated. The next section presents the updating scheme for lengths and orientations.

5.5.1 Updating lengths and orientations

A switching procedure is employed to find the best possible end node for each bolt. In this step, each bolt is updated separately. Sensitivity of each potential alternative for a bolt is evaluated using Eq. (5.5). This requires calculation of Π_b^e for each potential bolt b. For the existing bolts we have $\Pi_b^e = \Pi_b$ whose value is directly obtainable from the results of the finite element analysis. For the non-existing bolts, this value can be calculated based on the displacement results. Here an elastic-perfectly plastic material model is assumed for the rock bolts. Based on this model, we have

$$\Pi_b^e = \begin{cases} \frac{a_b E \delta_b^2}{2 l_b}, & \text{for } \delta_b \leq \delta_{Yb} = \frac{\sigma_Y l_b}{E} \\ a_b \sigma_Y \left(\delta_b - \frac{l_b \sigma_Y}{2E} \right), & \text{otherwise} \end{cases} \tag{5.6}$$

where σ_Y and E are the yield stress and elastic modulus of the bolt material respectively. δ_{Yb} is the elongation at which bolt b yields.

In the optimisation problem Eq. (4.1), we also have a volume constraint that needs to be satisfied. To make sure that switching bolts will not change the total volume, we need to adjust the cross section area of all the potential alternatives based on their lengths. This is similar to considering the strain energy density instead of the strain energy as the switching control parameter. The strain energy

density for bolt b can be expressed in the following form

$$\pi_b^e = \frac{\Pi_b^e}{V_b} = \begin{cases} \frac{E\delta_b^2}{2l_b^2}, & \text{for } \delta_b \leq \delta_{Yb} = \frac{\sigma_Y l_b}{E} \\ \sigma_Y \left(\frac{\delta_b}{l_b} - \frac{\sigma_Y}{2E} \right), & \text{otherwise} \end{cases} \tag{5.7}$$

where $V_b = a_b l_b$ denotes the volume of the bolt b.

Switching bolt i with bolt j is modelled by changing the value of t_i from 1 to 0 and the value of t_j from 0 to 1. The change in the objective function due to this switching (noting the volume adjustment explained above) can be approximated as follows

$$\Delta W \approx \frac{\partial W}{\partial t_i}\Delta t_i + \frac{\partial W}{\partial t_j}\Delta t_j = \Pi_i^e - \Pi_j^e = (\pi_i^e - \pi_j^e)V_i$$

To minimise W we need $\pi_j^e > \pi_i^e$. Hence, among all different potential alternatives for a rock bolt, the one with the highest value of π^e is the most efficient to be used and switching to it will result in the largest drop in the value of the objective function.

In the second step of updating, the optimisation algorithm goes through all the bolts one by one and switches them for their best potential alternative which is the one with the largest value of strain energy density. This switching procedure ensures that the objective function is decreasing and also the volume constraint is not violated.

The flowchart of the optimisation process is depicted in Fig. 5.3.

Note that in Eq. (5.6), δ_b is the only parameter which needs to be obtained through mechanical analysis of the model. This means that all the required sensitivities are calculable as long as one can obtain the displacement results for all the end nodes of all potential bolts. This makes the proposed optimisation approach extremely flexible: as long as one can provide the nodal displacement results for the design domain, irrespective of the method used for it, the proposed optimisation approach can be used to optimise the rock bolt design. As mentioned before, in this study we use finite element method for mechanical analysis of the model, but as just noted the optimisation method can as well be linked with any other suitable mechanical analysis method.

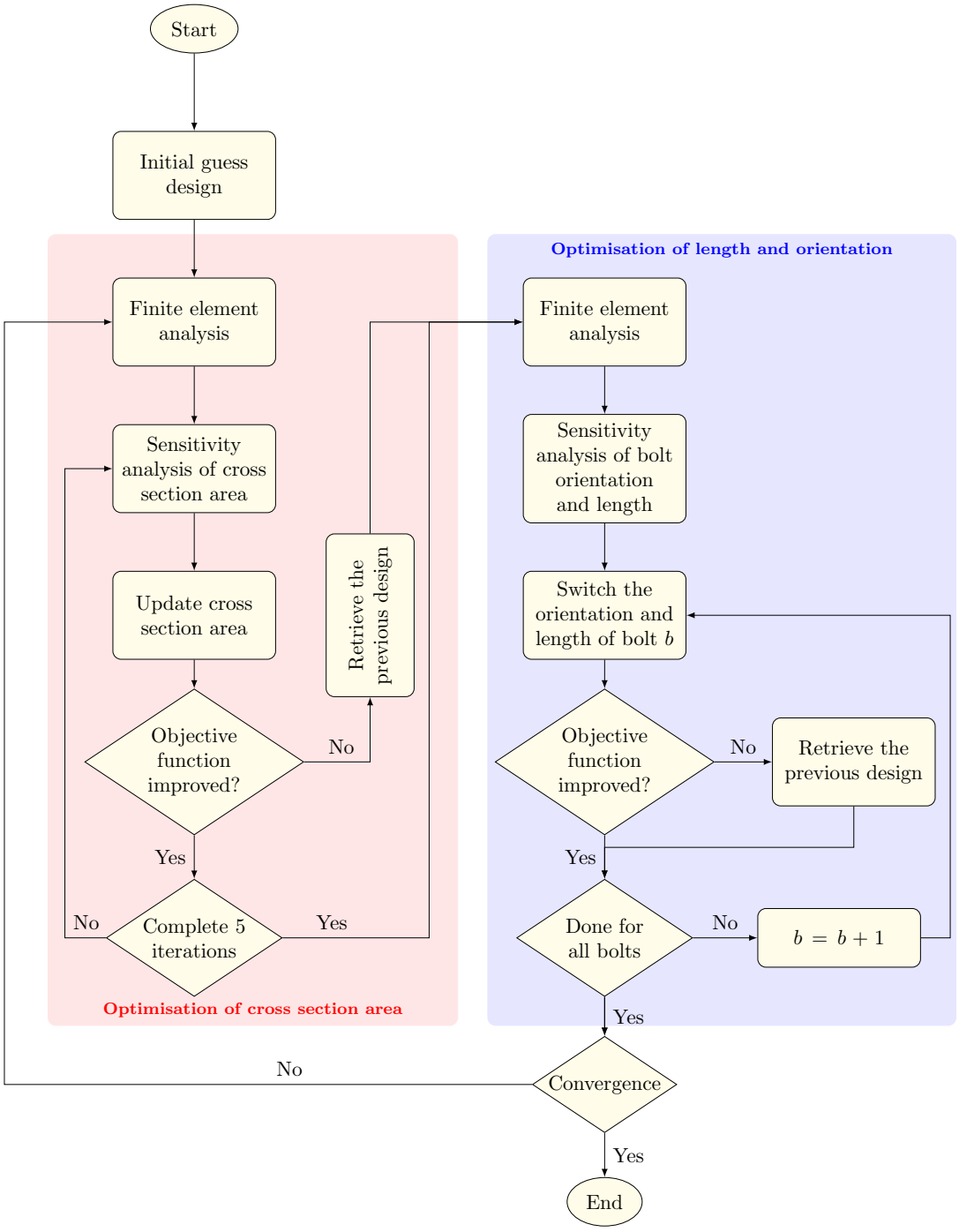

Figure 5.3: Flowchart of the proposed approach.

5.6 A basic example

The tunnel with initial bolt layout (Fig. 4.4) and material models described in §4.5 is also used in this example. The main material parameters used are summarised in Table 5.1. These input parameters will also be adopted in other examples in the following sections.

Table 5.1: Properties of rock and reinforcement materials

Material properties	Rock	Rockbolt	Shotcrete
Young modulus (GPa)	1.4	200	25
Poisson's ratio	0.3	0.3	0.2
Friction angle (°)	27	-	30
Dilation angle (°)	0	-	12
Cohesion (MPa)	0.3	-	3
Yield stress (MPa)	-	400	20

A hydrostatic *in situ* stress condition (horizontal to vertical stress ratio of $k = 1$) with a vertical stress of $\sigma_1 = 3\,\text{MPa}$ is investigated and the achieved optimisation outcomes are displayed in Fig. 5.4. To demonstrated the plastic zones around the opening, the plastic strain magnitudes computed as $\sqrt{\frac{2}{3}\boldsymbol{\varepsilon}^{pl} : \boldsymbol{\varepsilon}^{pl}}$ (where $\boldsymbol{\varepsilon}^{pl}$ is the plastic strain tensor) are illustrated by colour-filled contour lines.

In the displayed bolt configurations (Figs. 5.4a-5.4h), the values of bolt cross section areas are noted at the end of the bolts. As noted before, these values are actually cross section area required per unit length of the tunnel. Based on available bolt sizes and machinery, one can chose the required spacing along the longitudinal tunnel axis to satisfy the required cross section areas per length.

Generally, it can be observed that more bolts are distributed at the tunnel ribs and the tunnel floor which are experiencing larger and more widespread plastic strains. The bolts on the arched tunnel crown, on the other hand are generally shortened and weakened. This result matches the well-known supporting effect of arched roofs.

At the tunnel crown, the bolt orientations are almost similar to the initial layout with the radial alignment. On the other hand, in the optimised pattern, the bolts are not normal to the tunnel faces at the tunnel floor and the tunnel ribs.

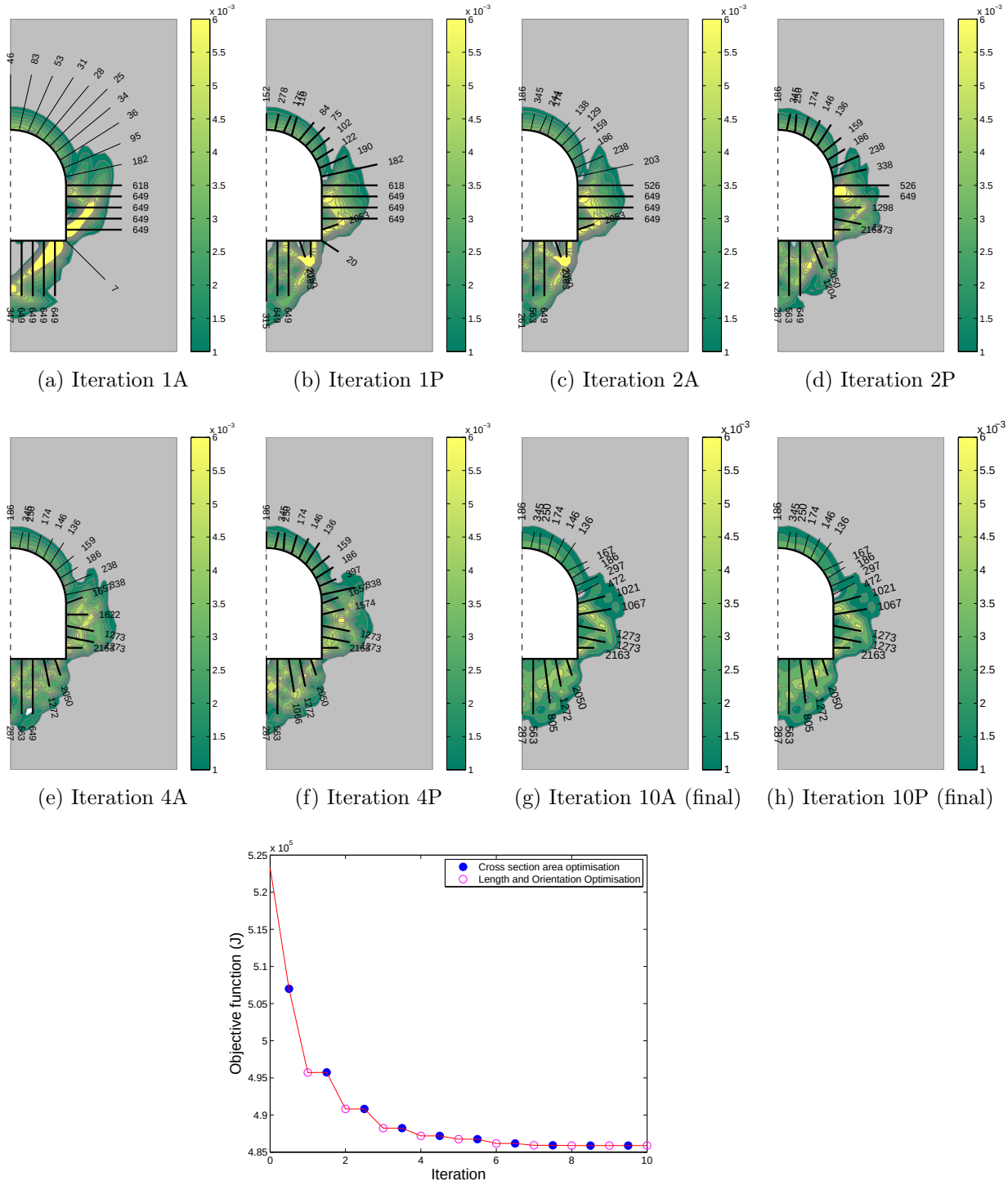

(a) Iteration 1A (b) Iteration 1P (c) Iteration 2A (d) Iteration 2P

(e) Iteration 4A (f) Iteration 4P (g) Iteration 10A (final) (h) Iteration 10P (final)

(i) Objective function variations

Figure 5.4: Optimised bolt layout and objective function variations for the case of $\sigma_1 = 3\,\text{MPa}$ and $k = 1$. Numbers at the end of bolts represent their cross section areas per unit length of the tunnel in mm^2/m. ("A" stands for area optimisation and "P" stands for patern optimisation)

Also, various bolt lengths are observed at various positions along these faces. It is expected that the shape of the opening is one of the main factors determining the optimal bolt layout. The effects of the tunnel shape on optimised bolt designs will be investigated in the Section 5.7.

Fig. 5.4i shows the evolution of the objective function with a gradual reduction before reaching the convergence. The external work of the initial bolt design is $523,254\,\mathrm{J}$, whereas that of the optimised bolt configuration is $485,880\,\mathrm{J}$. An improvement of 7.1% is hence achieved, verifying the effectiveness of the proposed optimisation algorithm.

In order to clearly differentiate between the improvement components obtained by cross section area optimisation and length and orientation optimisation, these steps are marked differently. In Fig. 5.4i and also in all the following figures depicting objective function variations, filled markers are used for the cross section area optimisation and hollow markers are used for length and orientation optimisation. It can be observed that initially the cross section area optimisation played a significant role in improving the design (lowering the objective function), but after that it was mainly the length and layout optimisation that improved the design. This of course demonstrates the significance of considering both bolt size and pattern in optimisation.

Apart from the value of the objective function, it is clearly observable that the optimised design reduced the plastic zone as well. In particular, the areas with large plastic strain magnitudes are significantly reduced in the optimised design. To further compare the initial uniform bolt layout and the optimised one, displacement profiles of the opening are displayed in Fig. 5.5 under each design. At the tunnel crown, the opening displacements for these two designs are almost similar. However, a significant reduction in tunnel convergence is recorded at the tunnel ribs and the tunnel floor. These observations can further approve the superiority of the optimised design over the initial one. This means that the uniform bolt layout advised by empirical methods is not necessarily optimal.

The proposed method can be used to provide optimised and improved bolt designs for different situations. We can thus use it to capture the effects of different

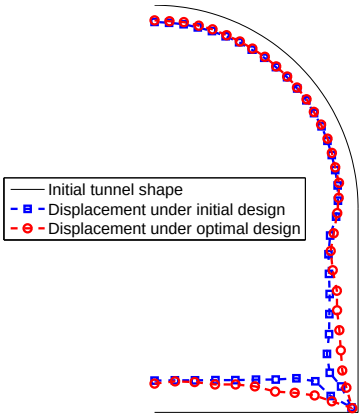

Figure 5.5: Tunnel displacements under uniform and optimised bolt layouts (the tunnel deformation is multiplied by a factor of 10).

crucial factors on tunnel reinforcement design, e.g. tunnel features and geological conditions. The following sections will explore the impacts of these factors on optimal bolt designs.

5.7 Studying the effects of tunnel shape on optimal bolt configurations

To investigate the effects of tunnel shape on the optimisation outcomes, different opening shapes are considered as shown in Fig. 5.6. A uniform bolt distribution is assumed as the initial design (Figs. 5.6a-e). Using symmetry, a quarter model is used for the circular (shape 1) and the square (shape 5) tunnels and a half model is used for the other shapes (shapes 2, 3 and 4). A hydrostatic stress condition ($k = 1$) with a stress magnitude of 3 MPa is assumed for all cases. Figs. 5.6f-j show the obtained optimised bolt configurations and Table 5.2 reports the initial and final values of the objective function.

In the case of the circular tunnel, as expected the bolt volume is distributed almost evenly around the opening (Fig. 5.6f). In other cases, there is a noticeable difference between the initial and the optimised bolt design. It is interesting to note that generally larger bolt volumes are required along the straight faces and/or curved faces with larger radius compared to faces with smaller radius (see Figs. 5.6g, 5.6h, and 5.6i). Another noticeable point is that the corner bolts are

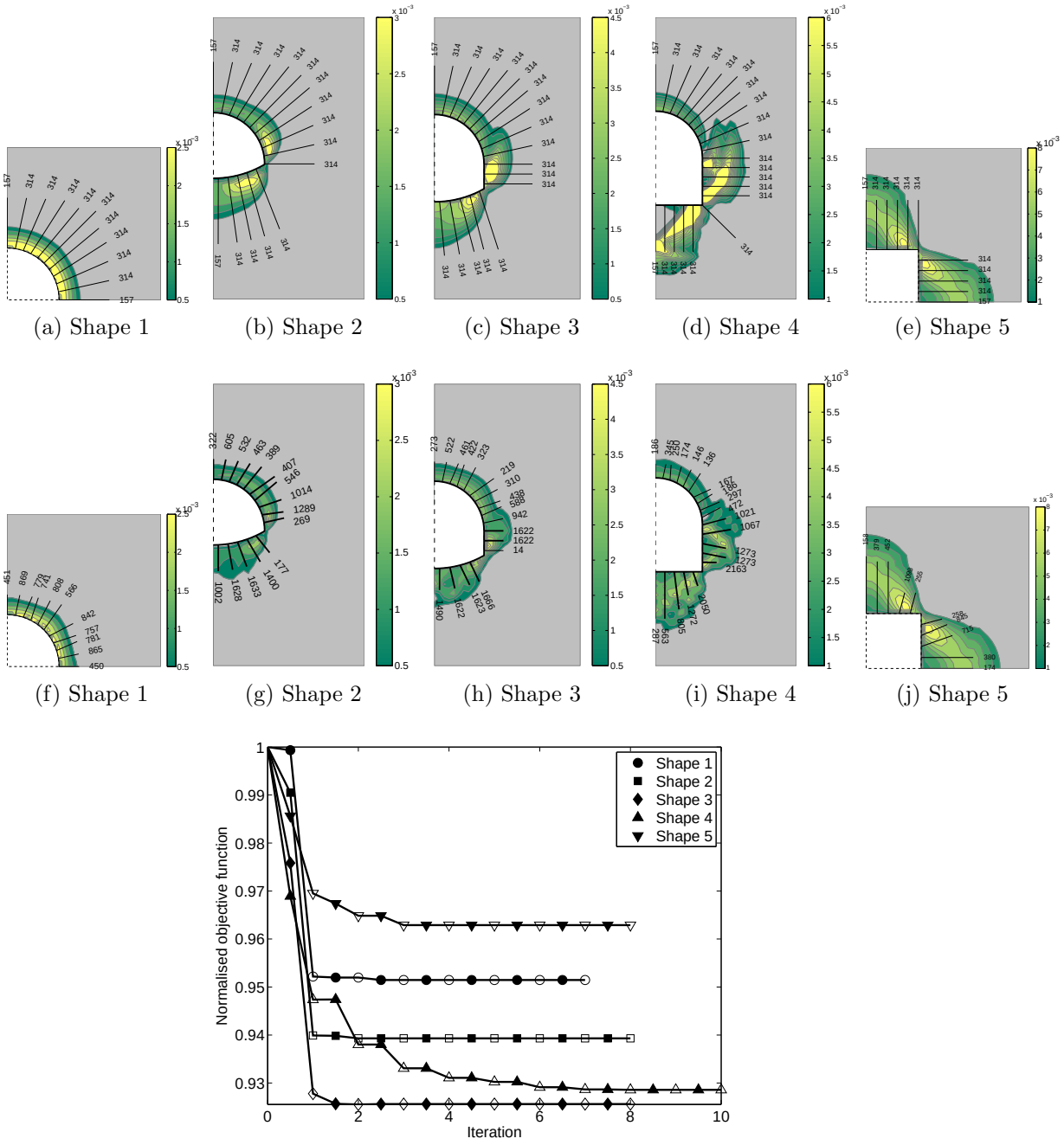

(a) Shape 1 (b) Shape 2 (c) Shape 3 (d) Shape 4 (e) Shape 5

(f) Shape 1 (g) Shape 2 (h) Shape 3 (i) Shape 4 (j) Shape 5

(k) Objective function variation

Figure 5.6: Initial and optimised bolt configurations for different tunnel shapes and corresponding objective function variations ($\sigma_1 = 3$ MPa and $k = 1$).

Table 5.2: Summary of the optimisation outcomes for different tunnel shapes ($\sigma_1 = 3$ MPa and $k = 1$)

Tunnel shape	Objective function		Improvement (%)
	Uniform (J)	Optimal (J)	
Shape 1	192 563	183 217	4.8
Shape 2	294 434	276 564	6.1
Shape 3	409 994	379 500	7.4
Shape 4	523 254	485 880	7.1
Shape 5	416 882	401 416	3.7

eliminated or significantly weakened in all cases.

Apart from the volume of bolts, their pattern also varies along different faces. Along the curved faces, the bolts are almost radially aligned and shorter lengths are preferable as is clearly observable in shapes 1 and 2, and also at the roof and floor of shape 3, and the roof of shape 4. On the other hand, the bolts emerging from the straight faces are not necessarily normal to the face and various bolt lengths are required along these faces as observable along the ribs of shapes 3 and 4, the floor of shape 4, and the square tunnel.

Looking at the variations of the objective function values, again it is noticeable that the contribution of optimising cross section areas is only significant in the initial stages. In all cases, a significant portion of the reduction achieved in the objective function value is due to updating the lengths and layout of bolts.

5.8 Consideration of discontinuities

Rock mass is naturally discontinuous and its mechanical behaviour is governed by the presence of rock discontinuities such as fractures, joints and other geological structures (Jing, 2003). A practical rock bolt design approach, should be able to explicitly capture the effects of discontinuities on proposed bolt layout. In the examples presented in §5.6 and §5.7, a homogeneous rock mass medium was modelled. This section is devoted to investigate the effects of rock mass discontinuities on the optimised rock bolt design. Two examples are considered here: one with a bedding plane and the other with two fractures in the rock mass.

Assuming that the discontinuity surfaces are cohensionless, the Coulomb's friction model is employed to model the slipping along the discontinuity. In this model, we have the following relationship at slippage,

$$\tau = \sigma_n \tan \phi. \tag{5.8}$$

Here τ and σ_n are the shear and normal stresses along the line of discontinuity respectively, and ϕ is the friction angle of the discontinuity surface.

5.8.1 Bedding Plane example

Bedding planes are commonly found between different layers of rock in sedimentary strata. A bedding plane at 1.5 m above the top of the tunnel is considered under two values of friction angle: $\phi = 10°$ and $\phi = 25°$. In order to solely investigate the effects of the bedding plane, the rocks above and below the bedding plane are assumed to possess the same material with properties defined in Table 5.1. A hydrostatic stress state of magnitude $\sigma_1 = \sigma_2 = 5$ MPa is considered.

The optimisation outcomes are presented in Fig. 5.7 and Table 5.3. To illustrate the slippage along the bedding plane, relative tangential displacements (RTD) are plotted along the bedding plane for the initial and optimised bolt layouts in Fig. 5.7. Looking at the initial designs (Figs. 5.7a and 5.7b), it can be seen that with $\phi = 25°$, the bedding plane is stable while slippage is occurring for $\phi = 10°$. The optimised rock bolt design reduces this slippage (Fig. 5.7c).

Table 5.3: Summary of the optimisation outcomes in consideration of effects of a bedding plane ($\sigma_1 = 5$ MPa and $k = 1$).

Friction angle	Objective function		Improvement (%)
	Uniform (J)	Optimal (J)	
$\phi = 10°$	1933504	1641544	15.1
$\phi = 25°$	1675770	1488113	11.1

With the friction angle of 10°, more bolt volume is distributed at the tunnel roof (Fig. 5.7c), which is a critical position due to the existence of the bedding plane. It is also interesting to note that two bolts at the large slippage areas are extended to the other side of the bedding plane, whereas the other bolts are

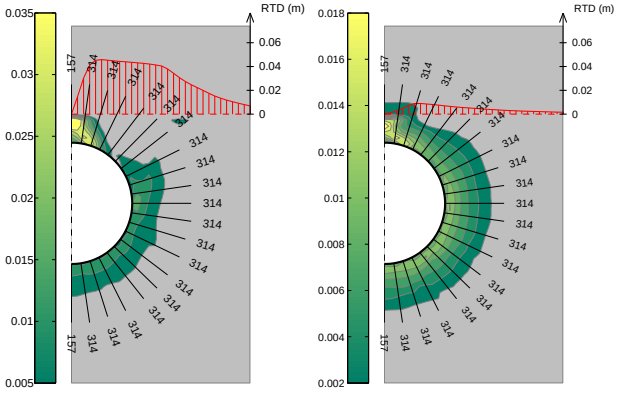

(a) Initial design, $\phi = 10°$ (b) Initial design, $\phi = 25°$

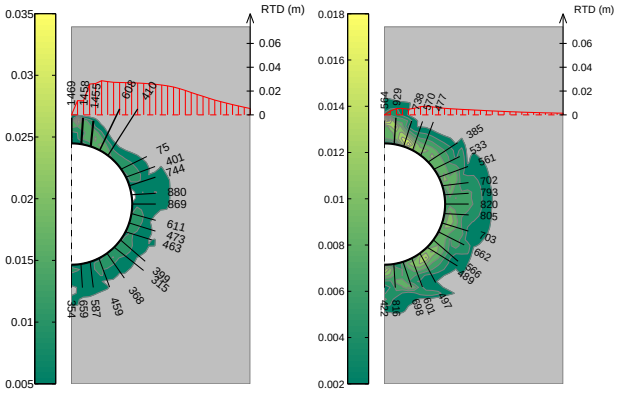

(c) Optimised bolt layout, $\phi = 10°$ (d) Optimised bolt layout, $\phi = 25°$

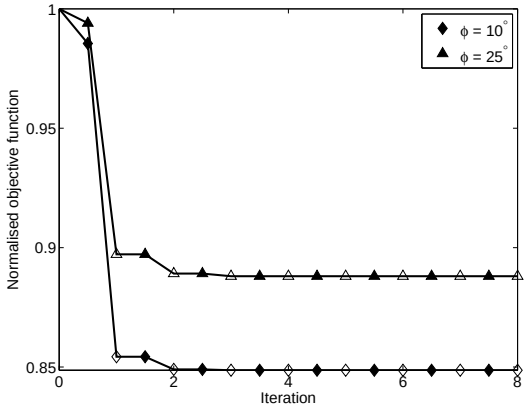

(e) Objective function variations

Figure 5.7: Effects of bedding plane on the optimisation outcomes ($\sigma_1 = 5\,\text{MPa}$ and $k = 1$).

shortened. Utilising the proposed bolt layout, an improvement of up to 15.1% is achieved as presented in Table 5.3. Although the considered objective function is not directly related to slippage, as noted before, the optimised design also considerably reduced the slippage along the bedding plane. Also noting at the plastic strain contours, it is clear the the optimised designs reduced the peak value and resulted in flatter distribution of plastic zone.

For the other case, the friction angle of 25° is very close to the friction angle of the intact rock material (27°). In the optimised design, the bolts are almost distributed evenly around the opening in the radial alignment and with short lengths (Fig. 5.7d). This bolt configuration is similar to that of the circular tunnel presented in Fig. 5.6f. It is clear that the existence of a bedding plane in this case has not resulted in any noticeable effect on the optimised bolt design.

Details of the objective function evolutions and their corresponding improvements are shown in Fig. 5.7e and Table 5.3. It is noted in Fig. 5.7e that the cross section area optimisation does not contribute much to the objective function improvements, while significant improvements are made by the length and orientation optimisation.

5.8.2 Fractured rock mass

A circular tunnel going through a rock mass with two major fractures as displayed in Fig. 5.8 is considered here as another example. It is assumed that the properties of these fractures are similar and two cases of friction angle of 10° and 25° are investigated. A hydrostatic *in situ* stress with a stress magnitude of 4 MPa is considered.

Fig. 5.9 shows the initial designs and optimisation results. Again, relative tangential displacements (RTD) are plotted along the fracture lines to illustrate the slippage.

Fig. 5.9g displays the objective function evolutions and Table 5.4 shows the initial and final objective function values and the achieved improvements. Apart from more that 7% improvement in the objective function values for both cases, it is

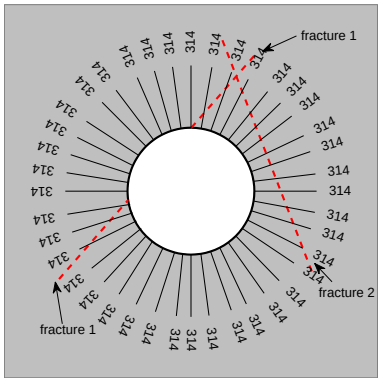

Figure 5.8: Model of the fracture rock mass

Table 5.4: Summary of the optimisation outcomes in consideration of effects of fractures ($\sigma_1 = 4$ MPa and $k = 1$)

Friction angle	Objective function		Improvement (%)
	Uniform (J)	Optimal (J)	
$\phi = 10°$	1573381	1454088	7.5
$\phi = 25°$	1376301	1279959	7.0

again interesting to note that the optimised rock bolt designs also significantly reduced the slippage along the discontinuities, reduced the peak plastic strains, and resulted in more uniform and flatter plastic zone around the tunnels.

A clear difference in the bolt volume distribution is observed for the case with $\phi = 10°$. The bolts in top left areas with no fracture are weakened to allow more bolt volume at more critical locations. Both bolt size and orientation are automatically adjusted in a way that reduces the movement along the discontinuities. Where the fractures were prone to slippage, bolt length are adjusted to staple the two sides of the plane of discontinuity. As seen in Fig. 5.9c, considerable reductions in the slippage magnitudes are obtained along the discontinuities. Particularly the peak values are significantly reduced.

For the case of $\phi = 25°$, the bolt volume around the "fracture 2" is just slightly higher than the other side. Three bolts are extended beyond this fracture plane where maximum slippage is expected. Noting the relatively small amount of slippage, as expected, the bolt orientations are almost similar to the initial design while shorter lengths are selected. The optimised design slightly reduced the slippage along the two discontinuities.

Again it is observable that the majority of the objective function improvement

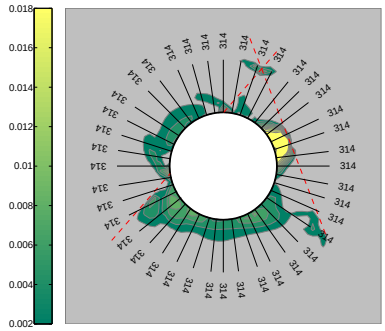

(a) Initial design, $\phi = 10°$

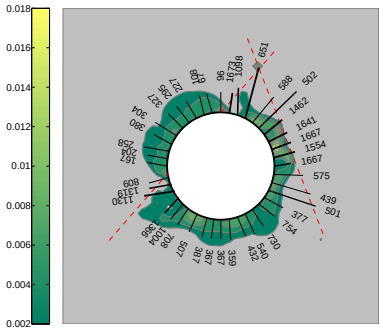

(b) Optimised design, $\phi = 10°$

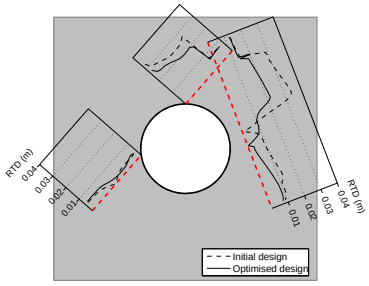

(c) Slippage, $\phi = 10°$

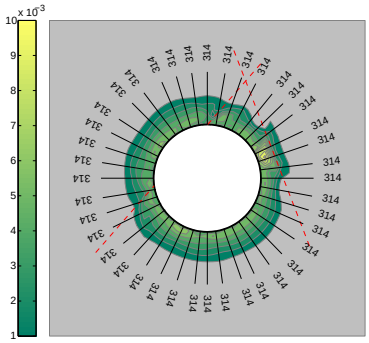

(d) Initial design, $\phi = 25°$

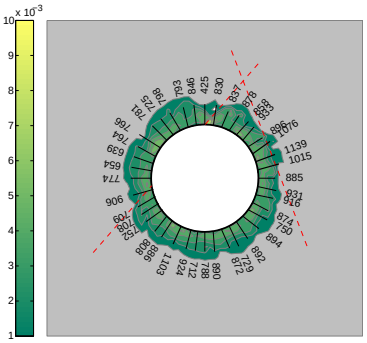

(e) Optimised design, $\phi = 25°$

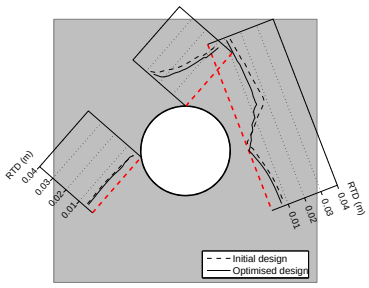

(f) Slippage, $\phi = 25°$

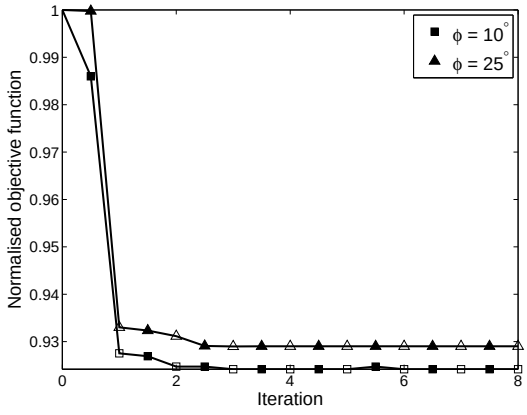

(g) Objective function variations

Figure 5.9: Effects of fractures on the optimisation outcomes ($\sigma_1 = 4$ MPa and $k = 1$)

in both cases is due to length and orientation optimisation.

5.9 Summary

In this chapter, an advanced optimisation algorithm is proposed which is capable of optimising all necessary parameters for a typical bolt design including cross section area, length and orientation. Compared to the previous works in this area, our proposed approach provides a significant improvement by explicitly considering bolt layout and length optimisation. The significant contribution of the length and orientation optimisation in the overall objective function improvement observed in all examples considered here proves the significance of the bolt pattern optimisation. Including bolt orientation and length in the optimisation algorithm not only results in more improvements in objective function values, but also extends the applicability of the proposed approach to more complicated and practical problems.

As the sensitivity results provided here solely depend on displacement results of bolts, any method of analysis which is able to provide displacement results can be adopted in this approach. Furthermore, because no assumption is included on the material models, the proposed method is directly applicable to any models of geomaterials and reinforcements. Considering the widespread availability of sophisticated numerical tools for analysing underground excavations, the proposed method is a potentially powerful tool in tunnel reinforcement design.

It is demonstrated that the uniform bolt layout as recommended by empirical methods is not necessarily an optimal design and more effective bolt layouts can be obtained. Obviously, the most appropriate bolt configuration needs to be found on a case-by-case basis by a thorough consideration of specific tunnel features and geological conditions.

Apart from a design tool, the proposed method can be used to study and investigate the effects of different parameters on rock bolt designs. A study of the effects of opening shape has been conducted by investigating various shapes of the tunnel. It is shown that generally a straight face or a large radius curved face

requires more reinforcement volumes than curved faces with smaller radii. Also, different bolt patterns can be advised based on the shape of the opening. The proposed approach has also been proved to work effectively with various geological conditions. Two sets of examples, one with the existence of a bedding plane and another with a fractured rock mass, have been demonstrated. The proposed approach automatically redistributes more reinforcement at critical positions and extend the bolts to cross the discontinuities where significant slippage is expected.

Although the direct objective of the proposed approach is to minimise a certain portion of the external work along the tunnel face, through several examples, it is demonstrated that other important improvements can also be achieved indirectly. This includes reduction of tunnel face deformation, slippage along planes of discontinuity, and plastic strain magnitudes. The proposed optimisation method is also able to extend to other useful objective functions and that topic will be presented in the next chapter.

Chapter 6

Looking at Displacement-based Objective Functions

6.1 Introduction

In chapters 3-5, a form of external work around the opening (which is a displacement functional) has been chosen as the objective function owing to its practical significance and ease of calculation. It should, however, be noted that at least in theory, the proposed optimisation approaches can be applied to any other objective function once the sensitivity of the utilised objective function is calculated with respect to the design variables. In this chapter, a general linear displacement-based objective function is considered, some forms of which are of particular interest in tunnelling design.

It is well known that minimisation of the settlement induced by tunnel excavation is important during both construction and operation phases. An excessive settlement might result in infringing serviceability requirements or in more serious cases, might cause critical damages to structures (Mair, 1998). For instance, significant ground movement due to shallow tunnel construction might lead to damage to the above structures. In the case of deep tunnels, tunnel heave and/or sidewall heave, which are particularly evident in squeezing and swelling rock (Hoek and Guevara, 2009; Kovári, 2009) are some of the displacement-related typical incidents. Apart from developing modern construction methods or en-

suring quality control, improving our understanding on reinforcement design is another crucial aspect to enhance an appropriate design with acceptable settlements. As a result, finding an optimised reinforcement distribution to minimise certain displacements is of interest and importance in many scenarios.

Using topology optimisation to minimise some displacement-based objective functions have been studied by Yin and Yang (2000a,b); Liu et al. (2008b); Ghabraie (2009). As mentioned previously, the common shortcomings of these studies are the usage of linear elastic material models and the homogenised isotropic material model for reinforced rock.

In this chapter, a sensitivity analysis for a general linear displacement-based objective function is presented considering general nonlinear material models. Verification of the derived sensitivity analysis is followed. Common problem faced in numerically calculating the sensitivities are discussed and a simple approach to estimate them will be proposed. Then, a tyical example is demonstrated to show the practicality of the proposed approach.

6.2 A general linear displacement-based objective function

An optimisation problem is defined as minimising a general linear displacement-based function $\Phi_d = \widetilde{\mathbf{f}} \cdot \mathbf{u}$, where $\mathbf{u} = [u_1, u_2, \ldots, u_n]$ is the displacement vector. Using topology optimisation approach, sensitivity analysis needs to be provided. To calculate a change in specified displacement components, a virtual load vector $\widetilde{\mathbf{f}} = [\widetilde{f}_1, \widetilde{f}_2, \ldots, \widetilde{f}_n]$ is applied to the system. It is noted that an element u_i of $\mathbf{u}$ would have a corresponding element $\widetilde{f}_i$ of $\widetilde{\mathbf{f}}$, and u_i and $\widetilde{f}_i$ have the same starting point and direction. The elements of $\widetilde{\mathbf{f}}$ are equal to a certain value at concerned displacement components and zeros at the others.

The minimisation problem can then be expressed as

$$\min \Phi_d = \widetilde{\mathbf{f}} \cdot \mathbf{u} \tag{6.1a}$$

$$\text{subject to:} \quad V_R = \sum_{b=1}^{m} a_b l_b = \bar{V}_R \tag{6.1b}$$

$$\mathbf{K} \cdot \mathbf{u} = \mathbf{f} \tag{6.1c}$$

where $\mathbf{u}$ and $\mathbf{K}$ are the displacement vectors and the stiffness matrix of the structure in its equilibrium condition respectively.

It can be seen in the optimisation algorithms shown in Figs. 4.2 and 5.3 that the proposed optimisation approach can be applicable to other objective functions provided that the sensitivity analysis is given. The sensitivity analysis for the general linear displacement-based objective functions is presented in the next section.

6.3 Sensitivity analysis

The sensitivity of the objective function with respect to an infinitesimal change in a general design variable ξ is

$$\frac{\partial \Phi_d}{\partial \xi} = \widetilde{\mathbf{f}} \cdot \frac{\partial \mathbf{u}}{\partial \xi} \tag{6.2}$$

In order to determine the sensitivity $\frac{d\mathbf{u}}{d\xi}$, the adjoint method is employed by introducing a Lagrangian multiplier vector $\boldsymbol{\lambda}$ and adding zero term $\boldsymbol{\lambda} \cdot \mathbf{R}$ to the objective function as

$$\Phi_d = \widetilde{\mathbf{f}} \cdot \mathbf{u} + \boldsymbol{\lambda} \cdot \mathbf{R} \tag{6.3}$$

where $\mathbf{R}$ is the residual force vector defined in Eq. (3.9)

The sensitivity of the modified objective function can then be derived as

$$\begin{aligned} \frac{\partial \Phi_d}{\partial \xi} &= \widetilde{\mathbf{f}} \cdot \frac{d\mathbf{u}}{d\xi} + \boldsymbol{\lambda} \cdot \left(\frac{\partial \mathbf{R}}{\partial \mathbf{u}} \frac{d\mathbf{u}}{d\xi} + \frac{\partial \mathbf{R}}{\partial \xi} \right) \\ &= \left(\widetilde{\mathbf{f}} + \boldsymbol{\lambda} \cdot \frac{\partial \mathbf{R}}{\partial \mathbf{u}} \right) \frac{d\mathbf{u}}{d\xi} + \boldsymbol{\lambda} \cdot \frac{\partial \mathbf{R}}{\partial \xi} \end{aligned} \tag{6.4}$$

In order to eliminate the unknown term $\frac{d\mathbf{u}}{d\xi}$, $\boldsymbol{\lambda}$ is chosen to satisfy the following system of nonlinear equations

$$-\boldsymbol{\lambda} \cdot \frac{\partial \mathbf{R}}{\partial \mathbf{u}} = \widetilde{\mathbf{f}} \tag{6.5}$$

Noting that the tangent stiffness matrix of the system can be expressed as

$$\mathbf{K}_T = -\frac{\partial \mathbf{R}}{\partial \mathbf{u}}, \tag{6.6}$$

Eq. (6.5) can be rewritten as

$$\boldsymbol{\lambda} \cdot \mathbf{K}_T = \widetilde{\mathbf{f}} \tag{6.7}$$

solving which, $\boldsymbol{\lambda}$ can be determined.

With the $\boldsymbol{\lambda}$ determined, Eq. (6.4) can be simplified to

$$\begin{aligned} \frac{\partial \Phi_d}{\partial \xi} &= \boldsymbol{\lambda} \cdot \frac{\partial \mathbf{R}}{\partial \xi} \\ &= -\boldsymbol{\lambda} \cdot \frac{\partial \mathbf{p}}{\partial \xi} \end{aligned} \tag{6.8}$$

As explained in the chapter 4, an infinitesimal change in the design variable merely leads to a change in the internal force vector of the bolts ($\mathbf{p}^S$) while the internal force vector of the rock remains unchanged. Eq. (6.8) can thus be rewritten as

$$\frac{\partial \Phi_d}{\partial \xi} = -\boldsymbol{\lambda} \cdot \frac{\partial \mathbf{p}_b^S}{\partial \xi} \tag{6.9}$$

Similar to the approach presented in §5.4, two variables included in the internal force vector of a bolt are the cross section area (a) and the matrix ($\mathbf{D}$), which is a function of the location of the bolt. Considering $\xi = a$, the cross section area can be optimised, whereas working with $\xi = \mathbf{D}$, one can optimise the length and orientation of the bolt. The previously defined interpolation schemes in Eqs. (4.2) and (5.3) can be used here to obtain the final formulae for the sensitivities with respect to the design variables a and $\mathbf{D}$ respectively.

Substituting Eq. (4.8) in Eq. (6.9) and replacing the general variable ξ by the

variable α_b, we obtain the following sensitivities with respect to cross section areas

$$\omega_A = \frac{\partial \Phi_d}{\partial \alpha_b} = -p\alpha_m^{p-1}\boldsymbol{\lambda} \cdot (\mathbf{p}_b^{S_{max}} - \mathbf{p}_b^{S_{min}}) \tag{6.10}$$

For sensitivites with respect to length and orientation of bolts, substituting Eq. (5.4) and Eq. (6.9) in Eq. (6.8), and replacing the general variable ξ by the variable t_b, we have

$$\omega_{OL} = \frac{\partial \Phi_d}{\partial t_b} = -\boldsymbol{\lambda} \cdot \mathbf{p}_b^{eS} \tag{6.11}$$

Once the sensitivities are determined, applying the variable updating scheme presented in §5.5, one can work out optimised bolt configurations. It should be noted again that the presented approach can be applicable to any displacement-related objective function and to any material model.

6.3.1 Calculation of λ

In order to obtain the sensitivities from Eqs. (6.10) and (6.11), λ needs to be solved from Eq. (6.7). A problem arises as the matrix $\mathbf{K}_T$ needs to be determined. As long as the finite element package is produced by the user, $\mathbf{K}_T$ can be conveniently recorded, and thus λ can be found. Obviously, using such approach would cause some inconveniences in tunnel modelling and hence restrict the practical applications of the presented method compared to using an external solver. On the other hand, when a commercial software is employed, obtaining the matrix $\mathbf{K}_T$ is challenging. This is due to the fact that for nonlinear materials, the matrix $\mathbf{K}_T$ changes accordingly with the application of the virtual load $\widetilde{\mathbf{f}}$. The ability to extract $\mathbf{K}_T$ is not always available for all finite element packages, leading to difficulties in handling the Eq. (6.7). It is evident that in tunnelling engineering with complicated simulation scenarios, employing a commercial software would bring us a lot of power and convenience in performing a practical simulation of the underground excavation. Therefore, one needs to compromise by using an appropriate method of analysis.

To the extent of this study, the Abaqus finite element package is utilised for modelling purpose. In order to overcome the challenges of solving the Eq. (6.7),

an approximation is introduced. By varying the virtual load $\widetilde{\mathbf{f}}$, corresponding $\boldsymbol{\lambda}$ can be determined and various sensitivities can be calculated using the proposed sensitivity analysis. A relationship between a measured sensitivity and a proposed sensitivity is established. The virtual load that gives the same value for the measured and the proposed sensitivity is selected. Further details on the approximation is presented in an example in the next section.

6.4 Minimising tunnel heave

This section is devoted to illustrate an example of minimising tunnel heave using the presented general sensitivity analysis. A horseshoe shape tunnel under biaxial stress condition is considered. It is known that the tunnel corners experience significantly smaller displacements while the centre of the floor experiences the largest displacement (see Figs. 4.6 and 5.5). The tunnel heave objective function can be defined as

$$\Phi_h = u_1 - \frac{u_2 + u_3}{2} \tag{6.12}$$

where u_1, u_2 and u_3 are the vertical displacements of the centre and the corners of the tunnel, respectively.

A load case is introduced with an upward load P at the centre of the tunnel floor and two downward half loads 0.5P at the tunnel corners as shown in Fig. 6.1.

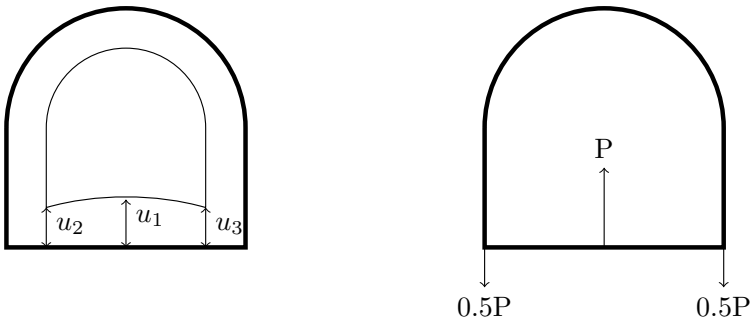

Figure 6.1: Load set to evaluate floor heave

6.4.1 Verification of sensitivity analysis

A problem of bolt cross section area optimisation is considered to minimise the tunnel heave under a bolt volume constraint. The tunnel model and the initial bolt layout are similar to those in the example in §5.6. The bolt identified as "tested bolt" in Fig. 6.2 is used for verification purpose.

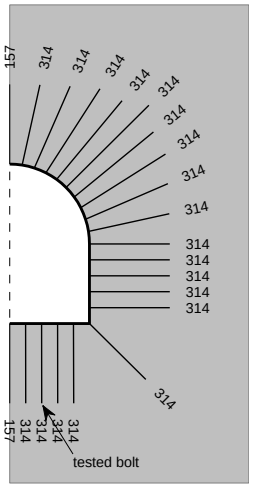

Figure 6.2: Initial bolt layout

The verification is based on the sensitivity analysis with respect to cross section areas (Eq. (6.10)). By creating a small change in the design variable (reducing the initial design variable α from 1 to 0.99), a comparison is made between the measured sensitivity number calculated as $\overline{\omega}_A = \frac{\Delta\Phi_d}{\Delta\alpha}$ and the proposed sensitivity (ω_A) in Eq. (6.10). By varying the value of P, a relationship between $\overline{\omega}_A$ and ω_A is then established to find out a P which gives the best fit of $\overline{\omega}_A$ and ω_A.

The following presents the verification results for two cases, case 1 with elastic materials and case 2 with elastic-plastic materials.

a. Case 1: Elastic materials

The host ground and the reinforcement materials are assumed to work in elastic regime with elastic material properties displayed in Table 5.1. Owing to the nature of the elasticity, $\mathbf{K}_T = \mathbf{K}$. From Eq. (6.7), we have $\boldsymbol{\lambda} = \widetilde{\mathbf{u}}$. Values of $\overline{\omega}_A$ and ω_A are then determined.

Fig. 6.3 shows the relationship between the ratios ($\overline{\omega}_A/\omega_A$) and various P.

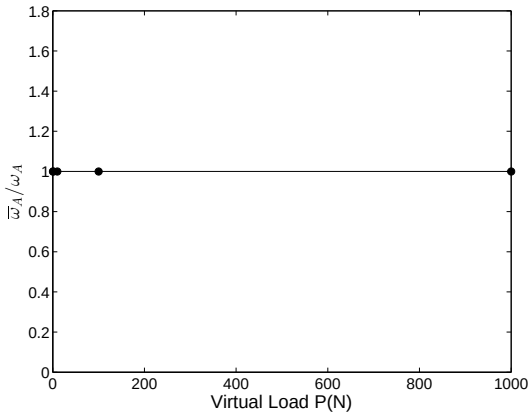

Figure 6.3: Approximation of virtual load for elastic case

Regardless of the applied values of P, the measured sensitivity number is almost the same as the proposed one ($\overline{\omega}_A/\omega_A \approx 1$). This is reasonably expected as for elastic materials, the sensitivity results should be independent of loading.

b. Case 2: Elastic-plastic materials

A similar procedure is applied for another set of material features. Material models and the related properties of rock, shotcrete and bolts are the same as the ones presented in §5.6. Under various magnitudes of the load P, the matrix $\mathbf{K}_T$ varies accordingly, leading to changes of $\boldsymbol{\lambda}$ and to the proposed sensitivity ω_A. Whereas the measured sensitivity remains unchanged in the testing condition, the ratio $\overline{\omega}_A/\omega_A$ varies accordingly with the varying of P as shown in Fig. 6.4. The relationship between the ratio of measured and estimated sensitivities and magnitude of P seems to be linear based on our numerical tests. It can be noted from the figure that $P = 60\,\mathrm{N}$ gives the desired result here. This value will, therefore, be used in the example to demonstrate the application of the proposed method.

6.4.2 Optimisation of bolt sizes

Using the optimisation algorithm shown in Fig. 4.2, the proposed sensitivity analysis for cross section area (Eq. (6.10)) and the suggested value of P, the outcome of an optimised bolt size is displayed in Fig. 6.5.

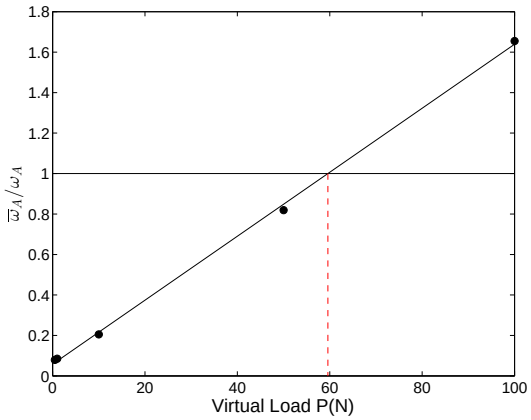

Figure 6.4: Approximation of virtual load for elastic-plastic case

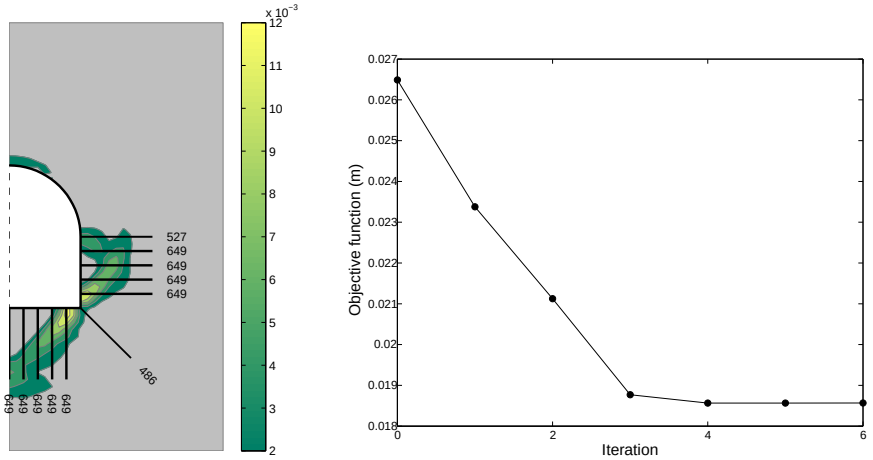

(a) Optimised bolt layout (b) Objective function variations

Figure 6.5: Bolt size optimisation for the tunnel heave objective function ($\sigma_1 = 3\,\mathrm{MPa}$, $k = 1$)

Fig. 6.5a shows an optimised bolt layout to minimise the floor heave in the tunnel. It can be seen that the bolts are all distributed at the tunnel floor and the ribs of the tunnel, leading to a significant reduction in the heave value as depicted in Fig. 6.5b. The initial value of the objective function is 0.0265 m, which is reduced to 0.0188 m. An improvement of 29% is thus achieved, showing the usefulness of the presented method.

6.5 Summary

Considering a general linear displacement-based objective function in the reinforcement optimisation problem, one would be able to cover a wide range of practical problems in tunnelling design including applications in both shallow and deep tunnels.

A challenge arising in the presented method is to solve the Eq. (6.7) and calculate the sensitivities numerically. One needs to make a decision on choosing a reasonable method of analysis. In the case that the simulation package is prepared by the user, the Eq. (6.7) can be solved directly and the sensitivity can be simply calculated. However, the practical application might be restricted due to limitations in the simulation capacity. On the other hand, if a commercial package is employed to take advantage of the simulation benefits, solving Eq. (6.7) cannot always be solved conveniently. An approximation approach therefore needs to be introduced to overcome the difficulty.

The achieved sensitivity analysis combined with the optimisation algorithm presented in the chapters 4 and 5 provides a powerful tool to seek out an optimised bolt configuration in consideration of a number of practical design requirements. It has been demonstrated in a typical example that the proposed method effectively minimises the assigned objective function by suggesting an optimised bolt layout.

Chapter 7

Conclusion

Despite its popularity and a great range of applications, topology optimisation has not been fully exploited in geomechanics and particularly in tunnelling, an area that requires a combination of theoretical and practical knowledge and experience. Owing to computational development and improvement of numerical methods, numerical analysis has become a powerful method of approximation in the last decades and also widely utilised in tunnelling design. A successful combination of optimisation methods and numerical analysis is proposed in this thesis to open up a new direction in designing reinforcement of underground excavations.

Like any other research work, in this thesis, a literature review was firstly performed. An introduction of special characters of geomaterials, the media in which the underground excavation is conducted has been given. Various methodologies of reinforcement design have been introduced and discussed. Issues on tunnel excavation simulation have been also mentioned.

A summary on optimisation methods has been presented as a continuation in the literature. Two commonly-used topology optimisation methods among others have been presented. The details of the methods, their general optimisation algorithms and typical examples have been demonstrated.

A brief review of previous works on applying topology optimisation on tunnel design has been given. Two main limitations in these works (linear elastic material model and modelling reinforced rock as a homogenised isotropic material) have

been pointed out and corresponding necessary improvements have been recommended.

To improve the previous works in this area, the simple assumption on using linear material has been removed and material nonlinearities have been considered in the optimisation methods. Behaviour of geomaterial and reinforcement materials can be modelled more accurately and more practical results can be obtained with this improvement. A revised optimisation algorithm has been provided. Various *in situ* stress states and opening shapes have been investigated in some typical examples to show the usefulness of the method. Also, an interpretation of the obtained homogenised reinforcement distribution is provided as an example to address the method's performance.

In chapter 4, the limitation of using the homogenised modelling technique is improved by explicitly modelling the reinforcement. More advanced optimisation approaches, therefore, need to be studied. An optimisation method has been proposed to optimise cross section areas of bolts by applying an interpolation scheme on the bolt size variable. The bolt spacing can also be indirectly controlled in this method. The method has been demonstrated to improve the conventional uniform bolt layout. Effects of various factors on an optimised bolt layout including *in situ* stress, bolt density and ground material features have been analysed. Also, penalisation effects are detailed in an example.

As a continued development, bolt pattern optimisation is taken into consideration in chapter 5. Stiffness matrix of bolt has been used as an optimisation variable to indirectly control the length and orientation of bolt. An optimisation algorithm has been proposed to simultaneously optimise size and pattern of bolts. The method has been proved to be an improvement on the conventional uniform bolt distribution and applicable to more complex and practical problems. Particularly, tunnel shape effects have been thoroughly presented. Moreover, presence of discontinuities in the media has been considered in some numerical examples. The effects of these ground conditions have been effectively captured using the proposed optimisation method by rearranging the bolt volume and pattern to the most critical positions. A comprehensive understanding of optimal bolt design

can be achieved by these kind of studies.

The proposed method aims at finding an optimised tunnel reinforcement that minimises the tunnel deformation under a given cost. A range of objective functions which are expressed as a functional of displacement and displacement-based functions can be utilised by the proposed methods provided that sensitivity analysis is obtained. A selection of a certain objective function is dependent on particular geological conditions and design requirements. In chapters 3-5, a particular functional of displacement (a form of external work along the opening surface) has been chosen as the objective function. The selection of objective function is then extended to a general linear displacement-based objective function in chapter 6. A wide range of practical problems in tunnelling design can be addressed with this general objective function formulation. An example has been demonstrated to search for an optimised bolt layout to minimise tunnel heave under a prescribed bolt volume.

An outstanding benefit of the presented optimisation methods is that they can be applicable to any model of both host ground and reinforcement materials. As long as the employed method of analysis is capable of providing the required outputs, the optimisation engine can be adopted to seek out an optimised reinforcement design.

Finding an optimal rock bolt design is a complicated problem which obviously needs to be studied in a case-by-case basis. The incorporation of advanced numerical modelling in the optimisation algorithms enables the proposed method to consider many significant factors in tunnelling design including construction sequences, geological conditions and tunnel features. Considering the widespread availability of numerical methods in tunnel excavation analysis, the proposed optimisation methods are a potentially promising tool in underground excavation design. Additionally, the concepts in the proposed methods can also be adopted in other engineering areas such as searching for optimised material distribution in multi-material problems, like the optimised distribution of steel bars in reinforced concrete structures, etc.

It can be seen in chapters 3-5 that neither a dramatic reduction in the objective

function nor a significant change in plastic zones have been observed. This is due to the fact that a large proportion of tunnel deformation is allowed before introducing the reinforcement, thus significantly reducing the loads that the reinforcements have to carry. Furthermore, the objective function of the external work is carried by the whole model which has considerably larger scale than the tunnel opening. If a local objective function is used, much higher improvements might be observed. This can be seen in the results obtained in chapter 6. A larger improvement of 29% has been achieved as the local displacement based objective function was utilised.

Apparently, this study did not cover all details in tunnel reinforcement design. Further improvements on modelling and optimisation approaches can be achieved by further studies. Application of the proposed methods to 3D models can probably be the first useful and most readily achievable extension. It is noted that regardless of the 2D/3D modelling selection, the methods can be used without any modifications. However, a great number of analyses would be required, resulting in an enormous consumption of time and computer resources. This study can also be extended to consider fully grouted bolt rather than the anchored bolt. Other problems in reinforcement design of shallow tunnels (e.g. minimising ground displacement) can be investigated. A case study using the proposed optimisation approaches would further illustrate the applicability of the methods.

References

ABAQUS (2013). *ABAQUS/Abaqus Analysis User's Manual. Hibbit, Karlsson and Sorenson Inc.*

Andreassen, E., Clausen, A., Schevenels, M., Lazarov, B. S., and Sigmund, O. (2011). Efficient topology optimization in MATLAB using 88 lines of code. *Struct Multidisc Optim*, 43:1–16.

Barton, N., Lien, R., and Lunde, J. (1974). Engineering classification of rock masses for the design of tunnel support. *Rock mechanics*, 6(4):189–236.

Bendsøe, M. P. (1989). Optimal shape design as a material distribution problem. *Structural Optimization*, 1:193–202.

Bendsøe, M. P. (1995). *Optimization of Structural Topology , Shape and Material*. Berlin: Springer.

Bendsøe, M. P. and Kikuchi, N. (1988). Generating optimal topologies in structural design using a homogenization method. *Computer Methods in Applied Mechanics and Engineering*, 71:197–224.

Bendsøe, M. P. and Sigmund, O. (2003). *Topology Optimization: Theory, Methods and Applications*. Springer, Berlin, Heidelberg.

Bernaud, D., de Buhan, P., and Maghous, S. (1995). Numerical simulation of the convergence of a bolt-supported tunnel through a homogenization method. *International Journal for Numerical and Analytical Methods in Geomechanics*, 19:267–288.

Bernaud, D., Maghous, S., de Buhan, P., and Couto, E. (2009). A numerical

approach for design of bolt-supported tunnels regarded as homogenized structures. *Tunnelling and Underground Space Technology*, 24:533–546.

Bieniawski, Z. T. (1973). Engineering classification of jointed rock masses. *Trans. S. Afr. Instn. Civ. Eng.*, 15(12):335–344.

Bieniawski, Z. T. (1974). Geomechanics classification of rock masses and its applications in tunneling. In ISRM, D., editor, *Proceedings of the Third International Congress on Rock Mechanism*, pages 27–32.

Bieniawski, Z. T. (1976). Rock mass classification in rock engineering. In *Proceedings of the Symposium on Exploration for Rock Engineering*, volume 1, pages 97–106, Cape Town. A. A. Balkema.

Bieniawski, Z. T. (1979). The geomechanics classification in rock engineering applications. In *ISRM Proceedings of the Fourth International Congress for Rock Mechanics, Montreux, Switzerland*, pages 41–48, Rotterdam. A.A. Balkerma.

Bieniawski, Z. T. (1984). *Rock Mechanics Design in Mining and Tunneling*. A.A. Balkerma, Rotterdam.

Bieniawski, Z. T. (1989). *Engineering Rock Mass Classification - A Complete Manual for Engineers and Geologists in Mining, Civil and Petroleum Engineering*. John Wiley & Sons, New York.

Bieniawski, Z. T. (1993). *Classification of rock masses for engineering: The RMR System and future trends, Comprehensive Rock Engineering, Practice & Projects, Rock testing and site characterization*, volume 3. Pergamon Press: Oxford, UK.

Bobet, A., Fakhimi, A., Johnson, S., Morris, J., Tonon, F., and Yeung, M. R. (2009). Numerical models in discontinuous media: Review of advances for rock mechanics applications. *Journal of Geotechnical and Goeenvironmental Engineering*, 135(11):1547–1561.

Brady, B. H. G. and Brown, E. T. (2006). *Rock Mechanics for Underground Mining*. Springer, Dordretcht, The Netherlands, 3rd edition.

Bruns, T. E. and Tortorelli, D. A. (2001). Topology optimization of nonlinear

elastic structures and compliant mechanisms. *Computer Methods in Applied Mechanics and Engineering*, 190:3443–3459.

Coda, H. (2001). Dynamic and static non-linear analysis of reinforced media: a BEM/FEM coupling approach. *Computers and Structures*, 79:2751–2765.

de Buhan, P., Bourgeois, E., and Hassen, G. (2008). Numerical simulation of bolt-supported tunnels by means of a multiphase model conceived as an improved homogenization procedure. *International Journal for Numerical and Analytical Methods in Geomechanics*, 32(13):1597–1615.

de Farias, M. M., Júnior, A. H. M., and de Assis, A. P. (2004). Displacement control in tunnels excavated by the NATM: 3-D numerical simulations. *Tunnelling and Underground Space Technology*, 19:283–293.

Dejean, M. and Raffoux, J. F. (1976). Role of rock bolting and parameters in its selection. *Mining Drifts and Tunnels: Tunnelling'76, London, Institute of Mining and Metallurgy*, pages 321–327.

Diaz, A. and Sigmund, O. (1995). Checkerboard patterns in layout optimization. *Structural Optimization*, 10:40–45.

Du, J. and Olhoff, N. (2004a). Topological optimisation of continuum structures with design-dependent surface loads - part i: New computational approach for 2d problems. *Str*, 27:151–165.

Du, J. and Olhoff, N. (2004b). Topological optimisation of continuum structures with design-dependent surface loads - part ii: Algorithm and examples for 3d problems. *St*, 27:166–177.

Fuchs, M. B., Jiny, S., and Peleg, N. (2005). The SRV constraint for 0/1 topological design. *Structural and Multidisciplinary Optimization*, 30:320–326.

Ghabraie, K. (2009). *Exploring topology and shape optimization techniques in undergorund excavation.* PhD thesis, RMIT University, Australia.

Ghabraie, K. (2015a). The ESO method revisited. *Structural and Multidisciplinary Optimization*, 51(6):1211–1222.

Ghabraie, K. (2015b). An improved soft-kill BESO algorithm for optimal distri-

bution of single or multiple material phases. *Structural and Multidisciplinary Optimization (accepted for publication).*

Ghabraie, K., Xie, Y. M., and Huang, X. (2008). Shape optimisation of underground excavation using ESO method. In *Innovations in Structural Engineering and Construction: Proceedings of the 4th International Structural Engineering and Construction Conference*, pages 877–882, Melbourne, Australia. London Taylor and Francis.

Ghabraie, K., Xie, Y. M., Huang, X., and Ren, G. (2010). Shape and reinforcement optimisation of underground tunnels. *Journal of Computational Science and Technology*, 4(1):51–63.

Grasselli, G. (2005). 3D Behaviour of bolted rock joints: experimental and numerical study. *International Journal of Rock Mechanics and Mining Sciences*, 42:13–24.

Grimstad, E. and Barton, N. (1993). Updating of the Q-system for NMT. In *International Symposium on Sprayed Concrete. Fagerness, Proceedings*, pages 46–66.

Hack, R. (1998). *Slope Stability Probability Classification, SSPC.* International Institute for Aerospace Survey and Earth Sciences (ITC).

Haftka, R. T. and Gurdal, Z. (1992). *Elements of structural optimization.* Kluwer, Dordrecht.

Harber, R. B., Jog, C. S., and Bendsøe, M. P. (1996). A new approach to variable-topology shape design using a constraint on perimeter. *Structural Optimization*, 11:1–12.

Harrison, J. P. and Hudson, J. A. (2000). *Engineering rock mechanics. Part 2: illustrative workable examples.* Sarkka P, Eloranta P, editors. Oxford: Pergamon.

Hinton, E. and Sienz, J. (1995). Fully stressed topological design of structures using an evolutionary procedure. *Engineering Computations*, 12(3):229–244.

Hoek, E. (1983). Strength of jointed rock masses - The Rankine Lecture. *Geotechnique*, 33(3):187–223.

Hoek, E. (1994). Strength of rock masses. *News Journal of ISRM*, 2(2):4–16.

Hoek, E. and Brown, E. T. (1980). *Undergorund Excavations in Rock*. The Institution of Mining and Metallurgy, London.

Hoek, E. and Brown, E. T. (1988). The Hoek-Brown failure criterion - a 1988 update. In *Proceedings of the 15the Canadian Rock Mechanics Symposium*, pages 31–38.

Hoek, E. and Brown, E. T. (1997). Practical estimates of rock mass strength. *International Journal of Rock Mechanics and Mining Sciences*, 34:1165–1186.

Hoek, E., Carranza-Torres, C., and Corkum, B. (2002). Hoek-Brown failure criterion - 2002 edition. In *Proceedings of the North American Rock Mechanics Symposium*, volume 1, pages 267–273, Toronto.

Hoek, E. and Guevara, R. (2009). Overcoming squeezing in the Yacambú-Quibor tunnel, Venezuela. *Rock Mechanics and Rock Engineering*, 42(2):389–418.

Hoek, E., Kaiser, P. K., and Bawden, W. F. (1997). *Support of Undergorund Excavations in Hard Rock*. A. A. Balkema, Rotterdam, The Netherlands.

Hoek, E., Wood, D., and Shah, S. (1992). A modified Hoek-Brown failure criterion for jointed rock mass. In In Hudson, J. A. e., editor, *ISRM Symposium: Eurock 92 - Proceedings of the International ISRM Symposium on Rock Characterisation*, pages 209–214, London. British Geotechnical Society.

Huang, X. and Xie, Y. M. (2007). Convergent and mesh-independent solutions for bi-directional evolutionary structural optimization method. *Finite elements in analysis and design*, 43(14):1039–49.

Huang, X. and Xie, Y. M. (2008). Topology optimization of nonlinear structures under displacement loading. *Engineering Structures*, 30:2057–2068.

Huang, X. and Xie, Y. M. (2009). Bi-directional evolutionary topology optimization of continuum structures with one or multiple materials. *Computational Mechanics*, 43:393–401.

Huang, X. and Xie, Y. M. (2010a). *Evolutionary Topology Optimization of Continuum Structures: Methods and Applications*. John Wiley & Sons, Ltd.

Huang, X. and Xie, Y. M. (2010b). A further review of ESO type methods for topology optimisation. *Struct Multidisc Optim*, 41:671–683.

Huang, X., Xie, Y. M., and Burry, M. C. (2006). A new algorithm for Bi-directional Evolutionary Structural Optimisation. *Japan Society of Mechanical Engineers International Journal Series C*, 49(4):1091–1099.

Jensen, J. S. and Sigmund, O. (2004). Systematic design of phonotic crystal structures using topology optimisation: low-loss waveguide bends. *Appl Phys Lett*, 84:2022–2024.

Jing, L. (2003). A review of techniques, advances and outstanding issues in numerical modelling for rock mechanics and rock engineering. *International Journal of Rock Mechanics and Mining Sciences*, 40:283–353.

Jog, C. S. (2002). Topology design of structures using a dual algorithm and a constraint on the perimeter. *International Journal for Numerical Methods in Engineering*, 54:1007–1019.

Jog, C. S. and Harber, R. B. (1996). Stability of finite element models for distributed-parameter optimization and topology design. *Comput. Meth. Appl. Mech. Engrg*, 130:203–226.

Jung, D. and Gea, H. C. (2004). Topology optimization of nonlinear structures. *Finite elements in analysis and design*, 40:1417–1427.

Karush, W. (1939). Minima of functions of several variables with inequalities as side constraints. Master's thesis, Department of Mathematics, University of Chicago, Illinois.

Kharmanda, G., Olhoff, N., Mohamed, A., and Lemaire, M. (2004). Reliability-based topology optimisation. *Str*, 26:295–307.

Kirsch, U. (1993). *Structural optimization*. Springer, Berlin.

Kovári, K. (2004). History of rockbolt and the sprayed concrete lining method. In

Proceedings of the Aachen International Symposium on Roofbolting in Mining, pages 39–85. Wissen-schaftsverlag Mainz in Aachen.

Kovári, K. (2009). Design methods with yielding support in squeezing and swelling rocks. In *World Tunnel Congress*, Budapest, Hungrary.

Kuhn, H. W. and Tucker, A. W. (1951). Nonlinear programming. In *Prcoceedings of 2nd Berkeley Symposium, Berkeley*, pages 481–492. University of California Press.

Lee, K. M. and Rowe, R. K. (1991). An analysis of three-dimensional ground movements: the thunder bay tunnel. *Canadian Geotechnical Journal*, 28:25–41.

Leite, L., Coda, H., and Venturini, W. (2003). Two-dimensional solids reinforced by thin bars using the boundary element method. *Engineering Analysis with Boundary Elements*, 27:193–201.

Li, Q., Steven, G. P., Querin, O., and Xie, Y. M. (1999). Evolutionary shape optimisation for stress minimisation. *Mechanics Research Communications*, 26(6):657–664.

Li, Q., Steven, G. P., and Xie, Y. M. (2001). A simple checkerboard suppression algorithm for evolutionary structural optimization. *Structural and Multidisciplinary Optimization*, 22:230–239.

Liu, H. Y., Small, J. C., and Carter, J. P. (2008a). Full 3D modelling for effects of tunnelling on existing support systems in the Sydney region. *Tunnelling and Underground Space Technology*, 23:399–420.

Liu, Y., Jin, F., Li, Q., and Zhou, S. (2008b). A fix-grid bidirectional evolutionary structural optimization method and its applications in tunnelling engineering. *International Journal for Numerical Methods in Engineering*, 73:1788–1810.

Mair, R. J. (1998). Geotechnical aspects of design criteria for bored tunnelling in soft ground. In *World Tunnel Congress '98 on Tunnels and Metropolises*, pages 183–199. Balkema, Sao Paulo, Brazil.

Matsui, K. and Terada, K. (2004). Continuous approximation of material distri-

bution for topology optimization. *International Journal for Numerical Methods in Engineering*, 59:1925–1944.

Maute, K., Schwarz, S., and Ramm, E. (1998). Adaptive topology optimization of elastoplastic structures. *Structural Optimization*, 15:81–91.

Menétrey, P. and Willam, K. J. (1995). Triaxial failure criterion for concrete and its generalization. *ACI Structural Journal*, 92:311–318.

Nguyen, T., Ghabraie, K., and Tran-Cong, T. (2014). Applying Bi-directional Evolutionary Structural Optimisation method for tunnel reinforcement design considering nonlinear material behaviour. *Computers and Geotechnics*, 55:57–66.

Nguyen, T., Ghabraie, K., and Tran-Cong, T. (2015a). Simultaneous pattern and size optimisation of rock bolts for underground excavations. *Computers and Geotechnics*, 66:264–277.

Nguyen, T., Ghabraie, K., Tran-Cong, T., and Fatahi, B. (2015b). Improving rock bolt design in tunnels using topology optimisation. *International Journal of Geomechanics (accepted 9 Jan 2015)*.

Palmstrom, A. (1995). *RMRi - a rock mass characterization system for rock engineering purposes*. PhD thesis, University of Oslo.

Palmstrom, A. (2000). Recent developments in rock support estimates by the RMi. *Journal of Rock Mechanics and Tunnelling Technology*, 6(1):1–19.

Palmstrom, A. and Broch, E. (2006). Use and miuse of rock mass classification systems with particular reference to the Q-systems. *Tunnelling and Underground Space Technology*, 21:575–593.

Palmstrom, A. and Stille, H. (2007). Ground behaviour and rock engineering tools for underground excavations. *Tunnelling and Underground Space Technology*, 22:363–376.

Panet, M. and Guenot, A. (1982). Analysis of convergence behind the face of a tunnel. In *Tunnelling'82*, pages 197–203, IMM, London.

Petersson, J. and Sigmund, O. (1998). Slope constrained topology optimisation. *International Journal for Numerical Methods in Engineering*, 41:1417–1434.

Potts, D. M. and Zdravković, L. (2001). *Finite Element Analysis in Geotechnical Engineering: Application*. Thomas Telford, London.

Querin, O. M. (1997). *Evolutionary Structural Optimisation Stress Based Formulation and Implementation*. Ph.D. thesis, Department of Aeronautical Engineering, University of Sydney, Sydney, Australia.

Querin, O. M., Steven, G. P., and Xie, Y. M. (1998). Evolutionary structural optimization (eso) using a bi-directional algorithm. *Engineering Computations*, 15:1031–1048.

Querin, O. M., Young, V., Steven, G. P., and Xie, Y. M. (2000). Computational efficiency and validation of bi-directional evolutionary structural optimisation. *Computer Methods in Applied Mechanics and Engineering*, 189:559–573.

Rabcewicz, L. V. (1964). The new austrian tunnelling method - part 1. *Water Power*, pages 511–515.

Rabcewicz, L. V. (1965). The new austrian tunnelling method - part 2. *Water Power*, pages 19–24.

Ren, G., Smith, J. V., Tang, J. W., and Xie, Y. M. (2005). Undergorund excavation shape optimization using an evolutionary procedure. *Computers and Geotechnics*, 32:122–132.

Ren, G., Zuo, Z. H., Xie, Y. M., and Smith, J. V. (2014). Undergorund excavation shape optimisation considering material nonlinearities. *Computers and Geotechnics*, 58:81–87.

Riedmüller, G. and Schubert, W. (1999). Critical comments on quantitative rock mass classifications. *Felsbau*, 17(3):164–167.

Rispler, A. R., Steven, G. P., and Tong, L. (2000). Photoelastic evaluation of metallic inserts of optimised shape. *Composites Science and Technology*, 60(1):95–106.

Rowe, R. K., Lo, K. Y., and Kack, K. J. (1983). A method of estimating sur-

face settlement above shallow tunnels constructed in soft ground. *Canadian Geotechnical Journal*, 20:11–22.

Rozvany, G. I. N. (2001). Aims, scope, methods, history and unified terminology of computer-aided topology optimization in structural mechanics. *Structural and Multidisciplinary Optimization*, 21:90–108.

Rozvany, G. I. N. (2009). A critical review of established methods of structural topology optimization. *Structural and Multidisciplinary Optimization*, 37:217–237.

Rozvany, G. I. N. and Querin, O. M. (2002). Combining eso with rigorous optimality criteria. *Int. J. Vehicle Design*, 28:294–299.

Russo, G., Kalammaras, G., and Grasso, P. (1998). A discussion on the concepts of geomechanical classes, behaviour categories, and technical classes for an underground project. *Gallerie e grandi opere soterranee*, 54:40–51.

Schubert, W., Goricki, A., Button, E., Riedm´uller, G., P´olsler, P., Steindorfer, A., and Vanek, R. (2001). Excavation and support determination for the design and construction of tunnels. In S´arkk´a, P. and Eloranta, P., editors, *Proceedings of the Eurock 2001*, pages 383–388, A.A. Balkema, Rotterdam.

Serafim, J. L. and Pereira, J. P. (1983). Consideration of the geomechanics classification of bieniawski. In *Proceedings of the International Symposium on Engineering Geology and Underground Construction*, pages 1133–1144.

Sigmund, O. (1994). *Design of material structures using topology optimisation*. PhD thesis, Depaerment of Solid Mechanics, Technical University of Denmark.

Sigmund, O. (1997). On the design of compliant mechanisms using topology optimization. *Mechanics of Structures and Machines*, 25(4):493–524.

Sigmund, O. (2001). A 99 line topology optimization code written in Matlab. *Structural and Multidisciplinary Optimization*, 21:120–127.

Sigmund, O. (2007). Morphology-based black and white filters for topology optimization. *Struct Multidisc Optim*, 33:401–424.

Sigmund, O. and Petersson, J. (1998). Numerical instabilities in topology opti-

mization: A survey on procedures dealing with checkerboards, mesh dependencies and local minima. *Structural Optimization*, 16(1):68–75.

Stolpe, M. and Svanberg, K. (2001a). An alternative interpolation scheme for minimum compliance topology optimization. *Structural and Multidisciplinary Optimization*, 22:116–124.

Stolpe, M. and Svanberg, K. (2001b). On the trajectories of penalization methods for topology optimization. *Structural and Multidisciplinary Optimization*, 21:128–139.

Swoboda, G. (1979). Finite element analysis of the new austrian tunnelling method (natm). In *Proceedings of the 3rd International Conference on Numerical Methods in Geomechanics*, volume 2, pages 581–586, Aachen.

Swoboda, G., Marence, M., and Mader, I. (1994). Finite element modelling of tunnel excavation. *International Journal of Engineering Modelling*, 6:51–63.

Tcherniak, D. and Sigmund, O. (2001). A web-based topology optimization program. *Struct Multidisc Optim*, 22:179–187.

Terzaghi, K. (1946). *Rock defects and loads on tunnel supports*. Harvard Univ., Graduate School of Engineering.

Vlachopoulos, N. and Diederichs, M. (2009). Improved longitudinal displacement profiles for convergence confinement analysis of deep tunnels. *Rock Mechanics and Rock Engineering*, 42(2):131–146.

Wickham, G. E., Tiedemamn, H. R., and Skinner, E. H. (1972). Support determination based on geologic predictions. In Lane, K. S. and Garfield, L. A., editors, *Proceedings of the North American Rapid Excavation Tunnelling Conference*, pages 43–64, New York. Society of Mineral Engineers, Americal Institute of Mineral, Metallurgical and Petroleum Engineers,.

Windsor, C. R. and Thompson, A. G. (1993). Rock reinforcement - technology, testing, design and evaluation. In *Comprehensive Rock Engineering*, pages 451–84, Pergamon: Oxford.

Wong, H. and Larue, E. (1998). Modelling of bolting support taking account

of non-simultaneous yielding of bolts and ground. In *Proceedings of the International Conference on the Geotechnics of Hard Soils - Soft Rock*, pages 1027–1038, Napoli, Italy. Balkema, Rotterdam.

Xie, Y. M. and Steven, G. P. (1992). Shape and layout optimization via an evolutionary procedure. In *Proceedings of International Conference on Computational Engineering Science*, page 471, Hong Kong.

Yang, X. Y., Xie, Y. M., Liu, J. S., Parks, G. T., and Clarkson, P. J. (2003). Perimeter control in the bidirectional evolutionary optimization method. *Structural and Multidisciplinary Optimization*, 24:430–440.

Yang, X. Y., Xie, Y. M., Steven, G. P., and Querin, O. M. (1999). Bidirectional evolutionary method for stiffness optimization. *AIAA Journal*, 37(11):1483–1488.

Yin, L. and Yang, W. (2000a). Topology optimization for tunnel support in layered geological structures. *International Journal for Numerical Methods in Engineering*, 47:1983–1996.

Yin, L. and Yang, W. (2000b). Topology optimization to prevent tunnel heaves under different stress biaxialities. *International Journal for Numerical and Analytical Methods in Geomechanics*, 24:783–792.

Yin, L., Yang, W., and Guo, T. (2000). Tunnel reinforcement via topology optimization. *International Journal for Numerical and Analytical Methods in Geomechanics*, 24:201–213.

Zhu, J. H., Zhang, W. H., and Qiu, K. P. (2007). Bi-directional evolutionary topology optimization using element replaceable method. *Computational Mechanics*, 40:97–109.